

# HYPOXIA IN SOLID TUMORS

BIOMARKER AND TARGET FOR INDIVIDUALIZED THERAPY

Elodie Melsens

Promotor: Prof. P. Pattyn; Co-promotor: Prof. W. Ceelen

Ghent 2017

Thesis submitted to fulfill the requirements for the degree of “Doctor in Medical Sciences”.

©Elodie Melsens, 2017

All rights reserved. No part of this thesis may be reproduced or transmitted in any form or by any means without prior written permission of the authors, of when appropriate, from the publishers of the publication.

Cover: by Nick Lagast

# **HYPOXIA IN SOLID TUMORS**

## BIOMARKER AND TARGET FOR INDIVIDUALIZED THERAPY

### **Promotor**

Prof. Dr. Piet Pattyn

Department of Gastro-Intestinal Surgery, University Hospital Ghent, Ghent,  
Belgium

### **Co-promotor**

Prof. Dr. Wim Ceelen

Department of Gastro-Intestinal Surgery, University Hospital Ghent, Ghent,  
Belgium

### **Members of the Examination Commission**

Prof. Dr. Boudewijn Brans

Department of Nuclear Medicine, University Hospital Ghent, Ghent, Belgium

Dr. Louke Delrue

Department of Thoracic and Abdominal Radiology, University Hospital Ghent,  
Ghent, Belgium

Prof. Dr. Anne Hoorens

Department of Pathology, University Hospital Ghent, Ghent, Belgium

Prof. Dr. Philippe Nafteux

Department of Thoracic Surgery, University Hospital Leuven, Campus  
Gasthuisberg, Leuven, Belgium

Prof. Dr. Marc Peeters

Department of Oncology, University Hospital Antwerp, Edegem, Belgium

Prof. Dr. Johan Vande Walle

Department of Pediatric Nephrology and Rheumatology, University Hospital  
Ghent, Ghent, Belgium



# **TABLE OF CONTENTS**

List of abbreviations		7
<b>Chapter 1</b>	Introduction	11
	1. Cancer and tumor microenvironment	13
	2. Tumor hypoxia	15
	3. Targeting tumor hypoxia	20
	4. Detecting tumor hypoxia	25
<b>Chapter 2</b>	Objectives and thesis outline	33
<b>Chapter 3</b>	Esophageal adenocarcinoma tumor model in mice	37
<b>Chapter 4</b>	Pilot study: <sup>18</sup> F-FAZA PET/CT in subcutaneous and orthotopic EAC xenografts	59
<b>Chapter 5</b>	Predictive value of <sup>18</sup> F-FAZA PET/CT and hypoxic modification with nimorazole	69
<b>Chapter 6</b>	Hypoxia as result of tumor angiogenesis and modification with cediranib	87
<b>Chapter 7</b>	General discussion and conclusion	109
<b>Chapter 8</b>	General relevance and future perspectives	121
<b>Chapter 9</b>	Summary/Samenvatting	127
References		137
Curriculum Vitae		147
Acknowledgments		151



## **LIST OF ABBREVIATIONS**

ARCON	Accelerated radiotherapy, carbogen and nicotinamide
ATF6	Activating transcription factor 6
ATP	Adenosine triphosphate
AUC	Area under the curve
BOLD	Blood oxygen level-dependent
CA	Contrast agent
CA9	Carbonic anhydrase 9
CAF	Cancer associated fibroblast
CFI	Colony formation index
CRC	Colorectal cancer
CT	Computed tomography
ATSM	Methyl-thiosemicarbazone
DAHANCA	Danish head and neck cancer group
DCA	Deoxycholate
DCE	Dynamic contrast enhanced
DFS	Disease free survival
DNA	Deoxyribonucleic acid
DSB	Double-strand breaks
DSWC	Dorsal skinfold window chamber
EAC	Esophageal adenocarcinoma
EC	Endothelial cell
EF5	Etanidazole pentafluoride
EGFR	Epidermal Growth Factor Receptor
EPO	Erythropoietin
EPRI	Electron paramagnetic resonance imaging
ESCC	Esophageal squamous cell carcinoma
FAZA	Fluoroazomycin arabinoside
FDG	Fluorodeoxyglucose
FETNIM	Fluoroerythronitroimidazole
FITC	Fluorescein isothiocyanate
FMISO	Fluoromisonidazole

GEJ	Gastro-esophageal junction
GEMM	Genetically engineered mouse model
GERD	Gastro-esophageal reflux disease
GFP	Green fluorescent protein
GLUT1	Glucose transporter 1
HAP	Hypoxia activated prodrug
HBO	Hyperbaric oxygen
Her2/Neu	Human epidermal growth factor receptor 2, ErbB-2
HIF	Hypoxia inducible factor
HNSCC	Head and neck squamous cell carcinoma
HSI	Hyperspectral imaging
HSP70, 90	Heat shock protein70, 90
Hypox	Hypoxia
IAZG	Iodo azomycin galactoside
IFP	Interstitial fluid pressure
IHC	Immunohistochemistry
IMRT	Intensity modulated radiotherapy
IP	Intraperitoneal
IRE1	Inositol-requiring protein 1
IV	Intravenous
IVIS	In vivo imaging system
IVM	In vivo microscopy, intravital microscopy
LARC	Locally advanced rectal cancer
LED	Light-emitting diode
Luc	Luciferase
MAPK	Mitogen-activated protein kinase
MCT1	Monocarboxylate transporter 1
MFI	Mean interstitial fluorescence intensity
MRI	Magnetic resonance imaging
mTOR	Mammalian target of rapamycin
MTS	3-(4,5-dimethylthiazol-2-yl)-5-(3-carboxymethoxyphenyl)-2-(4-sulfophenyl)-2H-tetrazolium
nCRT	Neoadjuvant chemoradiotherapy



NIRS	Near-infrared spectroscopy
Norm	Normoxia
NSCLC	Non-small cell lung carcinoma
OER	Oxygen enhancement ratio
ON	Overnight
OS	Overall survival
pCR	Pathologic complete response
PDX	Patient derived xenograft
PERK	PKR-like ER kinase
PET	Positron emission tomography
PFS	Progression free survival
PI3K	Phosphoinositide 3-kinase
pO <sub>2</sub>	Partial oxygen pressure
PSA	Prostate specific antigen
RCT	Randomized controlled trial
ROC	Receiver operating curve
ROI	Region of interest
RT	Radiotherapy
RTG	Relative tumor growth
SC	Subcutaneous
SD	Standard deviation
SER	Sensitizer enhancement ratio
SERCA	Sarco/endoplasmic reticulum Ca <sup>2+</sup> -ATPase
SNAP	S-nitroso-acetyl-penicillamine
SPECT	Single-photon emission computed tomography
StO <sub>2</sub>	Oxygen saturation
STR	Short tandem repeat
SUV	Standardized uptake value
T/B	Tumor to background ratio
TME	Tumor microenvironment
TT	Tumor take
TUNEL	Terminal deoxynucleotidyl transferase dUTP nick end labeling
UPR	Unfolded protein response

VEGF(R)      Vascular endothelial growth factor (receptor)  
VOI            Volume of interest

# **CHAPTER 1**

## **INTRODUCTION**



# CHAPTER 1: INTRODUCTION

## 1. CANCER AND TUMOR MICROENVIRONMENT

Cancer remains one of the most important causes of death worldwide and accounted for 8.8 million deaths globally in 2015 [1]. Briefly, cancer could be summarized as an uncontrolled growth of abnormal cells that are invasive, move to other sites in the body, and impair normal functioning of affected organs. Hanahan and Weinberg managed to comprehend this extremely complicated disorder by 10 hallmarks (Fig. 1).

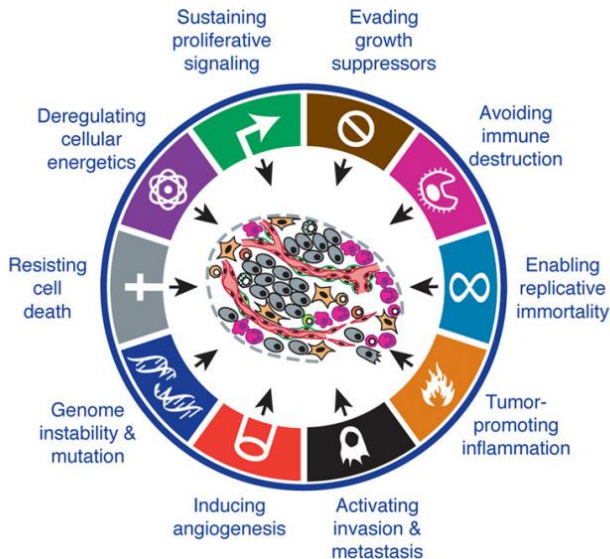


**FIGURE 1: Hallmarks of cancer.**

The hallmarks of cancer constitute an organizing principle for rationalizing the complexities of neoplastic disease. These acquired capabilities of cancer include (1) sustaining proliferative signaling, (2) evading growth suppressors, (3) resisting cell death, (4) enabling replicative immortality, (5) inducing angiogenesis, and (6) activating invasion and metastasis. Conceptual progress in the last decades led to addition of 4 more hallmarks: (7) genome instability, which generates the genetic diversity that expedites their acquisition, (8) inflammation, which fosters multiple hallmark functions, (9) reprogramming of energy metabolism and (10) evading immune destruction, leading to a total of 10 hallmarks. Adapted from [2].

Treatment of cancer has traditionally focused on eliminating cancer cells, by one, or a combination of the following treatments: surgery, chemotherapy and radiotherapy. Indeed,

tumors were formerly thought to be made of a nest of cancer cells only and research and therapies were focused only on the cancer cells (Fig. 2). At present, it is clear that the tumor microenvironment (TME) plays a crucial role in tumorigenesis. The TME consists of fibroblasts, immune cells and cells that comprise the blood vessels (pericytes, endothelial cells (EC's)) and is believed to be the second building block of the tumor. These seemingly normal environmental cells actively enable the malignant progression through cell-cell interactions (cancer versus environment) [3].

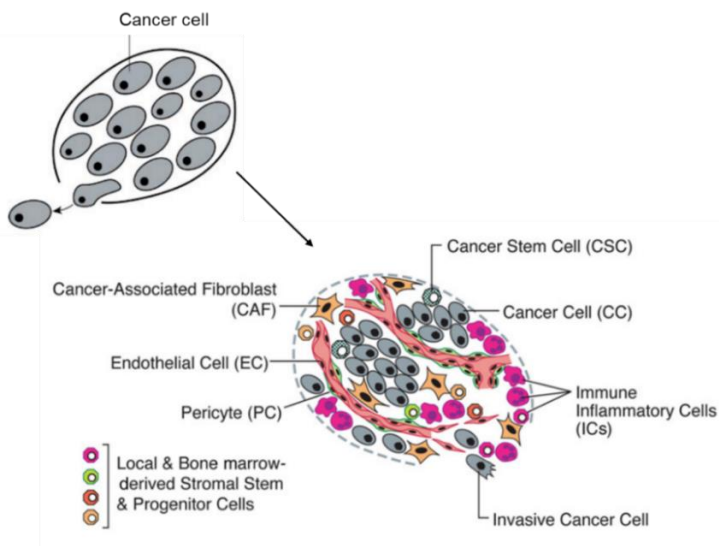


**FIGURE 2: Tumor micro-environment.**

The field of cancer research has largely been guided by a reductionist focus on cancer cells and the genes within them (above left). This view has evolved into a newer vision where tumors are seen as complex tissues in which mutant cancer cells have recruited seemingly normal cell types to act as active participants in their neoplastic development (beneath right). The interactions between the genetically altered malignant cells and the supporting microenvironmental cells are critical to understand cancer pathogenesis and to the development of novel, effective therapies. Adapted from [2, 3].

These important insights provided new approaches for cancer treatment that focused on the tumor as a whole (cancer cells + TME), like immunotherapy or anti-angiogenic therapy. An omnipresent feature of the TME is hypoxia. In the following sections, we describe the etiology of tumor hypoxia and highlight its importance as a potential target in cancer treatment, and as a predictive and prognostic biomarker.

## 2. TUMOR HYPOXIA

### A. *ETIOLOGY*

Oxygen is a key factor in cell metabolism. It is extracted from air in the lungs, bound to hemoglobin in the blood and transported to the capillaries where it enters tissue cells through diffusion. The critical oxygen level required for normal cell functioning is 10 mmHg [4]. Lower oxygen levels are considered hypoxic. In healthy tissues, oxygen delivery and consumption are well balanced, but tumors are prone to oxygen deficits for several reasons. First, consumption of oxygen is higher because cancer cells are highly proliferative. To meet this highly proliferative character, cancer cell's energy metabolism is reprogrammed to aerobic glycolysis instead of oxidative phosphorylation, known as the Warburg effect [5]. Second, oxygen delivery is compromised due to the limited diffusion distance of oxygen (limited to about 150-200  $\mu\text{m}$ ). Some tumor cells are located too far from existing blood vessels leading to diffusion-limited hypoxia (Fig. 3) [6].

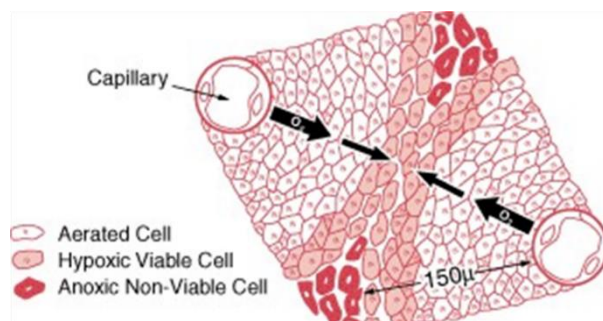


**FIGURE 3: Diffusion-limited hypoxia.**

Schematic illustration of oxygen diffusion from a capillary resulting in hypoxic cells. Oxygen diffuses an average of 150  $\mu\text{m}$  from the capillary. Cells beyond this region are anoxic and nonviable. Cells at the periphery of this radius are hypoxic but viable. Adapted from [7].

Oxygen delivery is further compromised due to the dysfunctional tumor vasculature (Fig. 4). This originates from the stimulation of tumor angiogenesis to cope with the fast growing tumor cells (one of the hallmarks of cancer [2]). Instead of forming well-structured functional vessels, tumor vessels are dilated, tortuous and the vessel wall is more permeable. These immature vessels eventually lead to a hypoxic and acidotic tumor microenvironment with high interstitial fluid pressures [8].

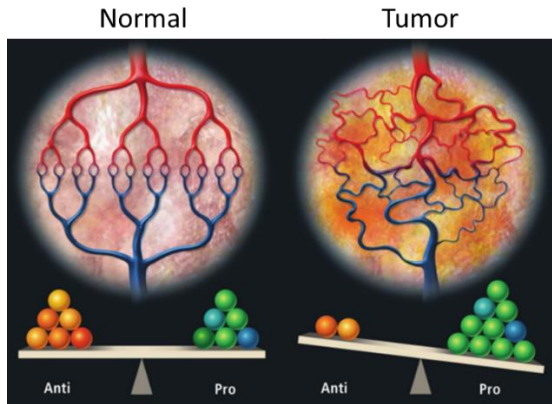


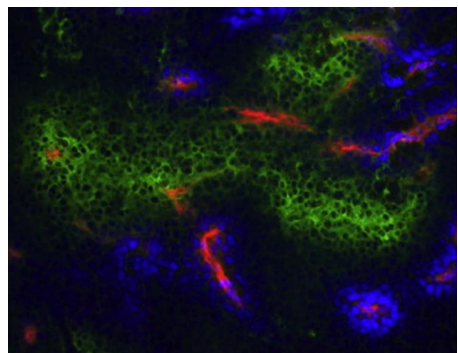
**FIGURE 4: Tumor angiogenesis.**

(Left) Normal vasculature. There is a balance between progrowth and antigrowth factor signals leading to an organized network, with large vessels regularly branching into smaller ones. (Right) Abnormal tumor vessels. There is an excessive number of proangiogenic factors, primarily vascular endothelial growth factor (VEGF), which causes an overgrowth of disorganized vessels that are typically permeable, dilated and tortuous. Adapted from [8].

Depending on the duration of hypoxia, two main types have been distinguished: chronic and cycling hypoxia, initially called acute hypoxia [9]. Chronic hypoxia is characterized by a deficit in  $O_2$  for a continuous period in time (at least several hours). This is believed to originate mostly from diffusion-limited hypoxia and the immature tumor vasculature. Cycling hypoxia, on the other hand, describes a hypoxia-reoxygenation pattern in which periods of poor and better perfusion alternate. It is believed to originate from perfusion-limited hypoxia where an intermittent constriction of tumor blood vessels lead to interruptions in tumor perfusion (Fig. 5).

**FIGURE 5: Cycling hypoxia.**

Immunofluorescence staining of a mouse tumor section depicting endothelial cells (red, CD31-staining), perfused vessels (blue, Hoechst 33342 injected 2 min before mouse sacrifice) and hypoxia area (green, pimonidazole staining). Note the existence of endothelial cells (red) in the hypoxic regions (green), reflecting ongoing angiogenesis or non-perfused blood vessels. Adapted from [9].





All these factors contribute to tumor hypoxia, which is distributed heterogeneously between tumor types, between individuals, and within the same tumor (space/time) and is present in up to 60% of locally advanced solid tumors [6, 10].

## B. TUMOR RESPONSE TO HYPOXIA

One could think that hypoxia leads to starvation of the tumor resulting in growth arrest, cell death and tumor growth inhibition, but the opposite occurs. Three main oxygen sensitive signaling pathways are activated independently where the Hypoxia Inducible Factor- 1 (HIF- 1) pathway is the most important one (Fig. 6). The Mammalian (or Mechanistic) Target Of Rapamycin (mTOR) and the Unfolded Protein Response (UPR) pathways are also activated. Through different intermediate steps, they lead to changes in cell metabolism and functioning and eventually result in adaptation and resistance of the cancer cells to hypoxia [6, 11-13].

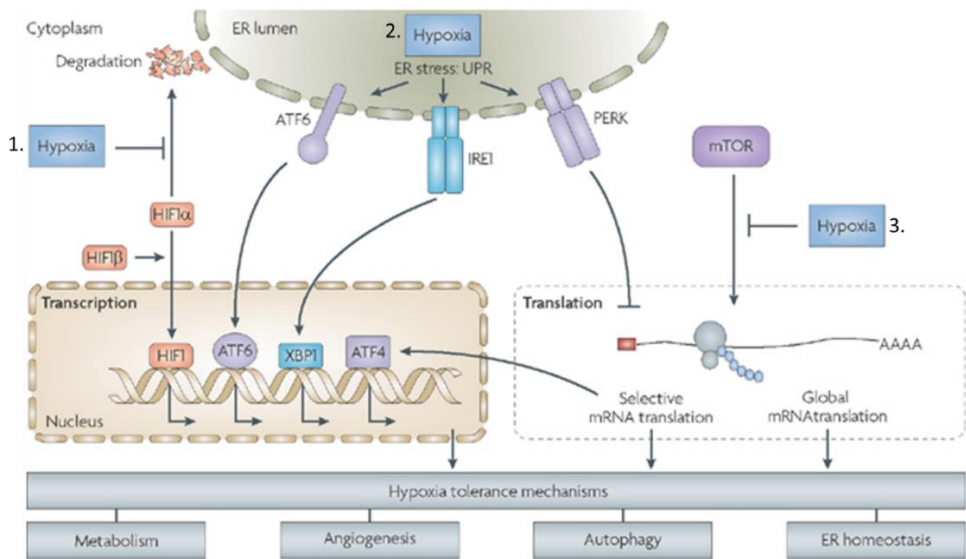


**FIGURE 6: Cellular response to hypoxia.**

(1) Hypoxia stabilizes hypoxia-inducible factor 1 $\alpha$  (HIF- 1 $\alpha$ ), facilitating heterodimerization with HIF- 1 $\beta$  and transcriptional activation of many genes. (2) Hypoxia triggers the unfolded protein response (UPR) by activation of the endoplasmic reticulum (ER) stress sensors PKR-like ER kinase (PERK), inositol-requiring protein 1 (IRE1) and, most probably, activating transcription factor 6 (ATF6). IRE1 and ATF6 both contribute to a transcriptional response whereas PERK causes inhibition of mRNA translation. (3) The activity of mTORC1, a complex containing the mammalian

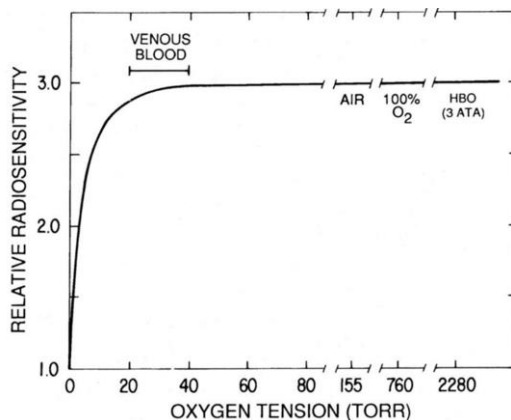
target of rapamycin (mTOR) kinase, which integrates and transmits positive and negative growth signals to the translational machinery, is inhibited by hypoxia. Together these three pathways influence the phenotype of hypoxic cells by altering metabolism, angiogenesis, autophagy and ER homeostasis. Adapted from [12].

Tumor cells do not only succeed in adapting their cell metabolism to the hypoxic circumstances, they also evolve to a more aggressive phenotype. It has been shown that tumor hypoxia is correlated with sustained angiogenesis [14], metastasis and invasion [15, 16], escaping apoptosis [17], suppression of the immune response [18] and genomic instability [19, 20], all hallmarks of cancer [2].

Further, clear associations with radio- and chemoresistance have been described [21-23]. The underlying mechanism of radioresistance is based on the crucial role of oxygen in the radiochemical process to cause DNA damage. Oxygen facilitates the making of DNA strand breaks by free radicals, as a result of ionizing radiation. In the absence of oxygen, 2-3 times higher doses of irradiation are needed to cause the same amount of DNA damage, also called the oxygen enhancement ratio (OER) and illustrated in Figure 7.

**FIGURE 7: Schematic representation of the relationship between radiosensitivity and oxygen tension.**

This graph summarizes the results of *in vitro* experiments with EMT6 mouse mammary tumor cells. Briefly, these were irradiated at different oxygen tensions with 250 kV x-rays. Cell survival was measured immediately after irradiation using a colony formation assay. Importantly this illustrates that the



radiosensitivity increases rapidly as the oxygen tension rises from anoxia to ~10 Torr. At higher concentrations of O<sub>2</sub>, similar to those found in venous blood, the radiosensitivity plateaus and does not increase greatly as the oxygen tension rises to that of cells equilibrated with air or with 100% O<sub>2</sub> at normal atmospheric pressure or even hyperbaric pressures (HBO). Adapted from [24, 25].

Tumor hypoxia was proven to be an independent negative predictive and prognostic factor in different solid tumors of which some examples are given in Table 1 [6, 26].

Measure of hypoxia	Probe	Clinical setting	Outcome for hypoxic tumours
Oxygen concentration	Eppendorf oxygen electrode	Chemoradiation of advanced HNSCC	Worse OS
		Radiotherapy of soft tissue sarcomas before surgery	Worse DFS owing to a higher rate of distant metastasis
		Brachytherapy of localized prostate cancer	Decreased biochemical control (shown by PSA levels)
Endogenous markers		Cervical carcinoma	Worse DFS in node-negative patients owing to a higher rate of distant metastases
	HIF1 $\alpha$	Node-negative breast cancer	Worse OS
	HIF1 $\alpha$	BRCA1 mutant breast cancer	Worse DFS
	HIF2 $\alpha$ , CA9	CHART trial in HNSCC	Worse local control and OS
	CA9	Adjuvant chemotherapy of breast cancer	Worse OS
	Osteopontin	Radiotherapy for HNSCC	Nimorazole (hypoxic radiosensitizer) improved local control and OS
Exogenous probes	Lysyl oxidase	Breast cancer	Worse metastasis-free survival
	Hypoxic gene signature	HNSCC and breast cancer	Worse outcome, multiple end points
	Hypoxic gene signature	Hepatocellular carcinoma	Worse OS
	Pimonidazole	Radiotherapy for advanced HNSCC	Worse local control
	EF5	Post-surgical radiotherapy of HNSCC	Worse DFS

**TABLE 1: Representative examples of the prognostic and predictive significance of hypoxia in human cancer.**

CA9= carbonic anhydrase 9= endogenous hypoxia marker; CHART= continuous hyperfractionated accelerated radiotherapy; DFS= disease free survival; EF5= etanidazole pentafluoride; HIF= hypoxia-inducible factor; HNSCC= head and neck squamous cell carcinoma; OS= overall survival. PSA= prostate specific antigen. Adapted from [26].

In conclusion, hypoxia is present to some extent in all solid tumors and has been correlated with treatment resistance and patients' prognosis. This makes it on the one hand an attractive target for therapy modifications and improvements, and on the other hand, an interesting biomarker to predict treatment response (predictive biomarker) and survival (prognostic biomarker).

### **3. TARGETING TUMOR HYPOXIA**

The importance of hypoxia in solid tumors has been recognized and investigated for over 100 years. Hereby, a diversity of therapies have been developed to act on this microenvironmental phenomenon. In this section we summarize some major mechanisms in targeting hypoxia.

#### ***A. ENHANCING OXYGEN DELIVERY***

Therapies to enhance the oxygen delivery by the blood were developed in the idea it would make tumors less radioresistant. Older studies tested the effect of blood transfusions and administration of erythropoietin (EPO) to increase hemoglobin levels and oxygen transport, but had questionable results as it was shown that EPO also increases tumor cell proliferation [27]. Later, different breathing schedules were tested like hyperbaric oxygen (HBO) or carbogen, a hyperoxic gas (95%- 98% O<sub>2</sub> and 2%- 5% CO<sub>2</sub>) [28]. Combination with nicotinamide, a vitamin B3 analog and vasoactive agent, and accelerated radiotherapy led to the ARCON strategy, accelerated radiotherapy with carbogen and nicotinamide. It would counteract cellular repopulation and reduce diffusion- and perfusion-limited hypoxia. ARCON seems the most promising with good local control rates in head and neck and bladder cancers in phase II trials [29].

However, the two main approaches to target hypoxia in cancer are the use of bioreductive prodrugs on the one hand, and drugs that inhibit molecular targets upon which hypoxic cell survival depends on the other hand [26].

#### ***B. BIOREDUCTIVE PRODRUGS***

The bioreductive prodrugs, also called hypoxia activated prodrugs (HAP's), are administered in their inactive state and are activated in hypoxic cells ensuring hypoxia

specific functioning [26]. Five groups of chemical structures have been identified with these hypoxia specific activation properties: nitro groups, aromatic N-oxides, aliphatic N-oxides, quinones and transition metals [30]. Figure 8 illustrates the chemical mechanism underlying the hypoxia dependent activation of HAP's with a nitro group, also called oxygen dependent redox cycling.

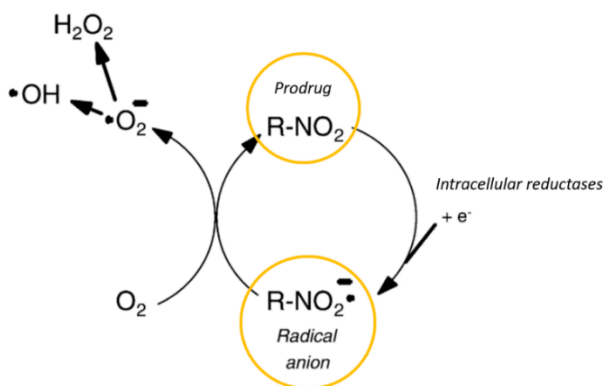
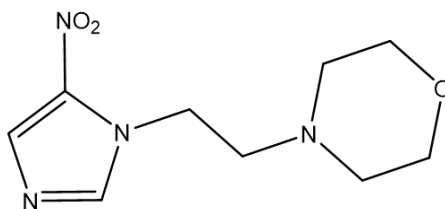


**FIGURE 8: Mechanism of hypoxia dependent activation of HAP's with a nitro group.**

The prodrug has entered the cell through diffusion and is reduced enzymatically by intracellular reductases. Under normoxic conditions, oxygen takes back the electron, reversing the reduction and returning the drug to its inactive state. Under hypoxic conditions, the reduction activates the prodrug to its active state of a radical anion. Adapted from [31].

The nitroimidazoles have besides the hypoxia specific cytotoxic activity also a hypoxic radiosensitizing effect. They are able to replace the effect of oxygen in the radiobiological process, in producing free radicals and generating cytotoxic DNA strand breaks. The oxygen enhancement ratio is valued at 1.5 to 2 maximally, thereby not reaching the level of normoxic conditions [32]. Misonidazole was the first tested nitroimidazole combined with radiotherapy. Several randomized clinical trials were performed, which proved the proof of principal, but due to high toxicities (neuropathy) and lack of major benefits on clinical outcomes, this was not adopted in daily clinic [33, 34]. Nimorazole however (Fig. 9), showed to improve clinical outcomes in head and neck cancer and is now used in daily practice in Denmark [35]. It is a 5-nitroimidazole with lower cytotoxicity and neurotoxicity. The lack of overall survival improvement is probably because no patient selection was performed.

**FIGURE 9: Chemical structure of nimorazole, 4-[2-(5-nitro-1H-1-imidazolyl)ethyl]morpholine.**



### C. TARGETING THE HYPOXIC CELL

The use of drugs that inhibit molecular targets upon which hypoxic cell survival depends, mainly concern the three primary hypoxia-sensing signaling pathways HIF, UPR and mTOR [26]. Different drugs have been developed that interfere with HIF1 $\alpha$  expression, HIF1 transcription, HIF1 target gene products (CA9, Glut1), receptor tyrosine kinases (VEGFR, EGFR), RAS-MAPK signaling, mTOR (autophagy, mTORC1) and UPR (SERCA, HSP90). Different examples of HIF-targeted therapies are summarized in Table 2.

Currently, no clear clinical evidence exists yet of antitumor activity due to direct HIF1 inhibition, UPR targeting is still in the *in vitro* phase and also mTOR inhibitors (e.g. rapamycin) are still in their preclinical phase. Targets downstream the primary hypoxia-sensing pathways are also investigated, like inhibiting autophagy (induced by UPR), inhibiting glycolysis (induced by HIF1 and mTOR), and targeting DNA damage response and repair pathways in response to hypoxia are investigated, like reactivating p53 to restore hypoxia-mediated apoptosis. These newer approaches are just at their start.

Targeting hypoxia induced angiogenesis on the other hand, has been studied extensively and will be discussed in the next section.

Inhibitory mechanism	Drug	Target	References	
mRNA/protein expression	Wortmannin	PI3K	Jiang et al., 2001	
	LY94002	PI3K	Jiang et al., 2001; Mohlin et al., 2015	
	GDC-0941	PI3K	Mohlin et al., 2015	
	PI-103	PI3K	Mohlin et al., 2015	
	Rapamycin	mTOR	Hudson et al., 2002	
	PP242	mTOR	Mohlin et al., 2015	
	Amino flavone	unknown	Terzuoli et al., 2010	
	Glyceollins	AKT/mTOR, Hsp90	Lee et al., 2015	
	Topotecan, PEG-SN38	Topoisomerase 1	Rapiscarda et al., 2004; Pastorino et al., 2010	
	EZN-2968	HIF-1 $\alpha$ mRNA	Greenberger et al., 2008	
	2ME2, ENMD-1198	Microtubules	Mabjeesh et al., 2003; LaVallee et al., 2008	
	Geldanamycin and analogs	Hsp90	Isaacs et al., 2002	
	Vorinostat	HDAC	Hutt et al., 2014	
HIF- $\alpha$ /HIF-1 $\beta$ dimerization	YC-1	unknown	Chun et al., 2001; Li et al., 2008	
	PX-478	unknown	Koh et al., 2008	
	PX-12, pleurotin	Thioredoxin-1	Welsh et al., 2003	
	Cardiac glycosides	unknown	Zhang et al., 2008b	
	FM19G11	unknown	Moreno-Manzano et al., 2010	
	HIF-2 $\alpha$ translational inhibitors	IRP1/IRE interaction	Zimmer et al., 2008	
	Acriflavine	HIF-1 $\alpha$ /2 $\alpha$ PAS-B domain	Lee et al., 2009	
	PT2385	HIF-2 $\alpha$ PAS-B domain	Scheuermann et al., 2013	
	Echinomycin	HRE	Kong et al., 2005	
	Polyamides	HRE	Olenyuk et al., 2004	
	Chetomin	p300 recruitment	Kung et al., 2004	
	Bortezomib	p300 recruitment	Kaluz et al., 2006; Shin et al., 2008	
	Amphotericin B	FIH-1 interaction and p300 recruitment	Yeo et al., 2006	
Triptolide	Hsp70	Zhou et al., 2010		
AJM290, AW464	Thioredoxin-1	Jones et al., 2006		
DNA binding				
	Transcriptional activity			

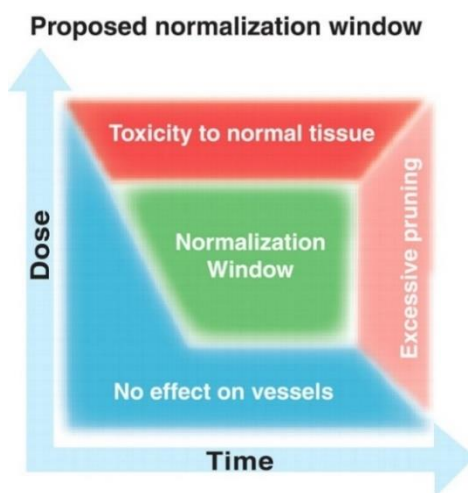
**TABLE 2: Inhibitors of HIF activity by different mechanisms and targets.** Adapted from [36].

## – VEGF(R) INHIBITION

In response to hypoxia, vascular endothelial growth factor (VEGF) is secreted by cancer cells and cancer associated stromal cells (EC, CAF's, macrophages). VEGF binds its receptor (VEGFR), mainly located on endothelial cells (EC) of blood vessels and lymphatic vessels, and induces angiogenesis by promoting survival, proliferation and migration of EC, increasing the display of adhesion molecules and increasing vascular permeability [37]. It is one of the major driving forces of survival of hypoxic cancer cells. Anti-angiogenic therapy through inhibition of VEGF(R) blocks these pathways. Depending on the resulting balance between pro- and anti-angiogenic factors, inhibition of VEGF(R) induces a normalization of the tumor vasculature (leading to better delivery of nutrients, oxygen (radiosensitizer) and drugs (chemo- or immunotherapy)), or the inhibition induces a regression of tumor vasculature (leading to tumor 'starvation' [38], but also an increase in hypoxia and a more hostile TME). With the eye on targeting hypoxia, normalization is aimed at. Radio-, chemo- and immunotherapy efficiency depend on tumor perfusion and oxygenation. Theoretically, combination with VEGF(R) inhibition could have synergistic effects and indeed this synergism has been proven for the combination with chemotherapy. Bevacizumab (Avastin®), for example, a VEGFA antibody, has been FDA-approved ((BLA) 125085) for treatment of different cancer types such as first line treatment of metastasized colorectal cancer in combination with chemotherapy [39]. Timing and dosage of VEGF(R) inhibition is important as is explained in figure 10 [40, 41].

**FIGURE 10: Normalization window.**

Proposed effect of drug dose and schedule on tumor vascular normalization. The efficacy of cancer therapies that combine antiangiogenic and cytotoxic drugs depends on the dose and delivery schedule of each drug. The vascular normalization model posits that a well-designed strategy should passively prune away immature, dysfunctional vessels and actively fortify those remaining, while incurring minimal damage to normal tissue vasculature. During this "normalization" window (green), cancer cells may be more vulnerable to traditional cytotoxic therapies and to novel





targeted therapies. The degree of normalization will be spatially and temporally dependent in a tumor. Vascular normalization will occur only in regions of the tumor where the imbalance of pro- and antiangiogenic molecules has been corrected. Adapted from [41].

In conclusion, numerous therapies exist to target hypoxia and improve treatment outcomes. Most of them showed promising results in the early trials, but eventually failed to confirm their benefit in phase III trials. For sure, this has to do with the lack of patient selection. The key to prove success of hypoxia modification lies in adequate patient selection. Therefore, methods to detect and quantify tumor hypoxia are needed and are discussed in the following section.

## 4. DETECTING TUMOR HYPOXIA [42-44]

### *A. pO<sub>2</sub> PROBE MEASUREMENTS*

Direct measurement of pO<sub>2</sub> with a polarographic needle electrode system (pO<sub>2</sub> histogram, Eppendorf, Hamburg, Germany) inserted in different tracks in the tumor, has long been the golden standard [45] (Table 3). This technique is based on the polarographic reduction of molecular oxygen at a cathode sensor, covered by a semipermeable membrane, inducing a current [46]. The magnitude of this current is linearly correlated with the amount of oxygen at the cathode and thus with the partial oxygen tension. In the clinical setting, it could confirm the hypothesis that hypoxia is a negative prognostic marker in different tumors (e.g. cervix cancer, soft tissue sarcomas, head and neck cancer) [47-49]. Later, the fluorescence-based fiberoptic probe followed (OxyLite, Oxford Optronix, UK) [50]. Short pulses of LED light are transmitted along the fiberoptic sensor and excite a platinum-based fluorophore at the sensor tip. The resulting emission of fluorescent light, quenched by the presence of oxygen molecules, is detected and the lifetime of fluorescence is inversely proportional to the concentration of dissolved oxygen.

These pO<sub>2</sub> probe systems proved their use, but major disadvantages remain, like their invasiveness, operator dependency, sample size dependency and most importantly their inapplicability for deeper lying pathologies and repetition of measurements. At present, they are very little used in the clinical setting.

pO <sub>2</sub> probe system	Advantage	Disadvantage
<i>Polarographic needle</i>	- rapid data sampling	- oxygen consumption during read-out - not reaching a steady state
<i>Fluorescence-based fiberoptic needle</i>	- measuring at individual locations over a prolonged period - absence of oxygen consumption	- stabilization period of 1-2 min before measuring

**TABLE 3: Comparison of polarographic and fluorescence-based pO<sub>2</sub> probe systems.**

### B. IMMUNOHISTOCHEMISTRY

Immunohistochemical detection of hypoxia is another frequently used quantification method. Endogenous hypoxia markers (e.g. HIF-1 $\alpha$  or CA9) or exogenous markers that are administered before biopsy (e.g. pimonidazole or EF5 (2-(2-Nitro-1H-imidazol-1-yl)-N-(2,2,3,3,3-pentafluoropropyl) acetamide)), are stained in tumor specimens [51] (Fig. 11). This technique however implies taken biopsies, is sample size dependent, difficult for deeper lying structures, difficult to repeat and difficult to quantify.

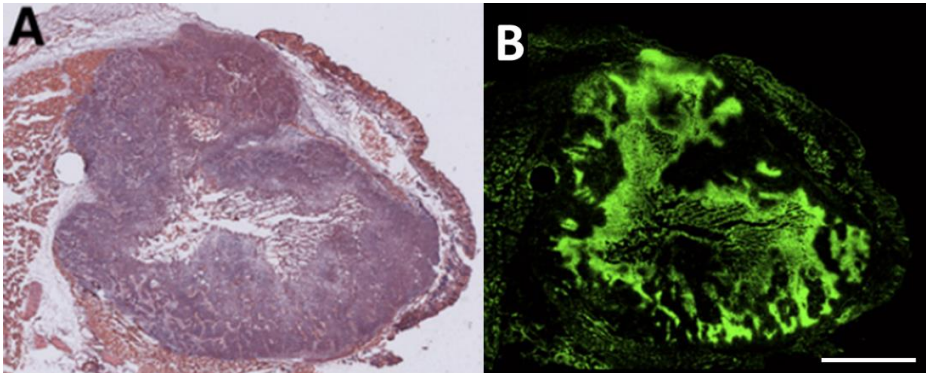


**FIGURE 11: Immunohistochemistry to detect hypoxia.**

SQ20b subcutaneous tumor in hind leg of nude mice. (A) H&E staining of tumor section. (B) Immunofluorescent pimonidazole staining of consecutive section (green). Pimonidazole was administered intravenously 90 min before sacrifice. The tumor was perforated with a 28-gauge angiocatheter after resection to facilitate tumor section orientation after staining (circular defect in the left upper corner). Scale bar= 2 mm. Adapted from [52].

### C. AUTORADIOGRAPHY

Autoradiography is the technique of recording an image of a preparation that contains radioactivity using a radiation-sensitive medium. The radioactive samples are placed directly against a film for a period to allow radioactive emissions from the sample to interact with the film emulsion and this creates an image (Fig. 12). When using a hypoxia tracer, the image represents hypoxic areas. This technique is mostly used for biodistribution studies or validity studies in tracer development, but is less suited for predictive and prognostic use because it requires tumor resections/biopsies and is sample size dependent.

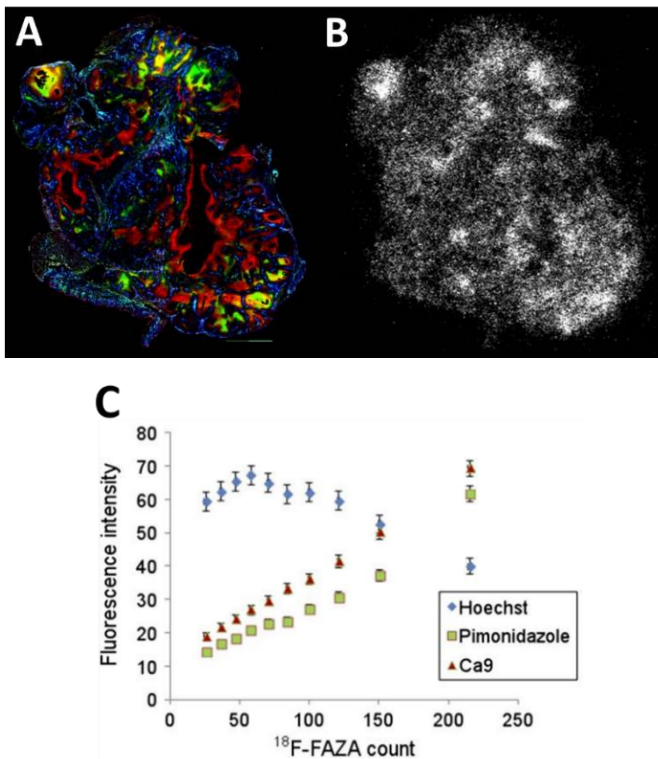


**FIGURE 12: Distribution of  $^{18}\text{F}$ -FAZA with autoradiography versus immunofluorescent staining.**

SQ20b murine xenografts. Registered 3-color immunofluorescent image (A) and corresponding autoradiography (B) from tumor section. Blue= Hoechst (perfusion marker); green= pimonidazole (hypoxia marker); red= CA9 (hypoxia marker); yellow= overlay of pimonidazole and CA9. (C) Rebinmed scatterplots showing relationship between fluorescence markers on y-axis, and indicated hypoxia radiotracer on x-axis. Areas of hypoxia on immunofluorescent staining correspond with areas of high  $^{18}\text{F}$ -FAZA activity on autoradiography. Adapted from [52].

## D. GENETIC MARKERS

Intense efforts have been made to identify a gene signature correlating with tumor hypoxia and having predictive and prognostic capacities. To date, 32 hypoxia gene expression signatures have been published and are summarized in a recent review [53]. An ongoing RCT investigates whether nimorazole with cisplatin-based CRT in patients with locally advanced head and neck cancer is superior to CRT alone, using a 15-gene hypoxia signature (ClinicalTrials.gov:NCT01880359). At our center, blood samples of esophageal cancer patients (pre, during and post treatment) are being collected in a biobank with the eye on identifying a predictive and prognostic gene signature.

## E. IMAGING METHODS

Besides genetic biomarkers, imaging modalities are another very interesting non-invasive method to detect hypoxia and are summarized in Table 4 [44, 54, 55].

Optical based methods are being used like phosphorescence or near-infrared spectroscopy (NIRS) [44]. These calculate the hemoglobin oxygen saturation ( $StO_2$ ) by measuring phosphorescence (oxygen dependently quenched) or optical absorption (different for oxy- and deoxyhemoglobin) (Fig. 13). Hyperspectral imaging (HSI), a third optical based imaging method, determines the electromagnetic spectrum of each pixel of an image [56]. As such, it can provide a very detailed image map of the hemoglobin saturation at the microvascular level. The major limitation of these optical based techniques is that they measure intravascular  $pO_2$  instead of tissue  $pO_2$  as a parameter for hypoxia.

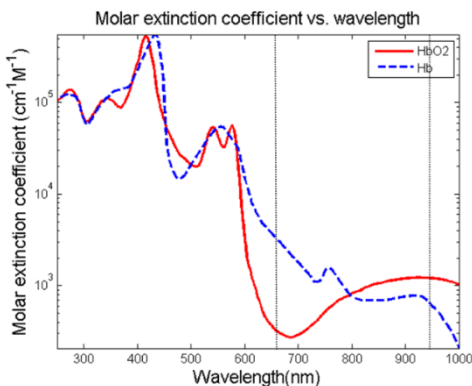


**FIGURE 13: Absorption spectra of oxy- and deoxyhemoglobin.**

The absorption spectra of oxygenated and deoxygenated hemoglobin differ. For example, at a wavelength of 660 nm (red light), deoxygenated hemoglobin absorbs more light than oxygenated hemoglobin. The opposite occurs at a wavelength of 940 nm (infrared light), where oxygenated hemoglobin absorbs more light than deoxygenated hemoglobin. By measuring the absorption at different wavelengths, the fraction of heme that is bound to oxygen can be determined. Adapted from [57].

Modality	Technique	Limitations
Optical-based	Phosphorescence	The measurement represents the vascular $pO_2$ , not tissue $pO_2$ .
	Near-infrared spectroscopy (NIRS)	The measurement provides information on vascular oxygenation, but not on tissue $pO_2$ .
MRI-based	Blood oxygen level-dependent magnetic resonance imaging (BOLD MRI)	The measurement provides information on changes in blood oxygenation, but not on the absolute oxygen concentration in tissue.
	$^{19}F$ -MRI or NMR (nuclear magnetic resonance)	The relaxation rate of $^{19}F$ may depend on other physiological factors present in the tissue and not only on $O_2$ concentration.
	Electron paramagnetic resonance imaging (EPRI)	The molecules may predominantly distribute in the vasculature, thus biasing in part measurements of tissue oxygenation.
	Proton-electron double resonance imaging (PEDRI)	The molecules may predominantly distribute in the vasculature, thus biasing in part measurements of tissue oxygenation.
	DCE-MRI (dynamic Gd-DTPA-enhanced MRI)	Low specificity, because the measurement provides information on both vascular and tissue oxygenation.
Nuclear-based	Single-photon emission computed tomography (SPECT)	Limited resolution dependent on voxel-based distribution of hypoxia.
	Positron emission tomography (PET)	Limited resolution compared to MRI and optical methods, but superior to SPECT.

**TABLE 4: Examples of non-invasive methods for hypoxia determination in living tissues.**

Adapted from [54].

Further, magnetic resonance imaging (MRI) based modalities are being used like blood oxygen level-dependent (BOLD-) MRI, electron paramagnetic resonance imaging (EPRI) or dynamic contrast enhanced (DCE-) MRI [58]. These have low specificity for tissue hypoxia because they actually measure perfusion and vascular oxygenation.

Finally and most importantly, nuclear imaging is being used which offers several advantages compared to the previously mentioned methods. It measures tissue hypoxia and not vascular oxygenation, the hypoxia distribution is imaged in a 3-dimensional way (3D), the imaging can be repeated allowing the evaluation of changes in hypoxia status, and whole tumor quantification is possible [59, 60]. A hypoxia specific tracer coupled to a radionuclide is injected and imaged with positron emission tomography (PET) or single-photon emission computed tomography (SPECT), according to the injected radionuclide. A good hypoxia tracer should be highly specific for hypoxia (oxygen-specific retention mechanism), have a fast uptake and homogeneous distribution in tissues, and thus be lipophilic to diffuse through the cell membrane, but at the same time have a fast washout from non-hypoxic tissue with fast elimination, and thus be hydrophilic [61, 62]. No tracer meets all criteria, but the family of nitroimidazoles showed the most promising results (Table 5).

Hypoxia specific tracer entrapment of nitroimidazoles is based on sequential reduction reactions of the  $\text{NO}_2$ -group under hypoxic conditions and eventually binding to intracellular macromolecules [31].  $^{18}\text{F}$ -FMISO (fluoromisonidazole) was the first to be developed and provided the broadest evidence as a hypoxia tracer (Table 5). Due to its lipophilic character, clearance from non-hypoxic tissues is slow and tumor-to-background contrast is not optimal [61]. Development of several second generation tracers followed, with slightly adapted pharmacokinetic properties to improve tumor-to-background contrast (Table 5).  $^{18}\text{F}$ -FAZA (fluoroazomycin arabinoside), for example, was developed as an adaptation of FMISO in which the alkyl side chain of FMISO was replaced by a polar arabinose sugar (Fig. 14) [63]. This increased the hydrophilicity of the molecule, leading to an increased clearance from blood and non-hypoxic tissues and an increased tumor-to-background contrast [62, 64].

Uptake mechanism	Tracer	Tumors imaged	Benefits	Limitations
Nitroimidazole-like uptake: reduction into RNO2 radicals and RNHOH compounds in hypoxic conditions. Then covalent binding to macromolecules [21, 59]	<sup>18</sup> F-MISO ( <sup>18</sup> F-fluoromisonidazole)	Head and neck tumors [35, 42-45] Locally advanced HNSCC [35, 46] Glioblastoma multiforme (GBM) [37, 47, 48] Breast cancer [49] NSCLC [32, 33, 50] Renal cell carcinoma [51]	Broadest evidence of value as a hypoxia tracer. Good correlation with immunohistochemistry and prognosis in most cases. Good availability	Lack of correlation in all tumors Low tumor-to-background ratio Variable reproducibility
	<sup>18</sup> F-FAZA ( <sup>18</sup> F-fluoroazomycin-arabinozide)	Head and neck tumors [52, 53] Cervical cancer [54] Prostate cancer [55] NSCLC [56, 57] Rectal cancer [58]	Good correlation with immunohistochemistry and prognosis in most cases. Faster diffusion and clearance with slightly higher tumor-to-background ratio than <sup>18</sup> F-MISO.	More limited evidence compared to <sup>18</sup> F-MISO.
	<sup>18</sup> F-FETNIM ( <sup>18</sup> F-fluoroerythronitroimidazole)	NSCLC [60] Esophageal cancer [61]	Promising tracer with possible correlation with outcome. Slightly higher tumor-to-background ratio than <sup>18</sup> F-MISO.	Limited evidence compared to <sup>18</sup> F-MISO.
	<sup>18</sup> F-EF5 ( <sup>18</sup> F-2-nitroimidazol-pentafluoropropyl acetamide)	Brain tumors [62] Soft tissue sarcoma [63] Head and neck tumors [64]	Promising tracer with possible correlation with outcome	Limited evidence.
	<sup>18</sup> F-EF3 ( <sup>18</sup> F-2-nitroimidazol-trifluoropropyl acetamide)	Rats bearing syngeneic rhabdomyosarcoma tumours [65] Head and neck tumors [66]	Promising tracer.	Very limited evidence, mostly preclinical.
	<sup>18</sup> F-FETA ( <sup>18</sup> F-fluoroetanidazole)	Mice bearing MCF-7, RIF-1, EMT6, HT1080/26.6, and HT1080/1-3C xenografts [67, 68] Hepatocellular carcinoma [69]	Promising tracer with better biodistribution than <sup>18</sup> F-MISO.	Preclinical evidence
	<sup>124</sup> I-IJZG ( <sup>124</sup> I-iodoazomycin galactopyranoside)	Tumor xenografted mice [70, 71]	Promising tracer	Preclinical evidence
	<sup>68</sup> Ga-labeled nitroimidazole analogs ( <sup>68</sup> Ga-NOTA-nitroimidazole, <sup>68</sup> Ga-DOTA-nitroimidazole, <sup>68</sup> Ga-SCN-NOTA-nitroimidazole)	Tumor xenografted rats/mice (a,b,c) Lung cancer (d,e,f) Head and neck cancer (g,h,i) Esophageal cancer (j) Pancreatic cancer (l)	More hydrophilic than <sup>18</sup> F-FMISO Good correlation with immunohistochemistry	More limited evidence compared to <sup>18</sup> F-FMISO and <sup>18</sup> F-FAZA.

**TABLE 5: Nitroimidazole hypoxia tracers for PET imaging.** Adapted from [54] and extended with information on  $^{18}\text{F}$ -HX4. References: (a, b, c) [52, 65, 66], (d, e, f) [67-69], (g, h, i) [68, 70, 71], (j) [72].

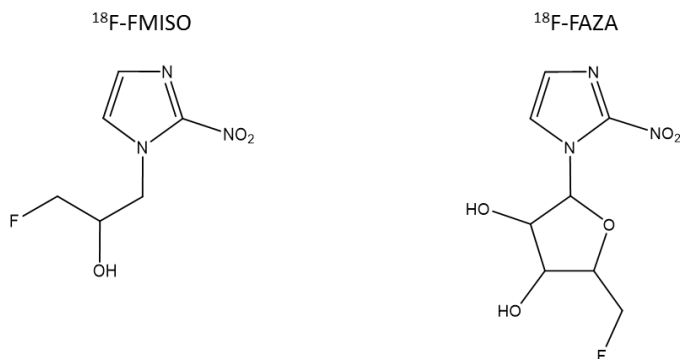


**FIGURE 14: Molecular structure of  $^{18}\text{F}$ -FMISO and  $^{18}\text{F}$ -FAZA.**

$^{18}\text{F}$ -HX4 (flortanidazole) [73],  $^{18}\text{F}$ -FETNIM (fluoroerythronitroimidazole) [74] and  $^{18}\text{F}$ -EF5 (2-nitroimidazol-pentafluoropropyl acetamide [75] are other examples of second generation nitroimidazole tracers that were developed to overcome the limitations of FMISO. Main studies, benefits and limitations are summarized in Table 5.

In the end, nitroimidazole-based PET tracers have proven reliability in measuring tumor hypoxia, with each tracer having its advantages and disadvantages, but overall only modest differences. This thesis focused on  $^{18}\text{F}$ -FAZA for several reasons.  $^{18}\text{F}$ -FAZA is a feasible tracer to detect tumor hypoxia and has indeed superior biokinetics compared to  $^{18}\text{F}$ -FMISO [76, 77].  $^{18}\text{F}$ -FAZA PET was studied in different tumors and showed to be predictive for treatment response in rhabdomyosarcoma and breast carcinoma (preclinical) [78, 79], and NSCLC and HNSCC (clinical) [80, 81]. Further, clinical trials are ongoing for rectal, lung, cervix and prostate carcinoma (ClinicalTrials.gov: NCT02624115, NCT02701699, NCT01989364, NCT01567800).



# **CHAPTER 2**

## **OBJECTIVES AND THESIS OUTLINE**



## CHAPTER 2: OBJECTIVES AND THESIS OUTLINE

Despite ongoing progression in oncology, there is a lack of patient-specific approaches based on biomarkers. The objective of this thesis was to use tumor hypoxia, an omnipresent feature of the TME, as a biomarker and target for treatment in solid tumors.

Two main research questions were investigated:

1. Can hypoxia imaging with  $^{18}\text{F}$ -FAZA PET/CT serve as a predictive biomarker and as a guidance for hypoxia targeting?
2. Can anti-angiogenic therapy reduce hypoxia by vascular normalization and enhance radiotherapy efficacy?

The first question was studied in an esophageal adenocarcinoma tumor model. Most patients with esophageal adenocarcinoma are diagnosed in a locally advanced stage and are standardly treated with neoadjuvant chemoradiotherapy followed by surgery. This treatment is associated with a considerable morbidity and treatment response is highly variable and unpredictable, making it an interesting pathology for a patient-tailored approach based on biomarkers [82]. Further, evidence exists (mostly histologically) that tumor hypoxia plays a role in treatment resistance in esophageal cancer [83, 84].

Because no appropriate tumor model was available for our research objective, our first aim was to develop an EAC model in mice, which is described in **chapter 3**.

Subsequently, we aimed to evaluate the feasibility of  $^{18}\text{F}$ -FAZA PET/CT in the orthotopic and subcutaneous EAC model which is outlined in **chapter 4**.

Finally, we aimed to use  $^{18}\text{F}$ -FAZA PET/CT as hypoxia detection method to predict radiation response in our tumor model. In **chapter 5** we describe the predictive value of  $^{18}\text{F}$ -FAZA PET/CT in EAC xenografts for radiation response. We further evaluated if  $^{18}\text{F}$ -FAZA PET/CT could identify tumors that might benefit from hypoxia targeted therapy to improve radiation response. To target hypoxia, we used nimorazole, a 5-nitroimidazole that mimics oxygen in the radiobiological process and has already showed to successfully increase radiation response in hypoxic HNSCC and rhabdomyosarcomas [35, 78].

The second research question, regarding the effect of anti-angiogenic therapy on hypoxia and radiotherapy, was discussed in **chapter 6** in a colorectal cancer tumor model. This model was chosen because CRC tumors are highly angiogenic and were one of the first tumor types that showed significant response to anti-angiogenic therapy. We were interested in the effects of anti-angiogenic agents on hypoxia and radiotherapy efficacy. This could be of special interest for patients with locally advanced rectal cancer (LARC), who receive chemoradiation before surgical resection. Anti-angiogenic agents might enhance pathological response and outcomes. We aimed to link tumor hypoxia with tumor angiogenesis and aimed to target it by administration of a pan-VEGFR inhibitor cediranib. We evaluated tumor hypoxia with a fluorescence based fiberoptic oxygen probe (Oxylite) and with immunohistochemistry (endogenous marker pimonidazole). The underlying structural and functional vascular changes were investigated by *in vivo* imaging in dorsal skinfold window chambers and by DCE-MRI of subcutaneous tumors.

**CHAPTER 3**  
**ESOPHAGEAL ADENOCARCINOMA**  
**TUMOR MODEL IN MICE**



## CHAPTER 3: ESOPHAGEAL ADENOCARCINOMA

### TUMOR MODEL IN MICE

To answer our first research question ‘Can hypoxia imaging with  $^{18}\text{F}$ -FAZA PET/CT serve as a predictive biomarker and as a guidance for hypoxia targeting?’, we first developed an esophageal adenocarcinoma model in mice, which is described in this chapter.

➔ This chapter is based on the following article:

*Melsens E, De Vlieghere E, Descamps B, Vanhove C, De Wever O, Ceelen W, Pattyn P. Improved xenograft efficiency of esophageal adenocarcinoma cell lines through in vivo selection. Oncol Rep, 38: 71-81, 2017.*

### ABSTRACT

**Background:** Esophageal adenocarcinoma is an aggressive disease with rising incidence rates. The need for development of new therapies is high and preclinical research plays herein a crucial role. However, there is a lack of preclinical (orthotopic) EAC models. We aimed to develop an EAC model in mice.

**Methods:** Two esophageal adenocarcinoma cell lines, OE33 and OACM5 1.C, and a third *in vivo* selected subpopulation, OACM5 1.C SC1, were used. One group of mice was injected subcutaneously in the hind legs. Tumor growth was followed with calipers. Another group was injected orthotopically in the distal esophageal wall through median laparotomy. Tumor development was evaluated macroscopically and confirmed microscopically and tumor take rates were calculated. A subset of mice was evaluated with MRI to follow tumor progression. Additionally, functional cell line characteristics were evaluated *in vitro* (clonogenic assays, collagen invasion assays, sphere formation assays and protein analysis of cell-cell adhesion and cytoskeletal proteins) to better understand xenograft behavior.

**Results:** OE33 cells were shown to be epithelial-like, whereas OACM5 1.C and OACM5 1.C SC1 were more mesenchymal-like. The three cell lines were non-invasive into native type I collagen gels. *In vivo*, OE33 cells led to 63.6% and 100% tumor nodules after orthotopic (n= 12) and subcutaneous (n= 8) injection, respectively. Adversely, OACM5 1.C cells did not lead to tumor formation after orthotopic injection (n= 6) and only 50% of subcutaneous injections led to tumor nodules (n= 8). However, the newly established cell line OACM5 1.C SC1 resulted in 33% tumor formation when injected orthotopically (n= 6) and in 100% tumors when injected subcutaneously (n= 8). The higher xenograft rate of OACM5 1.C SC1 ( $P < 0.05$ ) corresponded with a higher clonogenic potential compared to its parental ( $P < 0.0001$ ). All models showed local tumor growth without metastasis formation.

**Conclusion:** In conclusion, OACM5 1.C has a poor tumor take rate at an orthotopic and ectopic site. A subpopulation obtained through *in vivo* selection, OACM5 1.C SC1, gives a significant higher take rate ectopically. Further, OE33 establishes orthotopic (and subcutaneous) xenografts in mice. Our paper provides an orthotopic and subcutaneous xenograft EAC model in mice, which will hopefully contribute to further preclinical research on EAC.



## **INTRODUCTION**

Esophageal cancer is the eighth most frequent cancer worldwide [85]. Despite the latest evolutions in treatment, overall mortality of esophageal cancer patients remains high, with a 5-year survival of only 9.8% in Europe [86, 87]. Therefore, the need for development of new therapies is high and preclinical research plays herein a crucial role.

The majority of preclinical research in esophageal carcinoma has been performed in heterotopic models (subcutaneous xenograft tumors) [88]. However, orthotopic tumor models, where tumors are grown at their primary site, are preferred, because they resemble tumor development in patients more closely [89]. Furthermore, it has been proven that interaction between the tumor and its microenvironment plays a crucial role during carcinogenesis [2]. This tumor microenvironment is considerably different when esophageal tumors are grown subcutaneous (heterotopic), i.e. different blood supplies leading to different metastatic routes.

Some preclinical research in esophageal carcinoma has been performed on orthotopic models. Tumor cells were injected either directly in the esophageal wall, or subcutaneously in donor animals to transplant tumor fragments onto the surgically injured esophageal wall. The surgical procedures to induce orthotopic esophageal tumors are technically challenging due to the location and size of the esophagus in laboratory animals (mostly mice). Five surgical approaches to the esophagus have been described: (i) median laparotomy [90-95], (ii) median laparotomy combined with transgastric approach [96], (iii) subcostal laparotomy [97], (iv) transoral approach [98], and (v) cervical approach [99]. Tumor take varied between 0% and 100% (mean 80.06%) and seemed to depend more on the aggressiveness of the tumor cell line, than on the surgical technique. A total of 9 different esophageal squamous cell carcinoma (ESSC) cell lines (81-T, KYSE30, KYSE150, SLMT-1, TE1, TE8, TE4, TE10 and T.Tn) and 3 esophageal adenocarcinoma (EAC) cell lines (OE19 [92, 94, 100, 101], PT1590 [93, 102] and OE33 [92]) were described for orthotopic use. Because EAC has become the main subtype in patients in the United States and Northern and Western Europe [103], this study will focus on EAC. Overall, there is a lack of preclinical orthotopic EAC models. Of the 3 EAC cell lines previously described for orthotopic use, OE33 represents locally advanced EAC. This cell line was used by Habibollahi et al. for diagnostic properties [92], but only in 5 mice. They described orthotopic OE33 tumors of 2-3mm in diameter at 4 weeks after injection. OE19 and PT1590 on the other hand, are representative cell lines for aggressive metastatic EAC. Moreover, OE19 overexpresses

Her2, which is found in only a minority of EAC patients (17- 32% of gastro-esophageal junction tumors GEJ [104]).

The purpose of this study was to establish an orthotopic EAC model in the mouse based on two generally available human EAC cell lines, OE33 and OACM5 1.C. *In vivo* tumor take and growth were evaluated (orthotopic as well as subcutaneous) and *in vitro* cell line characterization was performed.

## **MATERIALS AND METHODS**

### **IN VITRO**

#### **CELL LINES**

The human EAC cell lines OE33 and OACM5 1.C were obtained from Dr. W. Dinjens, Department of Pathology, Erasmus MC, Rotterdam, the Netherlands, and are available at the European Collection of Authenticated Cell Cultures (ECACC), number 96070808 and 11012006 respectively. MDA-MB-231 GFP Luc, human mammary carcinoma cell line (ATCC: HTB-26), and HCT8/E11, human colon adenocarcinoma cell line (ATCC number: CCL-244), were controls for *in vitro* experiments. OE33, HCT-8/E11 and MDA-MB-231 GFP Luc were cultured at 37 °C in 10% CO<sub>2</sub> humidified atmosphere in DMEM medium (Life Technologies, Ghent, Belgium), supplemented with 10% fetal bovine serum, penicillin-streptomycin and fungizone. Doxycycline (50 µg/ 100 ml medium) was added to the medium of MDA-MB-231 GFP Luc to express GFP. OACM5 1.C and the *in vivo* selected cell line OACM5 1.C SC1 (see further) were cultured at 37 °C in 5% CO<sub>2</sub> humidified atmosphere in RPMI 1640 Medium (Life Technologies) supplemented with GlutaMAX™-I (Life Technologies), 10% fetal bovine serum, penicillin-streptomycin and fungizone. EAC cell lines and the *in vivo* selected cell line OACM5 1.C SC1 were authenticated by STR DNA profiling. Microscopic images were taken with a phase contrast microscope (Leica DMI3000B, Diegem, Belgium).

#### **SPHERE FORMATION ASSAY**

One million single cells were diluted in 6 ml culture medium in an Erlenmeyer flask (50 ml). They were incubated for 72 hours on a Gyrotory shaker at 37 °C and 70 rpm in 5 or 10% CO<sub>2</sub>. Aggregation was analyzed with a phase contrast microscope and was scored on at least 50 aggregates. They were scored as compacted (individual cells not visible) or loose

(individual cells still visible) (n= 2). HCT8/E11 and MDA-MB-231 GFP Luc were used as a control for a respectively compacted and loose sphere formation.

### ***COLLAGEN INVASION ASSAY***

The assay was performed according to De Wever et al. [105]. Briefly,  $1 \times 10^5$  cells were seeded as a single cell suspension on a 0.1% type I collagen gel (Santa Cruz). After 24 h incubation at 37 °C and 5 or 10% CO<sub>2</sub>, invasiveness was scored (n= 2x2) and expressed as a mean. HCT8/E11 and MDA-MB-231 GFP Luc were used as a control for a respectively low and high invasive cell line.

### ***COLONY FORMATION ASSAY***

1000 single cells were seeded in T75 falcons (15 ml culture medium) and cultured for 14 days at 37 °C. Colonies were stained with 0.5% crystal violet, scanned and counted using ImageJ software (NIH). Results were expressed as the mean percentage of colonies formed out of 1000 cells (colony formation index (CFI)) (n= 2x5). HCT8/E11 and MDA-MB-231 GFP Luc were used as a control for a respectively positive and negative colony formation cell line.

### ***WESTERN BLOT***

Cells were lysed and sonicated for 10 seconds on ice. Lysates were diluted to a protein concentration of 1 µg/ µl and boiled for 5 minutes at 95 °C. Equal amounts of proteins were separated on 8 and 10% gels and transferred to nitrocellulose membranes. Membranes were blocked (PBS, 5% non-fat milk, 0.5% Tween) and immunostained with primary antibodies: E-cadherin M106 (TaKaRa, The Netherlands), P-cadherin 610228 (BD Biosciences, Belgium), vimentin V6389,  $\alpha$ -catenin C2081,  $\beta$ -catenin C2206, and cytokeratin C2931, recognizing subtype (4, 5, 6, 8, 10, 13 and 18), (Sigma-Aldrich, St. Louis, MO, USA). Then, secondary antibodies were applied, either ECL<sup>TM</sup> Anti-Mouse IgG or ECL<sup>TM</sup> Anti-Rabbit IgG (GE Healthcare UK Limited, UK). Immunodetection was performed with Pierce ECL Western Blotting Substrate (Thermo Scientific, Rockford, IL, USA) and imaged with Proxima2850 (Isogen, Life Science, Belgium). HCT8/E11 was used as positive control for E-, P-cadherin and cytokeratin. MDA-MB-231 GFP Luc was used as a positive control for vimentin. Both cell lines were positive controls for  $\alpha$ - and  $\beta$ -catenin.

## IN VIVO

### ANIMALS

Animal experiments were approved by the Animal Ethical Committee of Ghent University, Belgium (ECD 14/82). Athymic mice (Foxn1nu male) were obtained from Envigo, the Netherlands, and were kept under environmentally controlled conditions (12 h normal light/dark cycle, 20- 23 °C and 50% relative humidity) with food and water ad libitum. At 8 weeks of age, tumor cells were implanted (subcutaneous or orthotopic) under general anesthesia (Isoflurane, Abbott, Belgium). At the end of the experiments, or when humane endpoints were reached, mice were euthanized by cervical dislocation.

### SUBCUTANEOUS TUMOR MODEL

Subcutaneous tumors were grown to evaluate overall growth behavior of the cell lines in mice and to provide tumors for *in vivo* selection of cancer cells. Under general anesthesia, tumor cells suspended in 100 µl of Matrigel/injection site were injected SC in both hind legs. Tumor nodules were measured biweekly with calipers and volumes were calculated according to the following formula:  $V = (length \times width)^{3/2} \times \pi/6$ .

### ORTHOTOPIC TUMOR MODEL

Mice were positioned supine on a heating pad. Under general anesthesia and analgesia (Ketoprofen, 5 mg/ kg, SC) a vertical skin incision of 10 mm was performed medially in the upper abdomen. Abdominal muscles were split and the peritoneum was opened through sharp dissection (Fig. 1.A). The liver was gently elevated with a moist Q-tip to give access to the abdominal esophagus. The stomach was lifted extra-corporeally by traction on the greater curvature with a forceps. A micro-forceps was positioned underneath the distal esophagus to lift it (Fig. 1.B). While the esophagus was stretched by gentle tension on the stomach by an assistant, a 30-gauge needle was inserted in the distal part of the esophageal wall and tunneled proximally for about 3 mm (Fig. 1.C). Tumor cells, suspended in 20 µl Matrigel/animal were injected slowly, resulting in a local bulging (Fig. 1.D). At body temperature, Matrigel solidifies within seconds, minimalizing the risk of intra-abdominal spilling of tumor cells. The stomach was cautiously repositioned and the abdominal wall and skin were closed with a running PDS 6-0 suture. Hartmann solution (500 µl) was given SC to prevent dehydration. Animals were followed daily and weighed 2 times per week.

Subcutaneous (TT<sub>sc</sub>) and orthotopic tumor take (TT<sub>orth</sub>) were defined as the percentage of macroscopic tumor nodules (confirmed on histology) on the total number of injections. At 7 weeks, mice were euthanized and tumors were excised for histopathology.

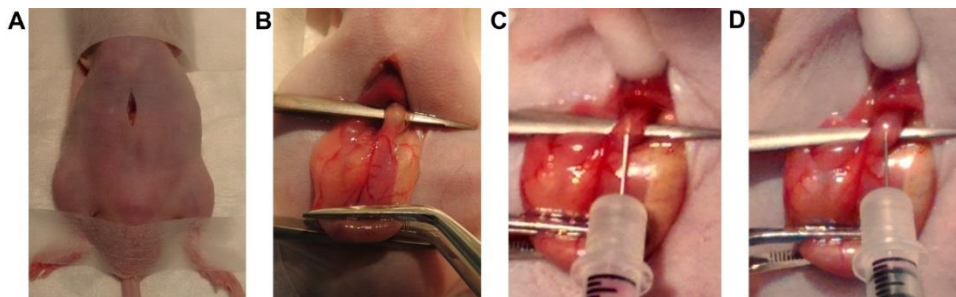


**FIGURE 1: Surgical technique of orthotopic injection of tumor cells.** (A) Upper abdominal median laparotomy in a mouse under general inhalation anesthesia, positioned using tape; (B) The stomach is lifted extra-corporal with a forceps. Another forceps (micro-instrument) is positioned underneath the esophagus to improve the access; (C) Insertion of a 30 G needle in the distal esophageal wall; (D) Injection of tumor cells in Matrigel resulting in a bleb in situ.

## ***MAGNETIC RESONANCE IMAGING***

A subpopulation of mice with orthotopic tumors (OE33 tumor nodules, n= 5) were evaluated by magnetic resonance imaging (MRI) at 1, 2, 3, 5, 8 and 12 weeks after tumor injection to follow tumor progression. MR images were acquired on a 7T system (Bruker PharmaScan 70/16, Ettlingen, Germany) with a mouse body volume coil. Mice were anaesthetized with isoflurane (5% induction, 1.5% maintenance, 0.3 L/ min) and warmed with a water-based heating blanket. Respiration was monitored using a respiration pad underneath the mouse. Anatomical information was obtained with a T2-weighted sequence (TurboRARE) with the following parameters: TR 3661 ms, TE 37.1 ms, 109  $\mu$ m in-plane resolution, 30 contiguous transverse slices of 600  $\mu$ m, and acquisition time 9'1". Mice were euthanized 15 weeks after tumor induction.

## ***IN VIVO SELECTION OF CANCER CELLS***

To obtain subcultures of cell lines that grow well in mice, tumors (SC and orthotopic) were excised under sterile conditions and divided into small pieces. Tumor fragments were dissociated (gentleMAX Dissociator, Miltenyl Biotec GmbH, Germany) together with a

collagenase 1 mg/ ml (Sigma- Aldrich) in PBS<sup>D+</sup> mixture to disrupt tissue structures. The suspension was filtered through a cell strainer (70  $\mu$ m) and centrifuged. Cells were seeded in T75 falcons and incubated. After 24 hours, non-adherent cells were cleared and replaced by fresh culture medium.

## **TUMOR SAMPLES AND HISTOLOGY**

Tumors were excised fixed with 4% formaldehyde, processed and embedded in paraffin. Tumor sections of 5  $\mu$ m were cut with a microtome (Microm HM355S, Thermo Scientific, Rockford, IL, USA). H&E staining and Ki67 staining (ready-to-use DAKO Envision+ system- HRP kit (K4011)) were performed according to standard protocols. Slides were scanned on 100x and 200x magnification and proliferation indices were determined by an overall visual scoring system. Tumors were categorized low, moderate or high proliferative. Microscopic images were taken with a light microscope (ColorView I, BX43F, Olympus, Tokyo, Japan).

## **STATISTICAL METHODS**

Statistical analysis was performed with GraphPad Prism6 (Graphpad Software, Inc.: La Jolla, CA, USA). Mann- Whitney test was used to compare *in vitro* results of the parental and *in vivo* selected cell line. Fisher's exact test was used to compare tumor take rates. Results were summarized as means with standard deviation (SD) and were considered statistically significant when the probability of a type I error was  $\leq 0.05$ .

## **RESULTS**

### **CELL CHARACTERIZATION OF OE33**

OE33 cells had an epithelial morphology, characterized by adherent cells, cell-cell contacts and a typical formation of islands (Fig. 2.A above). These cell-cell contacts resulted in the ability to form compact spheres under Gyrotory shaking (Fig. 2.A middle). On type I collagen gels, 21.6% (95% CI [8.12%, 35.04%]) of OE33 cells showed cellular extensions invading the matrix (Fig. 2.A under, B left). When seeded in a low density on tissue culture substrate, only a limited number of these cells were able to form a colony (mean CFI= 7.23%, 95% CI [6.24%, 8.23%]) (Fig. 2.B right). Additionally, Western blot was performed (Fig. 2.C). OE33 cells expressed cytokeratin, an intermediate filament supporting the

epithelial origin of the cancer cell line. Furthermore, cells showed expression of  $\alpha$ - and  $\beta$ -catenin and E- and P-cadherin, proteins important for cell- cell adhesion and tissue organization. They did not express vimentin, a major cytoskeletal component in mesenchymal cells.

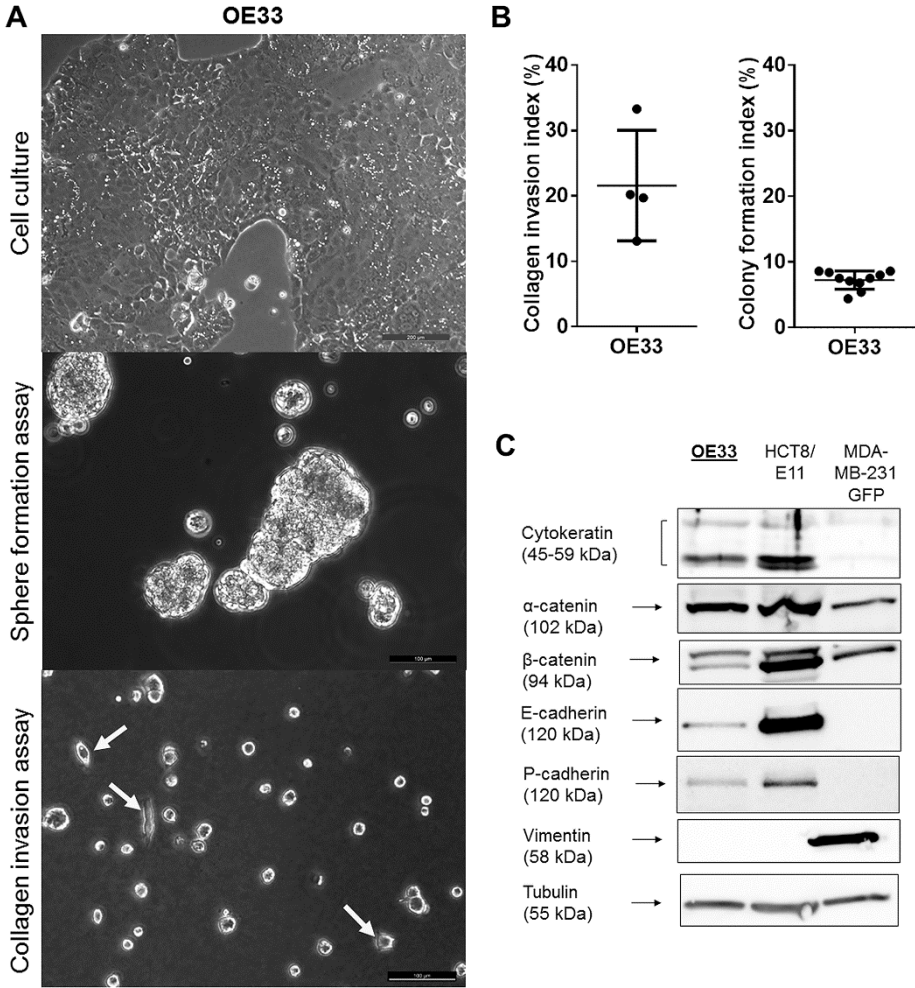


**FIGURE 2: *In vitro* characteristics of OE33.** (A) Above: Cell lines in culture, phase contrast image (scale bar= 200  $\mu$ m); Middle: Sphere formation assay 72 h after initiation, phase contrast image (scale bar= 100  $\mu$ m); Under: Collagen type I invasion assay 24 h after seeding, phase contrast image (scale bar= 100  $\mu$ m), yellow arrows show invasive cells in collagen type I gel. (B) Left: Collagen invasion

index (%); Right: colony formation index (%). Single values, mean, standard deviation. (C) Western blot of OE33 compared to HCT8/E11 and MDA-MB-231 GFP Luc.

## TUMOR DEVELOPMENT WITH OE33

Four mice were injected subcutaneously bilaterally with OE33 cells (Table 1). These all resulted in similar small tumor nodules, but volumes seemed to decrease progressively (Fig. 3.A). Histologically, nodules consisted of well differentiated tumor cells organized in islands and surrounded by infiltrating stromal cells connective tissue (Fig. 3.B-C). They were not invasive into surrounding tissues and Ki67 indices were low to moderate (Fig. 3.D). Two nodules were used for *in vivo* selection and were confirmed to contain tumor cells through that means.

Twelve mice were orthotopically injected with OE33 cells (Table I). Seven animals developed tumor nodules at the distal site of the esophagus without evidence for metastasis (liver, diaphragm, peritoneum and omentum were free of lesions) (Fig. 4. A). Tumors were located at the submucosal space and were not invasive into surrounding tissue (Fig. 4.B, D). They were well differentiated and had a low proliferation index (Fig. 4.C). Three nodules were used for *in vivo* selection and were confirmed to contain tumor cells through that means.

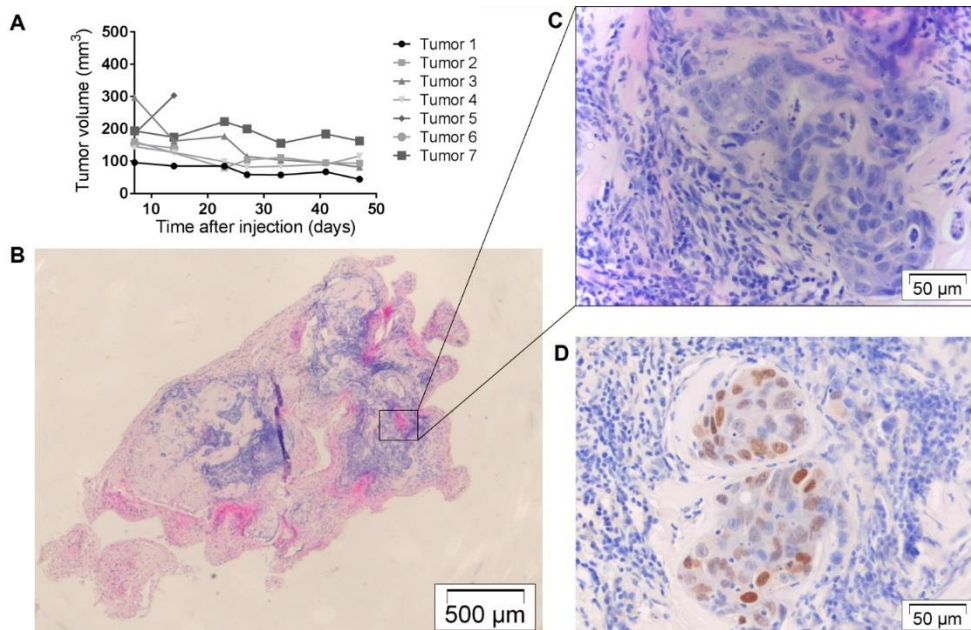




**FIGURE 3: SC xenograft OE33 tumor.** (A) Tumor volumes ( $\text{mm}^3$ ) of 7 SC tumors, time after injection of tumor cells; (B-C) H&E of SC tumor at different magnifications; (D) Ki67 staining of adjacent tumor slide.

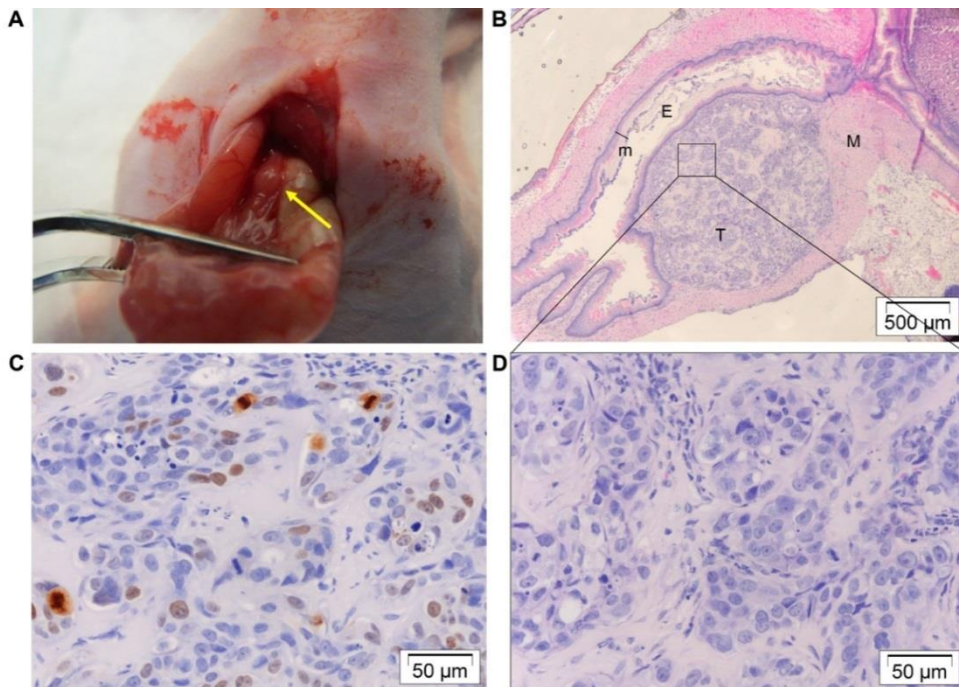


**FIGURE 4: Orthotopic xenograft OE33 tumor.** (A) Macroscopic tumor nodule at the distal site of the esophagus (yellow arrow). The stomach is pulled downwards with a forceps; (B, D) H&E of tumor nodule. E= esophageal lumen. T= tumor nodule. M= muscle layers of the esophageal wall. m= esophageal mucosa. The nodule is situated in the submucosal space and does not invade the mucosa. In the right upper corner, the transition to the stomach is situated; (C) Ki67 staining of adjacent tumor slide.

	OE33		OACM5 1.C		OACM5 1.C SC1			
	SC	Orthotopic	SC	Orthotopic	SC	Orthotopic		
Injected tumor cells ( $\times 10^6$ )	1	5	0.5	1	1.5	1	1.5	1
Number of tumor cell implantations	n=2	n=5	n=5	n=7	n=8	n=6	n=10	n=6
Macroscopic tumor nodule	2/2	5/5	3/4 <sup>a</sup>	4/7	4/8	0/4 <sup>b</sup>	10/10	2/6
Microscopic tumor cells	2/2	5/5	3/4	4/7	7/8	0/4	10/10	3/6
Tumor take (TT) (%)	100		63.6		50	0	100	33.3

<sup>a</sup>One mouse directly died post-operative; <sup>b</sup>2 mice were euthanized 5 days postoperative due to disease.

**TABLE 1: Summary of *in vivo* experiments.**

MRI scans were performed in a subset of mice (n= 5) to follow tumor development (Fig. 5. A). At the initial MRI scan 1 week post-tumor induction, all of them showed a clear tumor-like nodule at the distal site of the esophagus. During follow-up, volumes remained the same and at the end 4 out of 5 animals showed a tumor-like nodule on MRI. These were confirmed to contain tumor cells microscopically (Fig. 5. B-D).

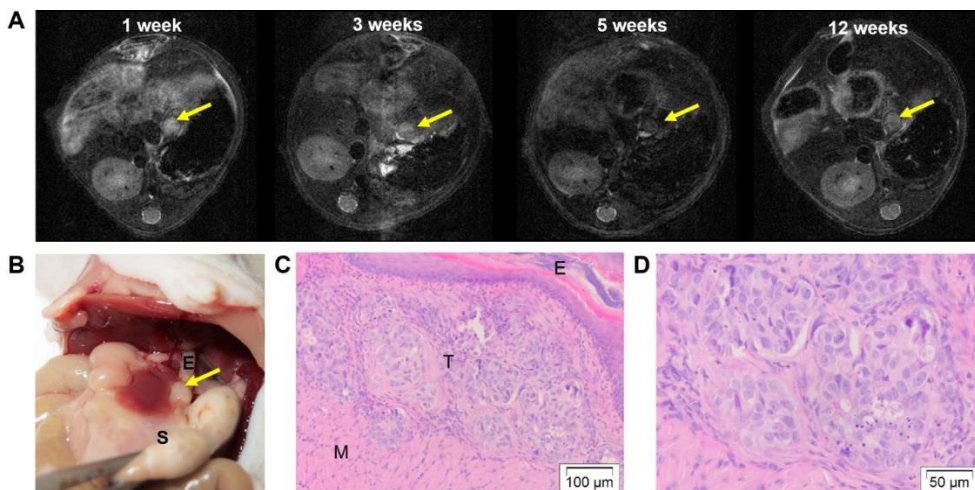


**FIGURE 5: MRI images of orthotopic OE33 esophageal tumor.** (A) Transverse MRI images at different time points (in weeks) after tumor induction. Yellow arrow= tumor nodule; (B) Macroscopic tumor (yellow arrow) at distal esophagus, E= esophagus, S= stomach; (C-D) H&E staining of tumor. T= tumor nodule. E= esophagus. M= muscle layer of esophageal wall.

## CELL CHARACTERIZATION OF OACM5 1.C

OACM5 1.C cells had two morphological subtypes: a majority of multicellular floating cell clusters, and some adherent cells with a fibroblast-like appearance, growing as single cells (Fig. 6.A above). These did not form cell-cell contacts and only very few cells were adherent to plastic. OACM5 1.C cells were not able to form compact spheres under Gyrotory shaking, but formed loose cell clusters with recognition of individual cells (Fig. 6.A middle). Furthermore, they were non-invasive into collagen gels (mean 1.38%, 95% CI [-0.30%, 2.47%]) (Fig. 6.A under, B above) and were not clonogenic (CFI= 0.10%, 95% CI [-0.001%, 0.201%]) (Fig. 6.B under). OACM5 1.C cells expressed cytokeratin on Western blot supporting the epithelial origin of the cancer cell line. They expressed  $\beta$ -catenin and poorly expressed  $\alpha$ -catenin but lacked expression of E-cadherin to consolidate cell-cell

contacts. OACM5 1.C expressed vimentin representing the mesenchymal characteristics of the cell line. (Fig. 6.C)

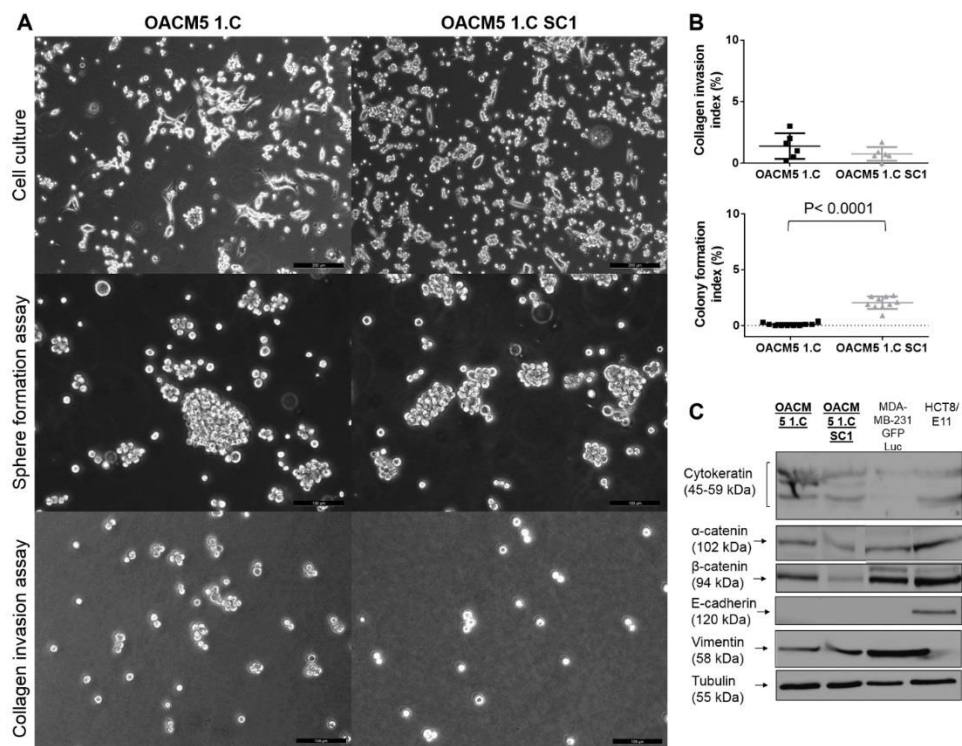


**FIGURE 6: *In vitro* characteristics of OACM5 1.C and OACM5 1.C SC1.** (A) Above: Cell lines in culture, phase contrast image (scale bar= 200 μm); Middle: Sphere formation assay 72 h after initiation, phase contrast image (scale bar= 100 μm); Under: Collagen type I invasion assay 24 h after seeding, phase contrast image (scale bar= 100 μm); (B) Above: collagen invasion index (%), single values, mean, standard deviation,  $P= 0.368$ ; Under: Colony formation index (%), single values, mean, standard deviation,  $P< 0.0001$ . (C) Western blot of OACM5 1.C and OACM5 1.C SC1 compared to MDA-MB-231 GFP Luc and HCT8/E11.

## TUMOR DEVELOPMENT WITH OACM5 1.C

Four mice were injected subcutaneously bilaterally with OACM5 1.C cells (Table 1). Four out of eight injections resulted in macroscopic tumor nodules. One nodule had an exponential growth curve, while the others remained stable (Fig. 7. A). Histology showed nodules packed with tumor cells with little infiltrating stromal cells. They were not invasive into surrounding tissues and Ki67 staining was overall low to moderate (Fig. 7. B-D).

Injection sites that did not develop macroscopic nodules (4/8) resulted in palpable fibrous remnants in which some loose tumor cell islands could be identified on histology. One nodule was used for *in vivo* selection and was confirmed to contain tumor cells through that means. An additional six mice were orthotopically injected with OACM5 1.C cells (Table 1). Of 4 mice evaluable, no tumor nodules, metastasis or involved lymph nodes were macroscopically visible and histology was negative for tumor cells.

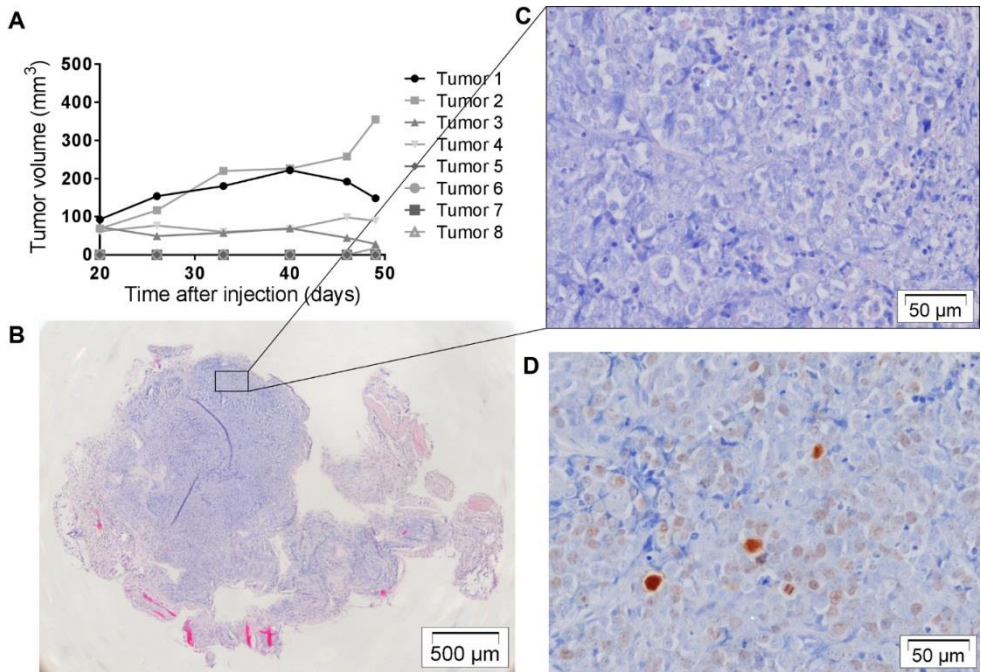


**FIGURE 7: SC xenograft OACM5 1.C tumor.** (A) Tumor volumes (mm<sup>3</sup>) of 8 SC tumors, time after injection of tumor cells. 4 out of 8 injections did not develop tumor nodules; (B-C) H&E of SC tumor at different magnifications; (D) Ki67 staining of adjacent tumor slide.

## ESTABLISHMENT OF NEW *IN VIVO* SELECTED CELL LINE OACM5 1.C SC1

OACM5 1.C cells harvested from a SC tumor nodule, were stable through different *in vitro* passages and could be re-injected in mice according to the above protocols. Five mice were injected subcutaneously bilaterally with OACM5 1.C SC1 cells, resulting in 10 macroscopically visible tumors (Table 1). 5 out of 10 were fast growing (Fig. 8. A). Histology showed presence of tumor cells in all nodules (Fig. 8. B-C) and Ki67 staining



was low to moderate (Fig. 8. D). An additional six mice were injected orthotopically with OACM5 1.C SC1 cells, leading to two small macroscopic tumor nodules (Table 1). No metastasis were observed. Histology confirmed presence of tumor cells and nodules did not invade surrounding tissues (Fig. 9. A-C). *In vivo* selection of OE33 cells was not successful (n= 5). Tumor cells were microscopically present, but did not survive different *in vitro* passages.

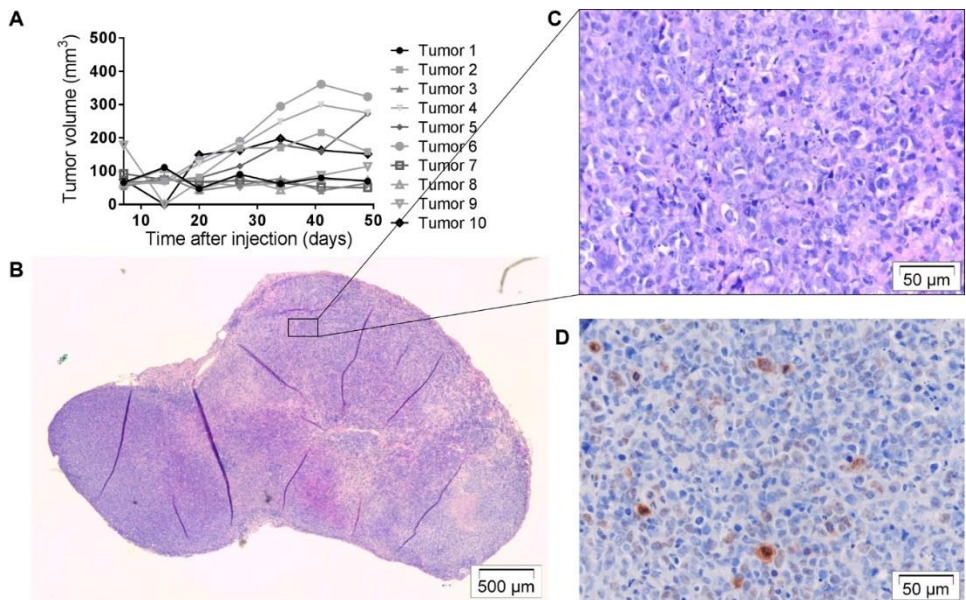


**FIGURE 8: SC xenograft OACM5 1.C SC1 tumor.** (A) Tumor volumes (mm<sup>3</sup>) of 10 SC tumors, time after injection of tumor cells; (B) H&E staining of SC tumor with close-up (C), packed with tumor cells; (D) Ki67 staining of adjacent tumor slide.

## COMPARISON OF OACM5 1.C AND OACM5 1.C SC1

Both cell lines had the same morphological appearance *in vitro* (Fig. 6.A above) and *in vivo* (Fig. 7 and Fig. 8). Further, they had the same cell line characteristics concerning sphere formation and collagen invasion (Fig. 6.A-B). Moreover, cell-cell adhesion and cytoskeletal protein expression were similar (Fig. 6.C). Yet, the *in vivo* selected cell line had higher subcutaneous tumor take rates than the parental cell line (TT<sub>SC</sub>= 100% versus 50% (P< 0.023) (Fig. 10). This can be related to the significant higher clonogenicity (P< 0.0001) of the *in vivo* selected cell line compared to the parental cell line *in vitro*.

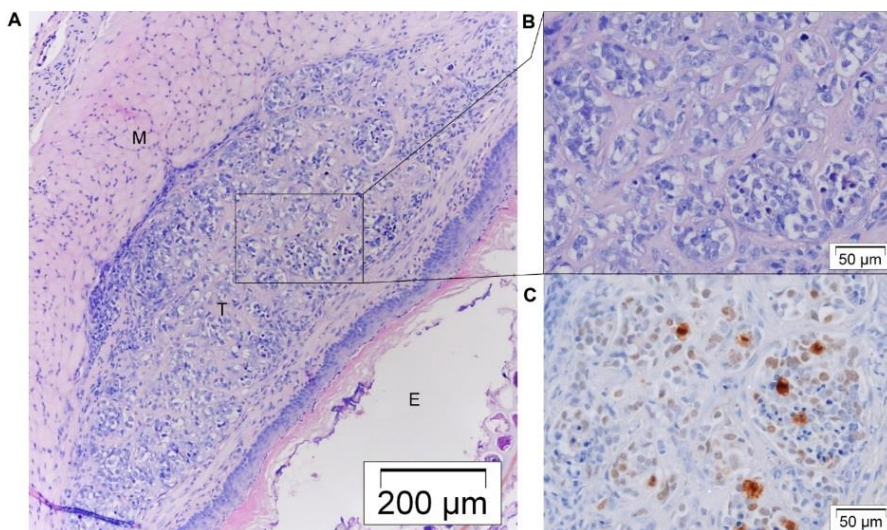


**FIGURE 9: Orthotopic xenograft OACM5 1.C SC1 tumor.** (A-B) H&E staining of orthotopic OACM5 1.C SC1 tumor nodule, situated at the submucosal space. E= esophageal lumen. T= tumor nodule. M= muscle layers of the esophageal wall; (C) Ki67 staining of adjacent tumor slide.

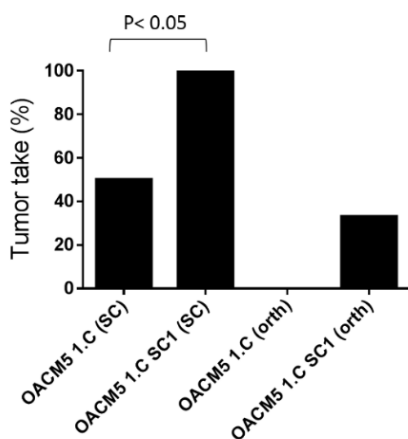


**FIGURE 10: Tumor take of OACM5 1.C and OACM5 1.C SC1.** SC and orthotopic tumor take were compared between the two cell lines. Development of tumors was expressed as a percentage of the total amount of implanted tumors: OACM5 1.C (SC) (n= 4/8) versus OACM5 1.C SC1 (SC) (n= 10/10); OACM5 1.C (orth) (n= 0/6) versus OACM5 1.C SC1 (orth) (n= 2/6). Subcutaneous tumor take was significantly increase with the *in vivo* selected cell line (OACM5 1.C SC1) compared to the parental cell line (OACM5 1.C) ( $P < 0.023$ ). The observed increase in orthotopic tumor take was not statistically significant ( $P = 0.4667$ ).

## **DISCUSSION**

This study investigated the orthotopic growth potential of two generally available EAC cell lines, OE33 and OACM5 1.C, and a third cell line obtained through *in vivo* selection,

OACM5 1.C SC1. Additionally, *in vitro* experiments were performed to better understand functional characteristics in relationship with *in vivo* growth behavior.

OE33 showed successful orthotopic xenografts in 63.6% (n= 12) of the cases. Nevertheless, volumes remained stable during follow-up, as can be seen on the serial MRI scans. Subcutaneous tumor take was higher (TT<sub>sc</sub>= 100%, n= 7) but resulted in similar small tumor nodules with stable to decreasing volumes. To our knowledge, only one previous study used OE33 cells for orthotopic use. The study was diagnostic and had similar results to ours. Small tumors of 2-3 mm in diameter at 4 weeks after injection (n= 5) were seen [92]. OE33 seems to be a low aggressive cell line with a high subcutaneous and orthotopic tumor take in nude mice, but extremely slow growth pattern. The decreasing subcutaneous volumes may be explained by clearance of Matrigel with slow replacement of tumor cells. In contrast to the OE33 cell line, OACM5 1.C cells were not able to develop orthotopic tumor nodules (TT<sub>orth</sub>= 0%, n= 6). Also subcutaneous tumor take was low (TT<sub>sc</sub>= 50%, n= 8). To improve these poor tumor take rates, a technique of *in vivo* selection of tumor cells was applied. As such, the new cell line OACM5 1.C SC1 was established and successfully led to a significant higher subcutaneous tumor take than the parental cell line (100% (n= 10) versus 50% (n= 8), P< 0.023). Orthotopic tumor take did not differ significantly (33.3% (n= 6) versus 0% (n= 6), P= 0.467). Cell lines had similar *in vitro* characteristics, except from the significant increased ability of the *in vivo* selected cell line to form colonies (P< 0.0001). The latter may partially explain the increased tumor take rate.

Another correlation between the *in vitro* and *in vivo* results was seen in the invasiveness of the cell lines. The investigated EAC cell lines were almost non-invasive in collagen type I gels *in vitro* and none of the xenografts in the mouse experiments invaded the surrounding tissues.

Beside *in vivo* selection, improved tumor take rates may be reached by simply increasing the amount of injected tumor cells. Unfortunately, the injection volume in the esophageal wall is limited. As such, the amount of injectable tumor cells is also limited to about  $1.5 \times 10^6$  cells per injection. This can be bypassed by transplanting a subcutaneous tumor fragment on the esophageal wall according to the technique of Gros et al. [93]. An additional experiment was performed with transplantation of 1 mm<sup>3</sup> tumor fragments of a subcutaneous OE33 tumor on the esophageal wall of 7 mice. Due to postoperative complications, three animals died within the first week postoperative. The remaining 4 did not show any vital tumor on the esophageal wall up to 70 days of follow up. We believe this is a technically

more difficult procedure, with a low success rate if fragments of slow growing tumor nodules are used and concluded this is not beneficial for the investigated cell lines.

It needs to be mentioned that the development of EAC in this tumor model differs from the situation in patients. While the pathogenesis is not yet fully understood, it is believed that chronic inflammation of the esophageal mucosa can develop dysplasia and eventually can evolve in EAC. As such, gastro-esophageal reflux disease (GERD) is one of the major risk factors for developing EAC, besides obesity [85]. In literature, several other models have been described, that reflect the clinical situation more closely [88]. On one hand, different reflux models have been used: surgical esophagojejunostomy [106] or drinking of caustic substances [107]. These reflux models lead to less than 50% cancer development in a time period of 6 months making it unreliable for therapeutic studies [88]. On the other hand, the use of genetically engineered mouse models (GEMMs) has been investigated. Transgenic mice with IL-1 $\beta$  overexpression were shown to develop moderate inflammation by 6 months, with a small percentage of mice developing high grade dysplasia or EAC after 20-22 months [107]. Best results with GEMMs were obtained in combination with the caustic substance deoxycholate (DCA), where 45% of mice developed EAC after a long follow-up period of 15 months [107]. The technique of injecting tumor cells in the esophageal wall is considered to be the best option available for the development of a relative rapid and reliable orthotopic mouse model.

Surprisingly, the three investigated EAC cell lines grew more efficient subcutaneously than orthotopically. To rule out technical issues with the orthotopic injection method, the technique was checked with a highly aggressive ovarian carcinoma cell line, SK-OV-3 Luc IP1 cells, that is known to be 100% tumorigenic in Foxn1nu mice, according to previous experiments in our research group [108]. Injection of  $5 \times 10^5$  SK-OV-3 Luc IP1 cells in the esophageal wall resulted in 100% tumor take and 100% exponential tumor growth (n= 5), confirmed on IVIS, MRI and histology (Fig. 11). After 4 weeks, exophytic tumors of about 8 mm diameter were observed. We believe the low orthotopic tumor take rates with the investigated EAC cells is due to a combination of low aggressive cells and the limited amount of injectable cells.



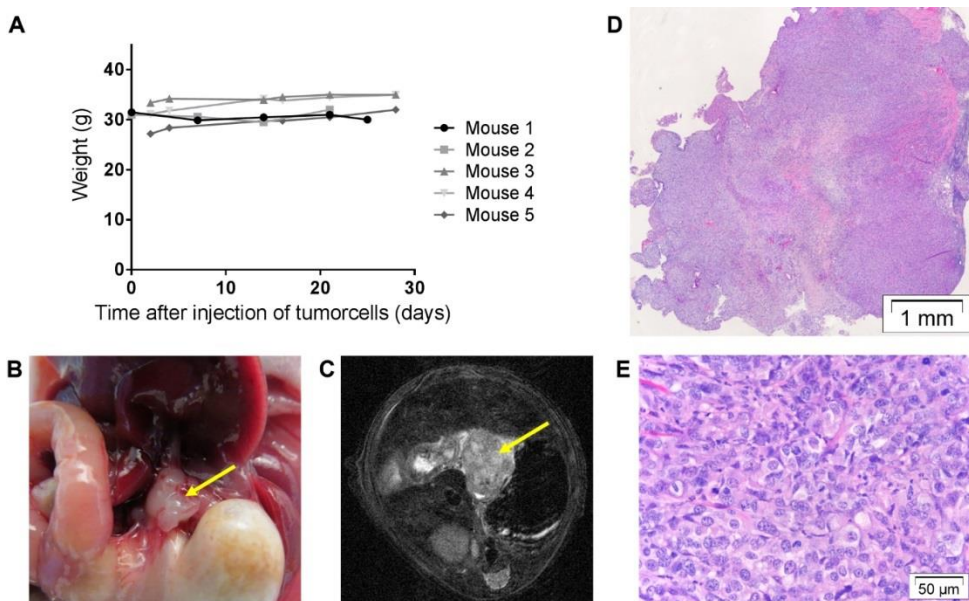


**FIGURE 11: SK-OV-3 Luc IP1 heterotopic esophageal tumor growth.** (A) Weight of mice with heterotopic SK-OV-3 Luc IP1 cells at the esophagus; (B) Macroscopic xenograft tumor (=yellow arrow) on the distal esophageal wall, with no sign of compression or dilatation of the proximal esophagus; (C) T2 weighed MRI, yellow arrow appoints the voluminous tumor; (D-E) H&E at different magnifications of a xenograft ovarian tumor at the esophageal wall.

The fact that the OACM5 1.C SC1 experiments are based on cells originating from one tumor nodule, could be point of discussion. Nevertheless, the *in vivo* selection technique is a validated technique to improve cell line characteristics (such as metastatic potential or take rates [108, 109]). Our aim was not to validate the technique, but to use it to improve tumor take rates and to show it can be of use for esophageal cancer models. The OACM5 1.C SC1 cell line was authenticated by STR assay, was stable through different passages and led to increased tumor take rates. The unsuccessful *in vivo* selection of OE33 was probably due to the small amount of tumor cells in the excised tumors and the low clonogenic potential of the cells. Repetitions would most probably lead to the same results. Finally, the follow-up of esophageal tumor growth in mice is challenging (i.e. due to its location). Performing a laparotomy at different time points is easy, fast and does not require specialized tools or knowledge. However, this causes intra-abdominal adhesions, making esophageal exposure more difficult after every laparotomy and could cause an inflammatory reaction influencing tumor development. MRI imaging was already confirmed to be feasible

and accurate for the follow-up of esophageal cancer in mice [93, 100, 101]. In this study, a dedicated small animal MRI scanner was used, leading to detailed images. Tumor nodules could be defined precisely as hyper-intense nodular structures, at a fixed location, slightly proximal of the gastro-esophageal junction. Also, the volumes of nodules could be measured accurately. However, MRI is not able to differentiate tumor tissue from inflammatory scar tissue or residual Matrigel. If volumes increase, viable tumor cells are plausible. If not, presence of tumor cells cannot be assured. It would be interesting to transfect the investigated EAC cell lines with luciferase, like shown by Gros et al. [93], to perform *in vivo* fluorescence imaging in case of stable nodules and be able to differentiate viable tumor cells from scar tissue and Matrigel.

This study can be of interest for future experiments. Especially the OE33 cell line is appropriate for orthotopic injection for diagnostic studies on EAC. Yet, some limitations, such as low aggressive cells, slow growth pattern and different etiology in patients should be kept in mind. It must be mentioned that this was the first study to describe growth behavior of OACM5 1.C in mice. OACM5 1.C had a poor tumor take rate at an orthotopic and ectopic site. The *in vivo* selected cell line OACM5 1.C SC1 showed higher subcutaneous take rates. The use of a more immunodeficient mouse strain (NOD SCID mice) could improve tumor take and should be considered for future research with these low aggressive cell lines.

## **CONCLUSION**

Little research is available about esophageal cancer, especially the EAC subtype, which is the more prevalent type in the Western world. Our paper provides an orthotopic and subcutaneous xenograft EAC model in mice, which will hopefully contribute to further preclinical research on EAC.

**CHAPTER 4**  
**PILOT STUDY:  $^{18}\text{F}$ -FAZA PET/CT IN**  
**SUBCUTANEOUS AND ORTHOTOPIC**  
**EAC XENOGRAFTS**



## CHAPTER 4: PILOT STUDY: <sup>18</sup>F-FAZA PET/CT IN SUBCUTANEOUS AND ORTHOTOPIC EAC XENOGRAFTS

In the previous chapter, we described the development of an orthotopic and subcutaneous EAC tumor model in mice that can be used to investigate our first research question ‘Can hypoxia imaging with <sup>18</sup>F-FAZA PET/CT serve as a predictive biomarker and as a guidance for hypoxia targeting?’. We tested the feasibility of <sup>18</sup>F-FAZA PET/CT in both tumor models in a pilot study, which is described in this chapter.

➔ The following researchers contributed to the pilot study:

*Melsens E, De Vlieghere E, Descamps B, Vanhove C, Kersemans K, De Vos F, Goethals I, Brans B, De Wever O, Ceelen W, Pattyn P.*

### **ABSTRACT**

**Aim:** In this chapter, we aimed to evaluate the feasibility of <sup>18</sup>F-FAZA PET/CT in the orthotopic and subcutaneous xenograft EAC models described in Chapter 3.

**Methods:** Subcutaneous tumors (OACM5 1.C SC1, human EAC) (n= 6) and esophageal tumors (SK-OV-3 IP1, human ovarian cancer) (n= 3) were used. The hypoxia tracer <sup>18</sup>F-FAZA (37 MBq) was injected in the tail vein of tumor bearing mice and PET/CT was performed 3 hours after tracer injection (30 min acquisition). Images were analyzed with AMIDE software and tumor to background ratios were calculated. Mice were euthanized on the same day of imaging, 1 hour after pimonidazole injection (IP). Tumors were excised and examined histologically.

**Results:** All subcutaneous tumors could be delineated on FAZA PET/CT and T/B rates could be calculated. The esophageal tumors could not be delineated due to insufficient soft tissue resolution on the CT scan and abundant background tracer activity in the liver region. Further, background activity was seen in the gall bladder, gastro-intestinal tract and urinary bladder.

**Conclusion:**  $^{18}\text{F}$ -FAZA PET/CT imaging is feasible in the subcutaneous OACM5 1.C SC1 model, but not in the orthotopic model.

## **MATERIALS AND METHODS**

### **SUBCUTANEOUS (SC) XENOGRAFTS**

To visualize hypoxia with  $^{18}\text{F}$ -FAZA PET/CT, a minimum tumor volume is needed. Most studies set the absolute minimum at a diameter of 5-10 mm or a volume of 200 mm<sup>3</sup> [62, 79, 110, 111]. We used SC OAMC5 1.C SC1 tumors, 7 weeks after tumor inoculation. According to the results of Chapter 3 these should have reached a volume of 100-200 mm<sup>3</sup>.

### **ORTHOTOPIC XENOGRAFTS**

The orthotopic EAC xenograft model with OE33 provided slow growing and small tumors, which is not ideal for this pilot. Therefore, we opted for the SK-OV-3 Luc IP1 ovarian cell line, described in Chapter 3 in the Discussion section, in which macroscopic bulky tumors were reached at the distal site of the esophagus, 5 weeks after tumor inoculation.

For more details on animals or cell lines, see Materials and Methods section of Chapter 3.

### **$^{18}\text{F}$ -FAZA PET-CT**

The radiosynthesis of  $^{18}\text{F}$ -FAZA was performed on a Synthra RNplus module (Synthra GmbH, Hamburg, Germany) using a fully automated procedure that was based on standard procedures [112, 113]. The precursor for the radiosynthesis, 1-(2,3-diacetyl-5-tosyl-( $\alpha$ -D-arabinofuranosyl)-2-nitroimidazole, was purchased from ABX GmbH (Radeberg, Germany) and all other required reagents and solvents were acquired from Sigma-Aldrich (Overijse, Belgium).

Mice were anaesthetized and a target activity of 37 MBq of  $^{18}\text{F}$ -FAZA was injected in the tail vein. Three hours after injection and under anesthesia, the animals were positioned on a heated animal bed of a small animal PET/CT scanner (TriFoil Imaging, Triumph II, Northridge, CA, USA). CT projection data were acquired using the following parameters: 256 projections, detector pixel size 50  $\mu\text{m}$ , focal spot size 100  $\mu\text{m}$ , tube voltage 50 kV, tube current 640  $\mu\text{A}$ , and a field-of-view of 90 mm. A 30 minutes PET scan was acquired in list mode, with a 75-mm axial field-of-view and a 1.3-mm spatial resolution, on the same scanner and without moving the animal. CT images were analytically reconstructed using a filtered back projection reconstruction algorithm (Cobra Version 7.3.4, Exxim Computing Corporation, Pleasanton, CA) into a 256x256x512 matrix with 200  $\mu\text{m}$  isotropic voxel size. The acquired PET images were reconstructed into a 200x200x64 matrix by a 2D maximum

likelihood expectation maximization (MLEM) algorithm (LabPET Version 1.12.1, TriFoil Imaging®, Northridge, CA) using 50 iterations and a voxel size of  $0.5 \times 0.5 \times 1.175 \text{ mm}^3$  (x, y, z). Each resultant CT image is inherently co-registered with the corresponding PET scan. PET and CT images were imported into A Medical Image Data Examiner (AMIDE) [114], where tumor-to-background ratios (T/B) were calculated as the mean tumor uptake divided by the background activity. Mean tumor uptake was quantified into a volume-of-interest that was semi-automatically delineated as the activity  $>40\%$  of the maximum activity using the 3D-isocontour tool, similar to Tran et al. [78], and a sphere with radius 1.5 mm was delineated in the foreleg muscle as background tissue.

## MRI

See Chapter 3, Materials and Methods.

## IMMUNOHISTOCHEMISTRY

The exogenous hypoxia marker pimonidazole (Hypoxyprobe, MA, USA) was administered 1 hour before sacrifice (60 mg/kg, IP) and stained on formalin-fixed paraffin-embedded tumor sections (5  $\mu\text{m}$ ) with the Hypoxyprobe anti-pimonidazole mouse IgG1 monoclonal primary Ab (HP1-100 Kit) (1/50, 1 h, RT) and the LSAB+ System-AP kit (DAKO K0675).

## **RESULTS**

A total of 6 animals were imaged: 3 mice with bilateral OACM5 1.C SC1 tumors (6 tumors in total) and 3 mice with a SK-OV-3 Luc IP1 tumor at the distal site of the esophagus. Overall, a high background staining was seen in the liver, gall bladder, small and large intestine and the urinary bladder (Fig. 1).

## SC XENOGRAFTS

All 6 tumors could be delineated on the PET/CT images and SUV values and T/B ratios were calculated (Table 1, Fig. 2).



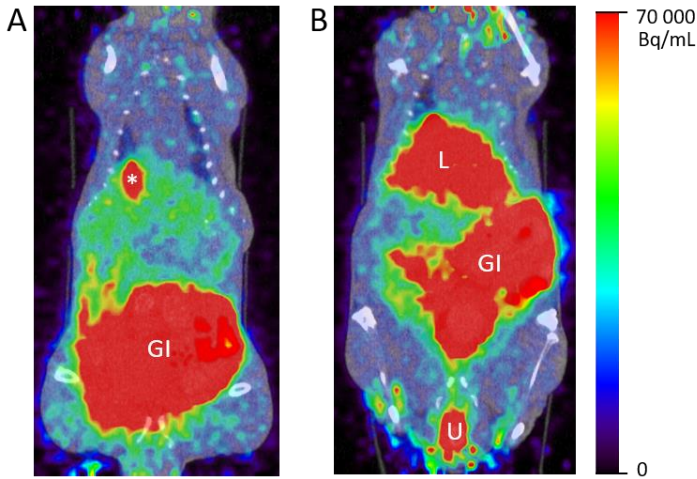


**FIGURE 1:  $^{18}\text{F}$ -FAZA PET/CT.**

Coronal images of  $^{18}\text{F}$ -FAZA PET/CT scans of 2 mice (A and B) illustrating the main regions of background activity: \*= gall bladder; L= liver; GI= small and large intestine; U= urinary bladder.

	Macroscopic tumor	Tumor Volume (mm <sup>3</sup> ) (CT/MRI)	IHC (pimonidazole)	Visualization of tumor on $^{18}\text{F}$ -FAZA PET/CT	$^{18}\text{F}$ -FAZA parameters	
					SUV	T/B
<b>SUBCUTANEOUS</b>						
Tumor 1	Yes	97.0	+/-	Yes	0.09	1.79
Tumor 2	Yes	78.8	+	Yes	0.09	2.40
Tumor 3	Yes	156.8	/	Yes	0.10	1.59
Tumor 4	Yes	91.7	+	Yes	0.13	3.90
Tumor 5	Yes	219.7	+	Yes	0.15	2.13
Tumor 6	Yes	231.2	+	Yes	0.17	2.73
<b>ORTHOTOPIC</b>						
Tumor 1	Yes	95.16	+	No	/	/
Tumor 2	Yes	116.3	+	No	/	/
Tumor 3	Yes	59.7	+/-	No	/	/

**TABLE 1: Results of  $^{18}\text{F}$ -FAZA PET/CT imaging.**

SUV= Standardized uptake value. Tracer uptake is quantified as percentage of the totally injected activity (%ID/g) and standardized to the animals' weight. T/B= Tumor to background. Mean tumor uptake was the activity in the >40% isocontour VOI. A sphere (radius 1.5 mm) in the foreleg muscle was background.

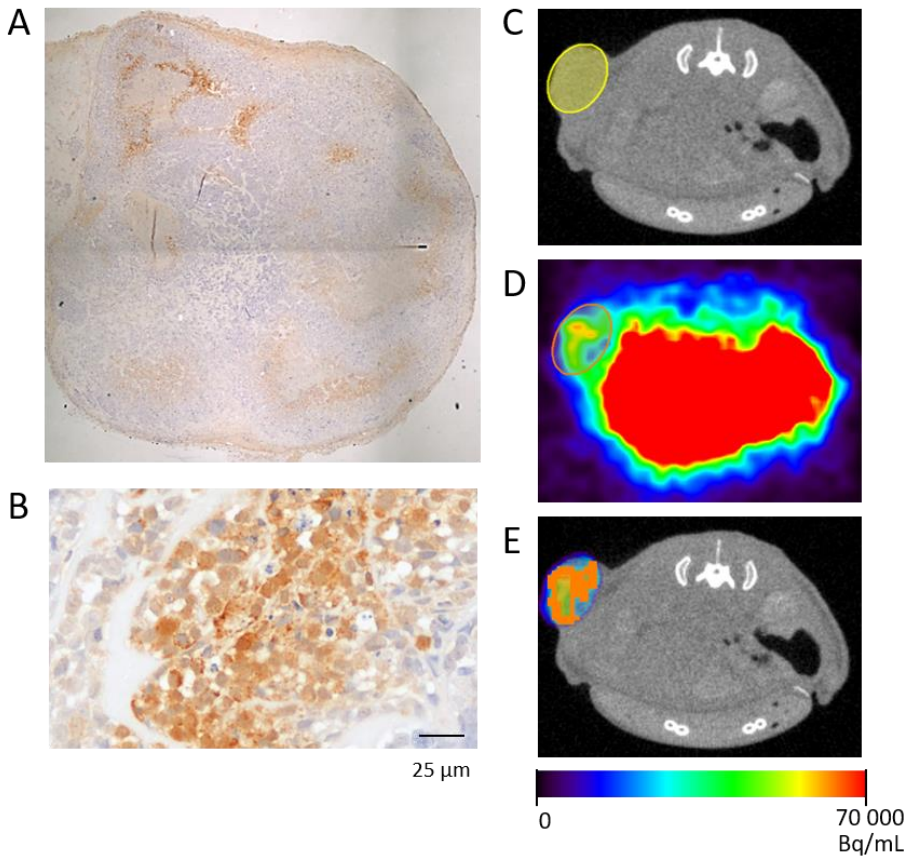


**FIGURE 2:  $^{18}\text{F}$ -FAZA PET/CT in SC xenografts.**

(A-B) Pimonidazole staining (=brown) of tumor section at different magnifications ((A) 40x and (B) 400x). Hypoxia is distributed heterogeneously in the tumor. (C-E) Transverse slices with mice in prone position on the PET/CT bed with right SC tumor on the hind leg. (C) CT image with tumor delineated spherically (yellow). (D)  $^{18}\text{F}$ -FAZA PET image. An irregular hypoxic area is visualized at this level of the tumor. The intense  $^{18}\text{F}$ -FAZA signal in the middle of the image is background activity from the gastro-intestinal tract. (E) Overlay  $^{18}\text{F}$ -FAZA PET/CT. The PET data exterior to the ROI was erased. Orange= ROI >40% isocontour.

## ORTHOTOPIC XENOGRAPHS

Three mice with SK-OV-3 Luc IP1 tumors at the distal site of the esophagus were imaged 5 weeks after tumor inoculation (Fig. 3). Tumor volumes were determined on MRI at the day of the  $^{18}\text{F}$ -FAZA PET/CT. Despite the clear presence of a voluminous tumors, it was

impossible to identify the tumors on PET/CT. First, soft tissue resolution on the CT was insufficient to differentiate the tumor from the neighboring tissues. Second, the intense background staining in the liver compromised tumor visualization on the PET images. As a result, no quantification of tumor hypoxia could be done on the  $^{18}\text{F}$ -FAZA PET/CT (Table 1). Yet, the presence of tumor hypoxia was confirmed histologically with pimonidazole staining in all 3 tumors (Fig. 3).

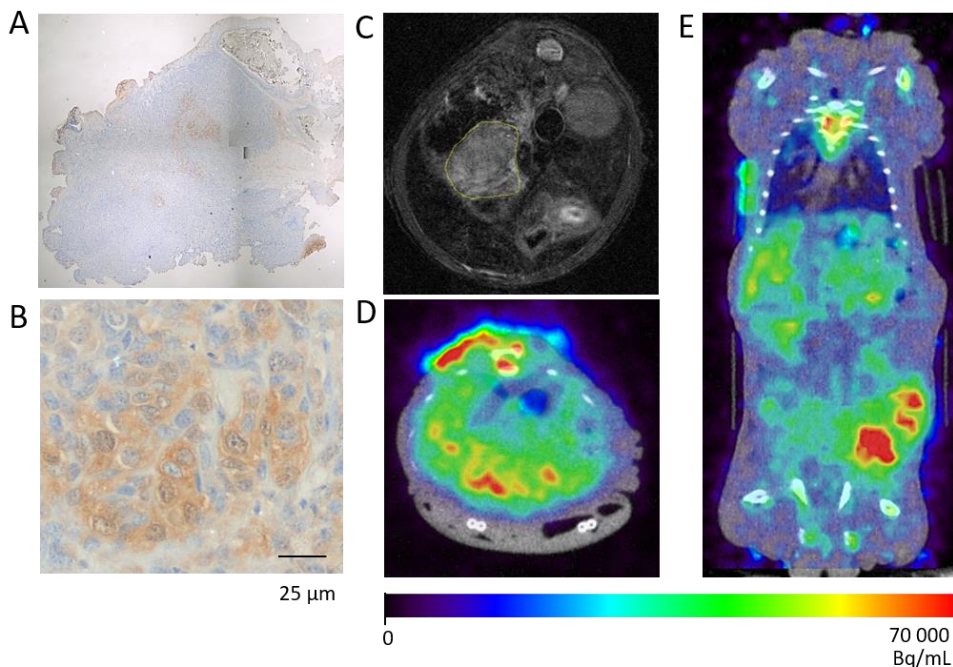


**FIGURE 3:  $^{18}\text{F}$ -FAZA PET/CT in orthotopic xenografts.**

(A-B) Pimonidazole staining (=brown) of tumor section at different magnifications ((A) 40x and (B) 400x). A small hypoxic zone is identified in the upper right quadrant of the tumor. (C) Transverse slice of MRI image. Tumor mass is delineated in yellow. (D-E) Transverse and coronal image of overlay  $^{18}\text{F}$ -FAZA PET/CT scan. The esophageal tumor mass clearly visible on MRI, could not be identified on the  $^{18}\text{F}$ -FAZA PET/CT scan.

## **DISCUSSION**

Overall, high background activity was observed in the liver, gall bladder, small and large intestine and urinary bladder, which is due to the pharmacokinetic properties of the tracer.  $^{18}\text{F}$ -FAZA is excreted through the gall bladder and gastro-intestinal tract, after hepatic

metabolization, and directly through the kidneys and the urinary bladder [62]. The SC tumors were localized outside these regions and could be visualized and delineated successfully on the  $^{18}\text{F}$ -FAZA PET/CT in all 6 tumors. The orthotopic xenografts were located near the liver, making visualization impossible.

This raises the question whether translation to the clinical setting would be feasible.

First, these experiments showed that the small dimensions of the mice, together with the low soft tissue resolution on the small animal PET/CT, were a primary cause of difficult tumor visualization. In the clinical setting, all esophageal cancer patients undergo CT-imaging as part of the standard staging modalities. Esophageal tumors are delineated more easily on CT images of patients than in mice which will be a first factor in favor of the clinical setting.

Second, not all tumors will be located in the field of background activity (liver). This tumor model represented esophageal adenocarcinomas (EAC) and was chosen because this has become the main subtype in the United States and Northern and Western Europe [103]. EAC is typically located at the lower 1/3 of the esophagus and at the gastro-esophageal junction [115], and thus near the liver. The second most common subtype is esophageal squamous cell carcinoma (ESCC). These tumors are mainly located in the proximal 2/3 of the esophagus [115], and thus outside any background activity fields, as can be seen on the scans (Fig. 1 and 3). The higher the tumor will be located, the easier visualization will be.

## **CONCLUSION**

$^{18}\text{F}$ -FAZA PET/CT imaging is feasible in the subcutaneous OACM5 1.C SC1 model, but not in the orthotopic model.

**CHAPTER 5**  
**PREDICTIVE VALUE OF**  
**<sup>18</sup>F-FAZA PET/CT AND HYPOXIC**  
**MODIFICATION WITH NIMORAZOLE**



## CHAPTER 5: PREDICTIVE VALUE OF <sup>18</sup>F-FAZA PET/CT AND HYPOXIC MODIFICATION WITH NIMORAZOLE

In chapter 3, we described the development of an orthotopic and subcutaneous EAC model in mice. Chapter 4 showed that only the subcutaneous model was feasible for <sup>18</sup>F-FAZA PET/CT hypoxia imaging. In this chapter, we investigated the first research question ‘Can hypoxia imaging with <sup>18</sup>F-FAZA PET/CT serve as a predictive biomarker and as a guidance for hypoxia targeting?’ in our subcutaneous EAC tumor model.

→ This chapter is based on the following article:

*Melsens E, De Vlieghere E, Descamps B, Vanhove C, Kersemans K, De Vos F, Goethals I, Brans B, De Wever O, Ceelen W, Pattyn P. Hypoxia imaging with <sup>18</sup>F-FAZA PET/CT predicts radiotherapy response in esophageal adenocarcinoma xenografts. Submitted.*

### **ABSTRACT**

**Background:** Esophageal cancer is an aggressive disease with poor survival rates. Standard treatment encompasses neoadjuvant chemoradiation (locally advanced stage). Response to neoadjuvant therapy is highly variable and difficult to predict. As it is known that tumor hypoxia is correlated with treatment resistance and worse prognosis in solid tumors, this could be an interesting predictive factor for esophageal cancer. By imaging hypoxia with <sup>18</sup>F-FAZA PET/CT, we aimed to predict treatment response of esophageal adenocarcinoma (EAC) xenografts. Further, we investigated hypoxic radioresistance and the radiosensitizing effect of the hypoxia modifier nimorazole *in vitro* and *in vivo*.

**Methods:** *In vitro* MTS cell proliferation assays were performed under normoxic and hypoxic conditions with 8 treatment groups: control, nimorazole, irradiation (5, 10 or 20 Gy) with or without nimorazole. *In vivo*, subcutaneous xenografts were induced in the hind legs of nude mice (human EAC cell line OACM5 1.C SC1). Mice were divided in 3

treatment groups: (A) control, (B) radiotherapy (RT) (5 Gy/d during 5 days) and (C) combination (nimorazole (200 mg/kg/d, IP) 30 min before RT).  $^{18}\text{F}$ -FAZA PET/CT was performed before and after treatment and tumor to background (T/B) ratios were calculated. Tumors were measured daily with calipers and relative tumor growth (RTG) was calculated. Tumor sections were examined histologically (hypoxia, DNA double-strand breaks (DSB), apoptosis and proliferation).

**Results:** A  $T/B \geq 3.59$  on pretreatment  $^{18}\text{F}$ -FAZA PET/CT was predictive for worse RT response in xenograft EAC tumors (sensitivity 92.3%, specificity 71.4%). Radiation induced growth inhibition was significantly less in hypoxic tumors ( $T/B \geq 3.59$ ) than normoxic tumors ( $T/B < 3.59$ ) ( $P= 0.0011$ ). Pre-treatment with nimorazole significantly decreased *in vitro* hypoxic radioresistance ( $P < 0.01$ ) and improved *in vivo* RT induced proliferation inhibition in hypoxic tumor areas (Ki67,  $P= 0.064$ ).

**Conclusions:**  $^{18}\text{F}$ -FAZA PET/CT is predictive for RT response in an EAC xenograft model. Pre-treatment with nimorazole may benefit treatment response in hypoxic tumors.



## **INTRODUCTION**

Esophageal cancer is an aggressive disease with poor survival rates. Patients are mostly diagnosed in a locally advanced stage and treated with neoadjuvant chemoradiation followed by surgery [82]. Response to chemoradiation is highly variable with a pathological complete response (pCR) in about 30%, but presence of residual carcinoma in the remaining 70% [116]. Therefore, identification of imaging biomarkers that allow to predict response to chemoradiation is an important challenge.

An attractive predictive factor is tumor hypoxia that is present in up to 60% of locally advanced solid tumors. It has been proven to be an independent negative predictive and prognostic factor and has been correlated with chemoresistance, radioresistance, invasiveness, propensity to metastasize, and genomic instability [6]. Also in esophageal cancer, hypoxia has been correlated with worse outcomes. Histologic examination of carbonic anhydrase 9 (CAIX) and hypoxia-inducible factor 1-alpha (HIF-1 $\alpha$ ), two factors that are overexpressed in hypoxic conditions, were correlated with worse outcomes and hypoxia imaging with <sup>18</sup>F-FETNIM (fluoroerythronitroimidazole) positron emission tomography (PET) showed that tracer uptake might be predictive for treatment response in esophageal cancer [83, 117, 118].

Here, <sup>18</sup>F-FAZA PET (fluoroazomycin arabinoside) was used to image and quantify tumor hypoxia and investigate its predictive potential in esophageal cancer. PET imaging has the advantages that it is non-invasive, it can be repeated and it gives a 3D-image of the hypoxia distribution [54]. <sup>18</sup>F-FAZA is a second generation 2-nitroimidazole with superior pharmacokinetics compared to <sup>18</sup>F-FMISO (fluoromisonidazole), resulting in a better tumor-to-background ratio [64]. The tracer entrapment is based on a reduction of the NO<sub>2</sub>-group followed by continued reduction under hypoxic conditions and eventually covalent binding to intracellular macromolecules [54]. <sup>18</sup>F-FAZA PET already showed to be predictive for treatment response in preclinical models of rhabdomyosarcoma and breast carcinoma [78, 79]. Clinically, FAZA imaging has been studied in non-small cell lung cancer and head and neck squamous cell cancer, while trials are ongoing in rectal, lung, cervix, and prostate carcinoma (ClinicalTrials.gov: NCT02624115, NCT02701699, NCT01989364, NCT01567800).

Further, we investigated whether this tumor hypoxia, diagnosed on <sup>18</sup>F-FAZA PET, could be modified and eventually enhance radiation response. We focused on the radiosensitizer nimorazole because it is easy applicable, has few side effects and is already part of daily

practice in Denmark for HNSCC patients [35] (DAHANCA guidelines). It is a 5-nitroimidazole and mimics oxygen in the radiochemical process by promoting fixation of free radicals [32].

In summary, this study investigated the predictive value of  $^{18}\text{F}$ -FAZA PET/CT for hypoxia-induced radioresistance in EAC xenografts and the radiosensitizing effect of nimorazole.

## **MATERIALS AND METHODS**

### **CELL LINE**

OACM5 1.C SC1 was established through *in vivo* selection from the parental cell line OACM5 1.C cell line, a human esophageal adenocarcinoma (EAC) cell line, as described previously [119], and was authenticated by short tandem repeat DNA profiling. This cell line was preferred over the parental cell line because it has increased tumor take rates. Cells were cultured at 37°C in 5% CO<sub>2</sub> humidified atmosphere in RPMI 1640 Medium (Life Technologies) supplemented with GlutaMAX™-I (Life Technologies), 10% fetal bovine serum and penicillin-streptomycin.

### **MTS ASSAY**

Cells were seeded ( $8 \times 10^5$ ) in T25 flasks and incubated overnight (ON) at normoxic (5% CO<sub>2</sub> in air) or hypoxic (Anaerobic Work Station, Baker Ruskinn, gas mixture 80% N<sub>2</sub>, 10% CO<sub>2</sub>, 10% H<sub>2</sub>) conditions. Hypoxia was confirmed with an anaerobic indicator (BR0055, ThermoScientific). Treatment was given 24 h after seeding. Flasks of the hypoxic group were closed in the anaerobic station to ensure hypoxia at the moment of irradiation. One dose of 5, 10 or 20 Gy was given, with or without pre-treatment with nimorazole (30 min before irradiation, 0.2 mg/mL in PBS). Controls received 100 µL PBS. RT was applied using the small animal radiation research platform (SARRP). The voltage of the X-ray source was fixed at 220 kV with a tube current of 13 mA, emitted from the 3 mm focal spot and filtered by a copper filter of 0.15 mm. A vertical radiation beam of 10x10 cm<sup>2</sup> was used that permitted simultaneous irradiation of 2 T25 falcons. Flasks were further incubated under standard conditions (37°C in 5% CO<sub>2</sub> humidified atmosphere) and MTS assay (3-(4,5-dimethylthiazol-2-yl)-5-(3-carboxymethoxyphenyl)-2-(4-sulfophenyl)-2H-tetrazolium) was performed 72 hours after treatment. MTS Reagent Powder (CellTiter 96® Aqueous MTS (Promega)) was dissolved at 2mg/mL in PBS<sup>D+</sup>. PMS (phenazine methosulfate,

dissolved at 0.92 mg/mL in PBS<sup>D+</sup>) was added at a concentration of 1/20 and 1 mL of the solution was added to each flask. After 90 min of incubation at 37°C and 5% CO<sub>2</sub>, absorbance was measured with Paradigm (490 nm) (SPECTRAMax Paradigm, Molecular Devices, USA). Cell viability was calculated relative to controls (%). Experiments were performed in duplicate and repeated 3 times (n= 3x2). An additional MTS assay was performed in a control group on the day of treatment (24 hours after seeding) to quantify cell viability at that time point.

## ANIMALS

Animal experiments were approved by the Animal Ethical Committee of Ghent University, Belgium (ECD 14/82). Athymic mice (Foxn1nu male) were obtained from Envigo, the Netherlands, and were kept under environmentally controlled conditions (12 h normal light/dark cycle, 20-23°C and 50% relative humidity) with food and water ad libitum. Inhalation anesthesia was performed with isoflurane (Abbott, Belgium), 5% induction, 1.5% maintenance, 0.3 L/min. Mice were euthanized by cervical dislocation under anesthesia one day post-treatment or when humane endpoints were reached.

## TUMOR MODEL AND TREATMENT

At 5 weeks of age,  $3 \times 10^6$  cancer cells suspended in 100 µl of Matrigel were injected subcutaneously in both hind legs under anesthesia. Tumors were grown for 7 weeks. Tumors with a minimum volume of 150 mm<sup>3</sup> were included and divided into 3 treatment groups. Daily treatment was given for 5 consecutive days: (A) Control (600 µl NaCl 0.9% intraperitoneally (IP)) (N= 5, n= 7), (B) RT (5 Gy/d) (N= 11, n= 20), (C) Combination (nimorazole (200 mg/kg/d IP) given 30 min before RT) (N= 13, n= 21). N= number of mice, n= number of tumors. Nimorazole (Adooq Bioscience LLC, USA) was dissolved in NaCl 0.9% at 10 mg/mL on the day of administration. The dosage and timing was according to previous literature [120]. RT was applied using the SARRP with X-ray source parameters as described above. A pair of parallel-opposed (anterior-posterior) radiation beams of 10x10 mm<sup>2</sup> were used. Mice were anesthetized and positioned on the bed of the SARRP. Guided by lasers, the bed was moved to position tumors at the isocenter of the beam. To allow parallel-opposed beam irradiations, mice were turned around when half of the dose was given. Doses of 5 Gy (2x2.5 Gy) were delivered daily during 5 consecutive days. Tumor nodules were measured daily with calipers and volumes were calculated according to the

following formula:  $V = (length \times width)^{3/2} \times \pi/6$ . Relative tumor growth (RTG) was calculated as the ratio of the volume at the day of euthanasia to the volume before treatment.

## <sup>18</sup>F-FAZA PET-CT

The radiosynthesis of <sup>18</sup>F-FAZA was performed on a Synthra RNplus module (Synthra GmbH, Hamburg, Germany) using a fully automated procedure that was based on standard procedures [121, 122]. The precursor for the radiosynthesis, 1-(2,3-diacetyl-5-tosyl-( $\alpha$ -D-arabinofuranosyl)-2-nitroimidazole, was purchased from ABX GmbH (Radeberg, Germany) and all other required reagents and solvents were acquired from Sigma-Aldrich (Overijse, Belgium).

<sup>18</sup>F-FAZA PET/CT was performed one day before treatment. Mice were anaesthetized and a target activity of 37 MBq of <sup>18</sup>F-FAZA (mean 37 MBq, SD 1.85) was injected in the tail vein. Three hours after injection and under anesthesia, the animals were positioned on a heated animal bed of a small animal PET/CT scanner (TriFoil Imaging, Triumph II, Northridge, CA, USA). CT projection data were acquired using the following parameters: 256 projections, detector pixel size 50  $\mu$ m, focal spot size 100  $\mu$ m, tube voltage 50 kV, tube current 640  $\mu$ A, and a field-of-view of 90 mm. A 30 minutes PET scan was acquired in list mode, with a 75-mm axial field-of-view and a 1.3-mm spatial resolution, on the same scanner and without moving the animal. CT images were analytically reconstructed using a filtered back projection reconstruction algorithm (Cobra Version 7.3.4, Exxim Computing Corporation, Pleasanton, CA) into a 256x256x512 matrix with 200  $\mu$ m isotropic voxel size. The acquired PET images were reconstructed into a 200x200x64 matrix by a 2D maximum likelihood expectation maximization (MLEM) algorithm (LabPET Version 1.12.1, TriFoil Imaging®, Northridge, CA) using 50 iterations and a voxel size of 0.5x0.5x1.175 mm<sup>3</sup> (x, y, z). Each resultant CT image is inherently co-registered with the corresponding PET scan. PET and CT images were imported into A Medical Image Data Examiner (AMIDE) [114], where tumor-to-background (T/B) ratios were calculated as the mean tumor uptake divided by the background activity. Mean tumor uptake (Bq/mL) was quantified in a volume-of-interest that was semi-automatically delineated as the activity >40% of the maximum activity using the 3D-isocontour tool, similar to Tran et al. [123], and a sphere with radius 1.5 mm was delineated in the foreleg muscle as background tissue. In a subset of mice (RT: n=7; combination: n=6), an additional <sup>18</sup>F-FAZA PET/CT was performed after treatment to evaluate the influence of treatment on hypoxia status.

## TUMOR SAMPLES AND HISTOLOGY

Consecutive 5 $\mu$ m sections of formaldehyde-fixed paraffin-embedded tumors were prepared. Standard H&E staining was performed and necrotic areas were excluded for further analysis. The hypoxia marker pimonidazole, administered 1 hour before sacrifice (60mg/kg, IP, Hypoxyprobe, USA), was stained with Hypoxyprobe anti-pimonidazole mouse IgG1 monoclonal Ab (HP1-100 Kit) (1/50, 1 h, RT) and the LSAB+ System-AP kit (DAKO K0675). Ki67 staining was performed with the primary rabbit monoclonal anti-human/mouse/rat anti-Ki67 Ab ([SP6] Abcam 16667) (1/100, ON, 4°C) and the labelled polymer HRP anti-rabbit secondary Ab (Dako, K4011) (40 min, RT). Proliferation indices (fraction of Ki67+ cells/total cells) were calculated in normoxic and hypoxic regions, according to pimonidazole staining (magnification 400x, 3x2 hotspots/tumor) (ImageJ (ImmunoRatio)).  $\gamma$ -H2AX was stained to evaluate DNA-DSB and confirm irradiation. The primary rabbit polyclonal anti-human/mouse anti-  $\gamma$ -H2AX Ab (Bethyl IHC-00059) (1/3000, ON, 4°C), the polyclonal goat anti-rabbit biotinylated secondary Ab (E0432) (1/200, 30 min, RT) and streptavidine-HRP (1/200, 30 min, RT) were used. Number of foci per nucleus (mean) were determined (magnification 400x, 5 at random areas, 15 cells per area). As last, cleaved caspase-3 (Asp 175) was stained with the primary rabbit monoclonal anti-mouse/human/rat anti-Asp175 Ab (Cell Signaling Technology, ab#9661) (1/400, ON, 4°C) and the labelled polymer HRP anti-rabbit secondary Ab (Dako, K4011) (30 min, RT). Sections were scanned (100x and 200x magnification) and apoptotic indices were determined by an overall visual scoring system: 0 means no staining and 10 means full staining.

Microscopy was performed with a light microscope (ColorView I, BX43F, Olympus, Japan).

## STATISTICAL METHODS

Statistical analysis was performed with GraphPad Prism6 (Graphpad Software, Inc.: La Jolla, USA). Data was tested for normality (Shapiro-Wilk), analyzed with the Mann-Whitney U test (non-parametric) or t-test (parametric) and summarized as medians or means with standard deviation (SD). ID50 values of the MTS-assay were calculated with non-linear regression analysis (log(inhibitor) vs. normalized response). The cut-off T/B ratio to predict treatment response was determined with ROC-analysis. T/B ratios of pre- and post-treatment scans were compared with the Wilcoxon matched-pairs signed rank test. Results

were considered statistically significant when the probability of a type I error was  $\leq 0.05$ . P-values were abbreviated as \* =  $P < 0.05$ , \*\* =  $P < 0.01$ , \*\*\* =  $P < 0.001$ , \*\*\*\* =  $P < 0.0001$ .

## RESULTS

### IN VITRO EFFECTS OF HYPOXIA AND NIMORAZOLE ON RT RESPONSE

Cell viabilities were analyzed 72 h after RT and represented the net result of cell growth and proliferation, and cell cycle arrest and apoptosis. As expected, RT was less efficient under hypoxic conditions, illustrated by an upwards movement of the dose-response curve (Fig. 1A). The ID50 was doubled (11.48 Gy versus 23.03 Gy) and cell viabilities were significantly higher for all radiation doses (5 Gy:  $P = 0.0004$ ; 10 Gy:  $P = 0.0012$ ; 20 Gy:  $P = 0.0012$ ) (Fig. 1C, Suppl Fig. 1). Hypoxia also induced a steepening of the dose-response curve (HillsSlope<sub>Norm</sub> = -0.64 (95% CI [-0.77; -0.51]) and HillsSlope<sub>Hypox</sub> = -1.32 (95% CI [-1.67 to -0.97])), meaning hypoxia-induced resistance decreased upon irradiation with higher doses.

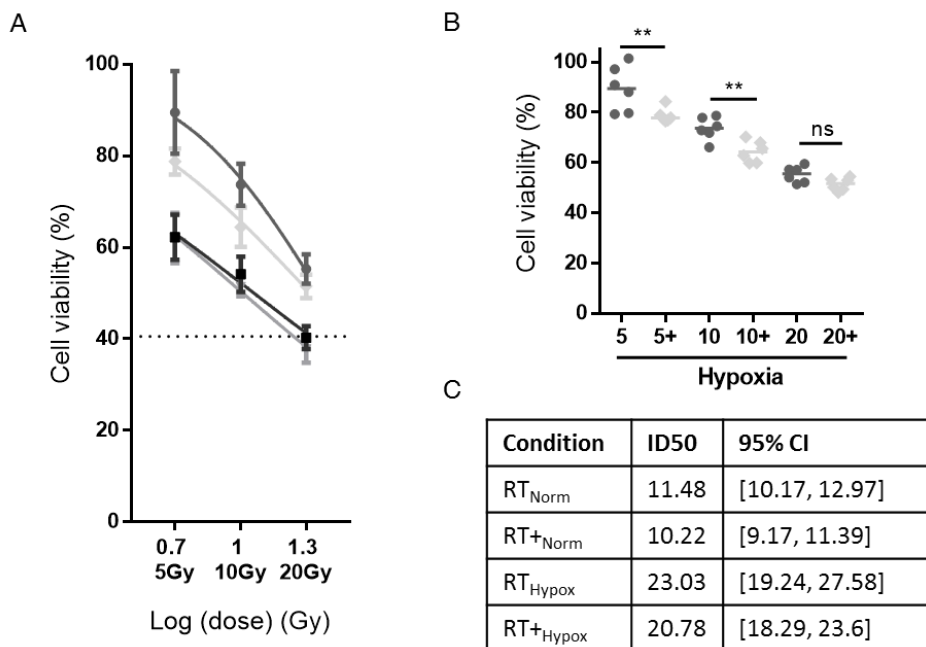


**FIGURE 1: *In vitro* effects of hypoxia and nimorazole on radiotherapy (RT) response.**

(A-B) ■ Normoxia; ● Hypoxia; ▼ Normoxia + nimorazole; ◆ Hypoxia + nimorazole. (A) Dose-response curve of MTS-assay with RT doses (x-axis, logarithmic) and cell viabilities (y-axis, mean, SD, non-linear regression fitted curve) relative to controls (0 Gy, cell viability=100%). Dotted line= cell viability at the day of treatment. (B) Effect of nimorazole on RT response in hypoxic conditions. X-axis: RT doses (5, 10 or 20 Gy) with (+) or without nimorazole. Y-axis: cell viabilities relative to controls (single values, medians). (C) Parameters derived from the dose-response curve. ID50 values represent the required radiation dose to inhibit 50% of the cell viability.

Nimorazole induced a radiosensitization of hypoxic cancer cells, represented by a downward movement of the dose-response curve under hypoxic conditions (Fig. 1A). Nimorazole significantly reduced treatment resistance for irradiation with 5 and 10 Gy ( $P= 0.0087$  and  $P= 0.0087$ ) (Fig. 1B), but did not enhance radiation response with 20 Gy, nor did it reduce the ID50 value (Fig. 1C). Further, nimorazole had no effect on RT efficacy in normoxic conditions.

## HYPOXIC RADIORESISTANCE AND RADIOSENSITIZING EFFECT OF NIMORAZOLE IN EAC XENOGRAPHS

Cancer cell proliferation was significantly reduced by RT and combination treatment in normoxic tumor areas compared to controls ( $P= 0.0012$  and  $P= 0.0022$ ) (Fig. 2A, 2D). Hypoxic areas were resistant to RT with significant higher proliferation indices than in normoxic areas ( $P= 0.0025$ ). Pre-treatment with nimorazole radiosensitized hypoxic cancer cells by reducing the proliferation indices in hypoxic tumor areas (trend,  $P= 0.064$ ) and not in normoxic areas (Fig. 2A, 2D).

Irradiation significantly induced DNA-DSB compared to controls ( $P< 0.0001$ ) (Fig. 2B, 2D). A minority of this DNA-damage led to cancer cell apoptosis. Controls scored 0-2, whereas 57% (8/14) of the irradiated tumors scored higher (3-5) (Fig. 2C-D). However, no tumors scored higher than 5. No difference between normoxic and hypoxic tumor regions was observed for DNA-DSB or apoptosis (Fig. 2D).

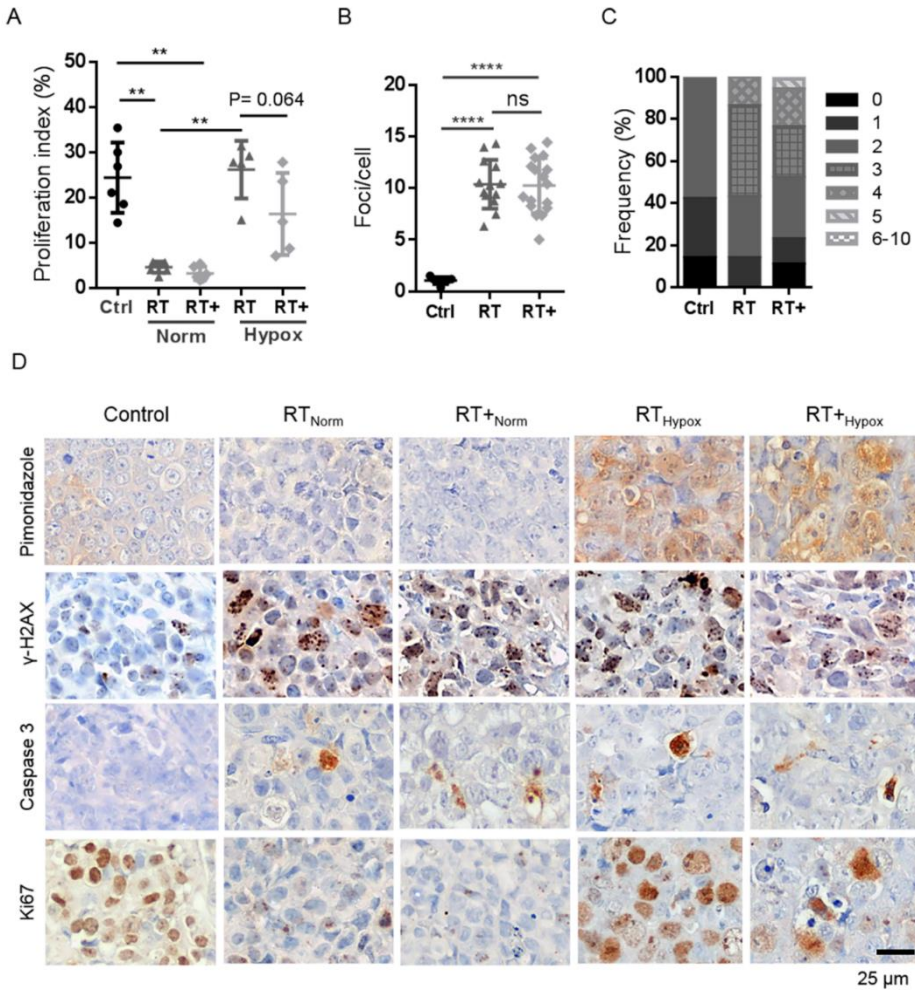


**FIGURE 2: Hypoxic radioresistance and radiosensitizing effect of nimorazole in EAC xenografts.**

● = Control; ▲ = RT; ◆ = Combination (RT+). (A) Cancer cell proliferation indices from Ki67 staining (single values, mean, SD). Normoxia/hypoxia was defined by co-localization of pimonidazole staining on consecutive sections. (B) Mean DNA-DSB/cancer cell nucleus, resulting from  $\gamma$ -H2AX staining (single values, mean, SD). (C) Number of tumors (%) for every apoptotic index (0-10) resulting from the cleaved caspase-3 staining. (D) Pimonidazole,  $\gamma$ -H2AX, cleaved caspase-3 and Ki67 staining of consecutive sections. Representative pictures of each treatment group. Irradiation caused DNA-DSB and apoptosis in all treatment groups with no difference between normoxic and hypoxic areas. There was less Ki67 staining in normoxic than hypoxic RT treated areas, representing hypoxic radioresistance.



## **<sup>18</sup>F-FAZA PET/CT AS A PREDICTIVE BIOMARKER**

Radiosensitive and radioresistant tumors were identified retrospectively based on RTG. Tumors that regressed after RT (RTG <100%) were defined radiosensitive (35%, n= 13) and tumors that continued growing (RTG >100%) radioresistant (65%, n= 7) (Fig. 3A). Pre-treatment <sup>18</sup>F-FAZA uptake (T/B ratios) was significantly higher in radioresistant tumors than in radiosensitive tumors (P= 0.046, Fig. 3B, 3D), demonstrating that more hypoxic tumors are more resistant to RT than less hypoxic tumors. ROC-analysis was performed to identify a cut-off value for predicting RT response with <sup>18</sup>F-FAZA PET/CT, which showed that a T/B of 3.59 predicted treatment response with the highest sensitivity and specificity (92.3% and 71.4% respectively, AUC 0.75). Based on pre-treatment <sup>18</sup>F-FAZA PET/CT, tumors were divided in normoxic (T/B < 3.59) and hypoxic (T/B ≥ 3.59). Irradiation inhibited tumor growth significantly better in normoxic tumors compared to hypoxic tumors (P= 0.0011) (Fig. 3C) and nimorazole seemed to improve tumor growth control in hypoxic tumors, but not significantly (Fig. 3C).

## **TUMOR REOXYGENATION AFTER RADIOTHERAPY**

T/B ratios were significantly reduced by RT (P= 0.047) and combination treatment (P= 0.031) (Fig. 4A, 4C). This reduction did not differ between RT or combination treatment (Fig. 4B) and no link was observed between reoxygenation status and treatment response (Fig. 4A). Although 3/4 hypoxic tumors reoxygenated, all 4 were radioresistant (Fig. 4A, red). Also after combined treatment 2 out of 2 hypoxic tumors reoxygenated, while one was radioresistant (Fig. 4A red) and the other was radiosensitive (green).

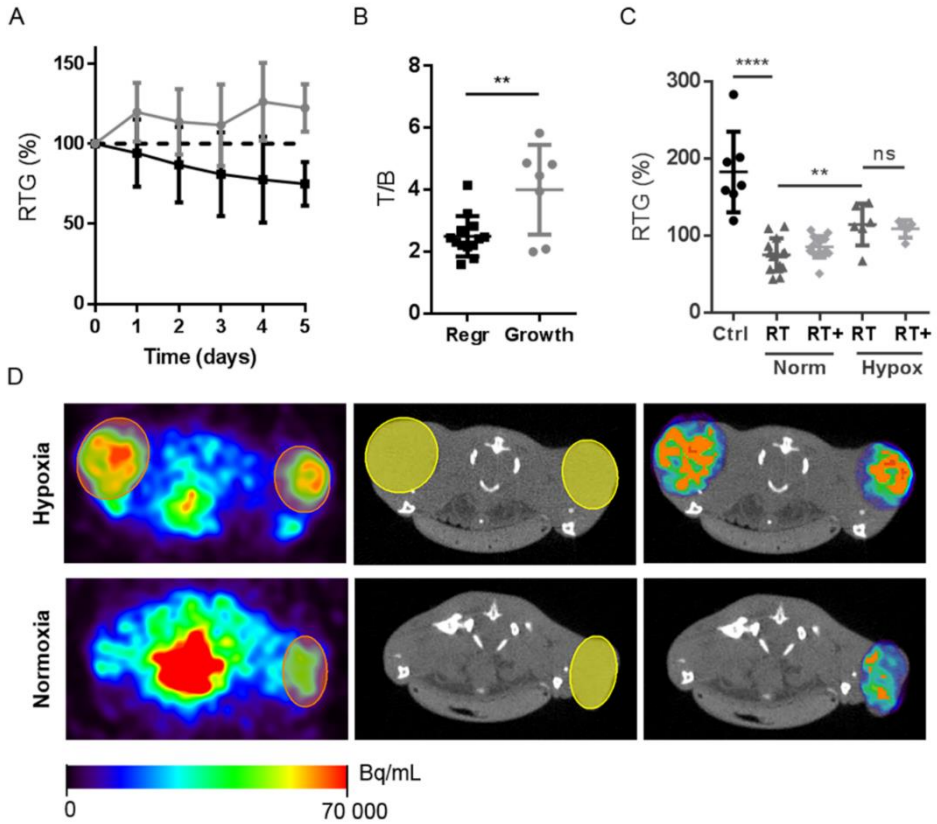


**FIGURE 3: Predictive value of  $^{18}\text{F}$ -FAZA PET/CT.**

(A) Relative tumor growth (RTG) of RT treated tumors (mean, SD). X-axis: time in days after start of treatment. Grey curve: tumors that continued growing (RTG at day 5 >100%= radioresistant, n= 7). Black curve: tumors that regressed (RTG at day 5 <100%= radiosensitive, n= 13). (B) Pre-treatment  $^{18}\text{F}$ -FAZA uptake of RT treated tumors, T/B ratios (single values, mean, SD). X-axis: tumors that regressed (radiosensitive) and tumors that continued growing (radioresistant) after RT. (C) RTG of EAC xenografts (single values, mean, SD). Hypoxia status was defined by  $^{18}\text{F}$ -FAZA PET/CT: T/B < 3.59 = normoxic; T/B  $\geq$  3.59 = hypoxic. (C) Transverse slices at the level of the hind legs with mice in prone position. Left:  $^{18}\text{F}$ -FAZA PET images with subcutaneous EAC tumors delineated spherically (orange). Middle: corresponding CT images. Right: Overlay  $^{18}\text{F}$ -FAZA PET/CT. The PET data exterior to the ROI's was erased. Orange= ROI >40% isocontour. Upper scans: bilateral tumors with high FAZA uptake, representative for hypoxic tumors. Lower scans: non-hypoxic tumor (left) with low FAZA uptake. High  $^{18}\text{F}$ -FAZA uptake was also seen in the urinary bladder due to renal excretion of the tracer.

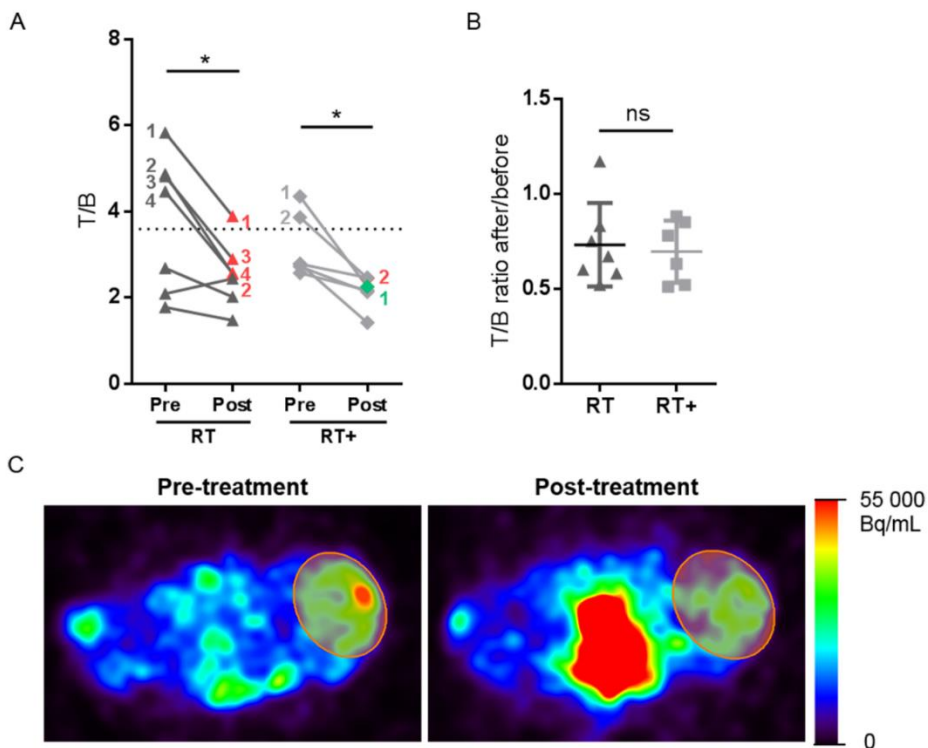


**FIGURE 4: Radiation induced tumor reoxygenation.**

▲ RT; ◆ = Combination (RT+). (A) T/B ratios (single values) of  $^{18}\text{F}$ -FAZA PET/CT (pre- or post-treatment). Dotted line= cut-off for hypoxic tumors ( $T/B \geq 3.59$ ). Hypoxic tumors are numbered. Colors refer to treatment response: red= radioresistant ( $\text{RTG} > 100\%$ ); green= radiosensitive ( $\text{RTG} < 100\%$ ). (B) Ratios of T/B after treatment to T/B before treatment (single values, mean, SD). (C) Transverse  $^{18}\text{F}$ -FAZA PET/CT slices at the level of the hind legs with a left subcutaneous tumor (orange). Mice in prone position. The clear hypoxic zone with high FAZA uptake that existed pre-treatment, disappeared after irradiation.

## **DISCUSSION**

This study investigated the predictive value of  $^{18}\text{F}$ -FAZA PET/CT for hypoxia-induced radioresistance in EAC and the radiosensitizing effect of nimorazole.

We confirmed the existence of hypoxia-induced radioresistance and the radiosensitizing effect of nimorazole in the OACM5 1.C SC1 cell line *in vitro* as well as *in vivo* in EAC xenografts. We showed that a T/B of  $\geq 3.59$  on pre-treatment  $^{18}\text{F}$ -FAZA PET/CT predicts radioresistance with a sensitivity of 92.3% and specificity of 71.4%. Further, we showed

that this cut-off also identifies tumors that could benefit from combination treatment with nimorazole.

It is difficult to compare the cut-off value of 3.59 with other studies, because no consensus exists for quantifying  $^{18}\text{F}$ -FAZA uptake. Some studies quantify tracer uptake as percentage of the totally injected activity (%ID/g or SUV (standardized uptake values) if standardized to the animals' weight). Because FAZA is excreted in urine and feces, individual tracer activity at the moment of the scan, i.d. 3 hours post-injection, varied substantially between animals. Therefore, like other studies [78, 124], we used tumor to background ratios, where tumor activity is compared to a reference non-hypoxic tissue. We calculated mean and maximum tumor uptakes and used lung or muscle as background tissue. We also calculated tumor uptake using the 40% isocontour VOI tool (available in Amide.exe 1.0.4), similar to Tran et al. [123]. The last method provided the strongest T/B parameter to predict treatment response and was chosen as predictive parameter for this model. Interestingly, the cut-off of 3.59 is in the range of the cut-off value proposed by Tran et al. [78]. They investigated  $^{18}\text{F}$ -FAZA uptake in a rhabdomyosarcoma xenograft model and found that  $\text{T/B} > 2.72$  identifies highly hypoxic tumors which benefit from pre-treatment with nimorazole.

As  $^{18}\text{F}$ -FAZA PET/CT has already been proven to be safe in the clinical setting and this study proved its predictive value in EAC xenografts, we believe it would now be interesting to analyze  $^{18}\text{F}$ -FAZA PET/CT in EAC patients. However, certain difficulties may arise. EAC tumors are preferentially localized at the distal esophagus [115]. Because FAZA is excreted biliary (after hepatic metabolization) and renally [62], there is a lot of background tracer activity in those regions, which could impede tumor visualization. We tested the feasibility of  $^{18}\text{F}$ -FAZA-PET/CT in a distal esophageal tumor mass in an additional mouse experiment. Tumor delineation was not possible due to intense liver tracer uptake combined with poor soft tissue resolution of the small animal CT. Nevertheless, we believe visualization in patients will be better because the higher soft tissue resolution on human CT scans. For esophageal squamous cell carcinomas, typically located in the thoracic part of the esophagus, this should not be a problem.

The benefit of nimorazole was more evident in the *in vitro* experiments than in the xenograft model. Probably, the RT regimen itself had radiosensitizing effects. *In vitro*, single doses were used, where *in vivo* we used a hypofractionated schedule because a clinically relevant schedule was aimed at (23 x 1.8 Gy according to the recent CROSS trial [82]). Because copying the exact clinical regimen would be impracticable, we opted for a hypofractionated

schedule of 5 x 5 Gy. On the one hand, as was seen *in vitro*, higher irradiation doses cause less hypoxic radioresistance than smaller doses. On the other hand, fractionation is known to cause tumor cell reoxygenation between the doses and enhances RT efficacy as such [125, 126]. Indeed, post-treatment <sup>18</sup>F-FAZA PET/CT showed a normalization of hypoxia status in 5/6 hypoxic tumors after RT alone or combined with nimorazole.

Predicting treatment response in the clinical setting offers possibilities for individualized treatments. For example, if a tumor is predicted to show a good response, it is worth to administer neoadjuvant treatment before surgery. Meanwhile, if a tumor is predicted to be resistant to neoadjuvant treatment, it could be better to perform the surgical resection earlier or to modify the neoadjuvant treatment and decrease radioresistance, like modifications to the RT regimen itself (e.g. dose-painting [127]) or addition of a hypoxia modifier (e.g. nimorazole [128]). Still, tumor hypoxia is distributed heterogeneously in space and over time [6]. For sure, hypoxia distribution and status of the tumors will change during the neoadjuvant treatment. Repetitions of <sup>18</sup>F-FAZA PET/CT during treatment are needed to reevaluate tumor's hypoxia status and indications for radiosensitizers.

## **CONCLUSION**

This study on esophageal adenocarcinoma showed that a T/B  $\geq 3.59$  on <sup>18</sup>F-FAZA PET/CT is predictive for worse RT response. The benefit of nimorazole in hypoxic tumors seems doubtful and should be limited to individuals with proven hypoxic tumors on <sup>18</sup>F-FAZA PET/CT.



**CHAPTER 6**  
**HYPOXIA AS RESULT OF TUMOR**  
**ANGIOGENESIS AND MODIFICATION**  
**WITH CEDIRANIB**





## CHAPTER 6: HYPOXIA AS RESULT OF TUMOR

### ANGIOGENESIS AND MODIFICATION WITH

### CEDIRANIB

In the previous chapters, we developed an EAC tumor model that was feasible for  $^{18}\text{F}$ -FAZA PET/CT imaging and that was used to answer the first research question ‘Can hypoxia imaging with  $^{18}\text{F}$ -FAZA PET/CT serve as a predictive biomarker and as a guidance for hypoxia targeting?’. We showed that tumor hypoxia imaging with  $^{18}\text{F}$ -FAZA PET/CT is a useful predictive biomarker for treatment response in an EAC model in mice. We further showed that targeting of hypoxia with nimorazole seemed to improve radiation response of hypoxic tumor (identified with  $^{18}\text{F}$ -FAZA PET/CT).

In this chapter, we investigated the second research question: ‘Can anti-angiogenic therapy reduce hypoxia and enhance radiotherapy efficacy?’

→ This chapter is based on the following article:

*Melsens E, Verberckmoes B, Rosseel N, Vanhove C, Descamps B, Pattyn P, Ceelen W. The VEGFR Inhibitor Cediranib Improves the Efficacy of Fractionated Radiotherapy in a Colorectal Cancer Xenograft Model. Eur Surg Res. 2016;58(3-4):95-108.*

### ABSTRACT

**Background:** Radiotherapy (RT) increases local tumor control in locally advanced rectal cancer, but complete histological response is seen in only a minority of cases. Anti-angiogenic therapy has been proposed to improve RT efficacy by ‘normalizing’ the tumor microvasculature. Here, we examined whether Cediranib, a pan-VEGF receptor tyrosine

kinase inhibitor, improves microvascular function and tumor control in combination with RT in a mouse colorectal cancer (CRC) model.

**Methods:** CRC xenografts (HT29) were grown subcutaneously in mice. Animals were treated for 5 consecutive days with vehicle, RT (1.8 Gy daily), cediranib (6mg/kg PO), or combined therapy (cediranib 2 hours prior to radiation). Tumor volume was measured with calipers. Vascular changes were analyzed by dynamic contrast enhanced-MRI, oxygenation and interstitial fluid pressure probes and histology. To investigate vascular changes more in detail, a second set of mice were fitted with titanium dorsal skinfold window chambers, wherein a HT29 tumor cell suspension was injected. In vivo fluorescence microscopy was performed before and after treatment (same treatment protocol).

**Results:** IVM analyzes showed that VEGFR-inhibition with cediranib led to a 'normalization' of the vessel wall, with decreased microvessel permeability ( $p < 0.0001$ ), tortuosity ( $p < 0.01$ ) and a trend to decreased vessel diameters. This seemed to lead to lower tumor hypoxia rates in the cediranib and combination groups compared to the control and RT groups. This led to an increased tumor control in the combination group compared to controls or monotherapy ( $p < 0.0001$ ).

**Conclusions:** The combination of RT with cediranib enhances tumor control in a CRC xenograft mouse model. Microvascular analyses suggest that cediranib leads to vascular normalization and improved oxygenation.

## **INTRODUCTION**

Colorectal cancer (CRC) is the third most frequent cancer and the fourth most frequent cause of cancer related death worldwide [129]. Standard therapy consists of surgical resection with or without adjuvant chemotherapy or radiotherapy (RT). The addition of neoadjuvant RT has been shown to increase local tumor control and sphincter preservation in case of locally advanced rectal cancer (LARC), compared to surgery alone [130]. Nevertheless, this did not lead to a significant benefit in overall survival. Despite regimens combining RT with chemotherapy, complete histological response is seen in only a minority of cases and has been linked to patient's prognosis. As such, there is a need to enhance the efficacy of RT.

An important cause of radioresistance is related to the vascular tumor microenvironment [131]. Because tumor cells are highly proliferative, angiogenesis is stimulated to cope with the increased need for oxygen and nutrients. Tumor vessels are typically dilated, hyperpermeable and tortuous, and lead to an abnormal tumor microenvironment characterized by an increase in interstitial fluid pressure (IFP), hypoxia and acidosis, leading to chemo and radioresistance [8].

The key pro-angiogenic factor in tumor angiogenesis is vascular endothelial growth factor (VEGF). The VEGF family consist of 5 signal proteins, of which VEGF-A is the most important for angiogenesis. After binding with one of the three tyrosine kinase receptors, angiogenesis (VEGFR-1 and -2) or lymphangiogenesis (VEGFR-3) is stimulated. Activation of the VEGF signaling pathway has stimulating effects on endothelial cells (migration, survival and proliferation) and increases vascular permeability [37]. As such, inhibition of the VEGF signaling pathway is a promising way to rebalance tumor angiogenesis and 'normalize' the hostile tumor microenvironment, making tumors more acceptable for chemo and RT.

In this study, cediranib (AZD2171) was investigated, an orally active, highly potent tyrosine kinase inhibitor that acts on all 3 VEGF-receptors. Cediranib may lead to a more pronounced anti-angiogenic effect than for instance bevacizumab (Avastin), which specifically binds VEGF-A. Previous *in vitro* and *in vivo* experiments in colon, head and neck and non-small cell lung cancer models, demonstrated the inhibitory effects of cediranib monotherapy on tumor angiogenesis and tumor growth [132-135]. Clinical trials showed promising results for cediranib combined with chemotherapy in patients with metastatic CRC (mCRC), but results for progression free survival (PFS) and overall survival

(OS) were rather disappointing when compared to chemotherapy with bevacizumab (HORIZON trials) [136-138]. Yet, combination of cediranib and RT in CRC has not been studied except for one [139]. Williams et al. performed a mouse xenograft study (colon tumors (LoVo)) and illustrated a significant higher tumor growth inhibition with cediranib and RT compared to RT alone. Unfortunately, underlying anti-angiogenic effects were only studied in lung carcinoma xenografts.

Here we investigated the effects of combination treatment of fractionated RT and cediranib on tumor growth and tumor microvessels and microenvironment in a CRC xenograft mouse model. Understanding the potential enhancement of RT efficacy in CRC through VEGF signaling inhibition with cediranib is important for future clinical studies and could change neoadjuvant therapy regimens.

## **MATERIALS AND METHODS**

### **TUMOR MODEL**

The human colon cancer cell line HT29 was kindly provided by the Department of Experimental Cancer Research, Ghent University, Belgium. Cells were cultured at 37°C in 5% CO<sub>2</sub> humidified atmosphere in McCoy's Medium (Life Technologies, Ghent, Belgium), supplemented with 10% fetal bovine serum, penicillin-streptomycin and fungizone. Cells were authenticated by STR DNA profiling.

Animal experiments were approved by the Animal Ethical Committee of the Ghent University, Belgium (approval code 14/02). Athymic mice (Foxn1<sup>nu</sup> male) were obtained from ENVIGO, the Netherlands, and housed with access to tap water and standard pellet food. At 8 weeks of age, tumors were induced under general anesthesia (Isoflurane, 5% induction, 2% maintenance) at two locations: subcutaneously (SC) or in dorsal skinfold window chambers (DSWC). At the end of the experiments, or when humane endpoints were reached, mice were euthanized by cervical dislocation.

### **DSWC**

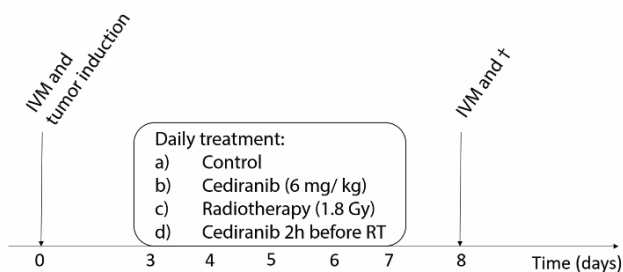
Under general anesthesia (Isoflurane) and analgesia (Ketoprofen, 5mg/kg, SC) DSWC were implanted on a heating pad. First, the posterior part of the titanium frame was sutured on the back of the mouse. Then, a circular skin flap (dermis and subcutis) was unilaterally removed and the anterior part of the frame was attached. The open wound was humidified

(saline water) and closed with a cover glass. After initial *in vivo* microscopy (day 0), tumor cells ( $1 \times 10^6$  HT29 cells suspended in  $20 \mu\text{L}$  Matrigel® (Corning BV, Amsterdam, the Netherlands)) were injected into the chamber (Fig 1.A).

## SC XENOGRAFTS

$1.5 \times 10^6$  HT29 cells suspended in  $40 \mu\text{L}$  Matrigel were injected (30G needle) bilaterally SC in the hind legs of the animal. One nodule was used for DCE-MRI imaging and immunohistochemistry, the other for probe measurements. Pimonidazole hydrochloride (Hypoxyprobe®, Burlington, MA, USA) ( $60 \text{mg/kg}$ , IP), a hypoxia marker, and Hoechst®-33342 (Sigma- Aldrich, Diegem, België) ( $15 \text{mg/kg}$ , IV), used as perfusion marker, were administered in the tail vein 2 hours and 1 minute before sacrifice, respectively. Tumor dimensions were measured weekly with calipers and daily during therapy. Tumor volumes (V) were calculated as  $V = (\text{length} * \text{width})^{3/2} * \pi/6$  (Fig 1.B).

### A. Dorsal skinfold window chamber tumors



### B. Subcutaneous xenograft tumors

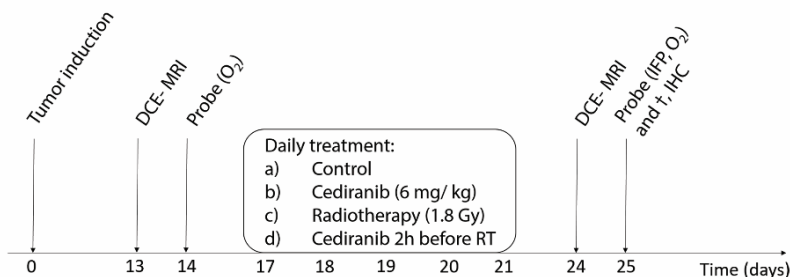


**FIGURE 1: Experiment timeline.** (A) Induction of HT29 tumors in DSWC in mice at day 0. Four treatment groups. Daily treatment from day 3 to 7. IVM before and after treatment. Euthanasia after last measurement. (B) Induction of HT29 tumors subcutaneous in the hind legs of mice at day 0. Four

treatment groups. Daily treatment from day 17 to 21. DCE-MRI and pO<sub>2</sub> measurements before and after treatment. IFP measurement after treatment. Euthanasia after last measurement.

## EXPERIMENTAL THERAPY

Treatment was started at day 3 (DSWC) and day 17 (SC xenograft) after tumor induction and given for 5 consecutive days (Fig 1). Mice were divided into 4 groups. A control group received 150 µl of 1% Polysorbate 80 orally once daily. A second group received cediranib (Recentin™, AZD2171, Astra Zeneca, Brussels, Belgium) (6mg/kg/day, orally). The third group received RT at a dose of 1.8 Gy/day, while the fourth group was treated with combined cediranib and RT with cediranib administered 2 hours before RT. Cediranib was dissolved in 1% polysorbate 80 (tween 80) with deionised water and sterilised by autoclaving.

RT was applied using the small animal radiation research platform (SARRP, XStrahl LTD, Surrey, UK). Mice were anesthetized and positioned on the bed of the SARRP. Guided by lasers, the bed was moved to position tumors/DSWC at the isocenter of the beam. A pair of parallel- opposed (anterior- posterior) radiation beams of 10x10mm<sup>2</sup> were used. The voltage of the X-ray source was fixed at 220 kV with a tube current of 13 mA, emitted from the 3 mm focal spot and filtered by a copper filter of 0.15 mm. Doses of 1.8Gy were delivered daily for 5 consecutive days.

## EXPERIMENTAL MEASUREMENTS

### *IN VIVO MICROSCOPY (IVM)*

Fluorescence IVM was performed on day 0 and day 8 after tumor implantation. Mice were anesthetized (Isoflurane) and positioned on a heating pad. A catheter (30G) was placed in the tail vein for administration of fluorescent tracer, the cover slip was removed from the chamber and the animal was placed under the microscope (modified BX51W, Olympus, Aartselaar, Belgium). In case of dehydration of the chamber, saline water was locally applied. Mice received a bolus of 30 µL of IV Fluorescein isothiocyanate (FITC)-dextran (MW 40 kDa) in NaCl 0.9% (20 mg/mL). At the same time, registration of images (dynamic and static) started (magnification 100x). Fluorescence microscopy was performed using a HBO 50W mercury lamp (Osram, Zaventem, Belgium) and a FITC filter set (excitation filter 460-490nm). Images were saved on a computer using a high sensitivity digital camera (model C8484-05, Hamamatsu, Louvain-la-Neuve, Belgium). To analyze vascular

permeability, one location was imaged over 15 minutes at 4 time intervals (0'-0'30"; 1'30"-2'00"; 4'30"-5'00"; 15'00"-15'30"). Two other locations were imaged (each 30") at the right upper and left lower quadrants of the tumor.

### ***MICROCIRCULATORY ANALYSIS***

Off-line analysis was performed with the CapImage software package (H Zeintl Engineering, Heidelberg, Germany) and included the calculation of: number of microvessels per area (N/A, count/mm<sup>2</sup>), microvessel diameter (d, μm) and centerline red blood cell velocity (V<sub>RBC</sub>, mm/s). Microvessel diameter and V<sub>RBC</sub> were analyzed for 10 randomly chosen microvessels of interest crossing a vertical line in the middle of the image at 3 locations, as described previously [140]. Considering the parabolic velocity profile of blood in microvessels, the volumetric blood flow (VQ) was calculated by  $VQ = \pi * (d/2)^2 * V_{RBC}/K$ , where K (=1.3) represents the Baker/Wayland factor [141]. Post- to pre-treatment rates were calculated and compared between groups. Additionally, microvessel tortuosity (T) and mean interstitial fluorescence intensity (MFI<sub>inter</sub>) were calculated with the NIH ImageJ software (Version 1.48, available from <https://imagej.nih.gov/ij/>). T was calculated from 6 randomly chosen microvessels at 3 locations and was defined as T (%) = (1-SP/L)\*100, where SP represents the shortest distance between 2 branching points (i.e. the distance between two branching points along a straight line) and L represents the segment length (i.e. the distance between the branching points along the vessel), according to Norrby et al [142]. MFI<sub>inter</sub> was calculated from 10 randomly chosen regions-of-interest (ROIs) that were drawn in the interstitial space at 3 locations. Using the TimeSeriesAnalyzer plugin, the mean fluorescence intensity (=mean grey value) was calculated as a function of time and curve analysis was performed.

### ***DYNAMIC CONTRAST-ENHANCED MRI (DCE-MRI)***

Animals were scanned before and after treatment (day 13 and 24) on a 7 tesla magnet (PharmaScan 70/16, Bruker, Ettlingen, Germany) with a mouse body volume coil. Mice were anesthetized with isoflurane (5% induction, 1.5% maintenance, 0.3L/min) and warmed with a water-based heating blanket. Respiration was monitored using a respiration pad underneath the mouse. Anatomical information was obtained with a T2-weighted sequence (TurboRARE) with the following parameters: TR 3661ms, TE 37.1ms, in-plane resolution 109 μm, 30 contiguous transverse sections of 600 μm, and acquisition time 9'1".

Pre- and post-contrast injection, T1-weighted images were obtained with a RARE sequence with parameters TR 1464 ms, TE 9.1 ms, in-plane resolution 117  $\mu\text{m}$ , 30 contiguous sections of 600  $\mu\text{m}$ , and acquisition time 4'17". DCE-MRI images were acquired for a single slice using a FLASH sequence with the following parameters: TR 12 ms, TE 3.4 ms, in-plane resolution 268  $\mu\text{m}$ , 550 repetitions, temporal resolution 1.344 seconds, and acquisition time 12'19". An oblique slice was chosen such that both tumors were imaged. One minute after the start of acquisition, the gadolinium-based contrast agent Vistarem® (50 mmol/kg IV, Guerbet, Villepinte, France) was injected. Total acquisition time per session was 35 minutes. Dynamic time series were analyzed with MIStar version 3.2.62.03 (Apollo MIT, Melbourne, Australia) using curve analysis. The following parameters were calculated: area under the curve (AUC), maximum uptake slope (MUS), maximum washout slope (MWS), area under the curve until time to peak (rAUC ttp). ROIs were manually drawn around tumors (ROI) and mean values were calculated.

### *TISSUE OXYGENATION AND INTERSTITIAL FLUID PRESSURE*

At day 14 and 25, tumor oxygenation was measured with a fluorescence based fiberoptic probe (OxyLite System, Oxford, Optronix, Oxford, UK), as described previously [143]. Mice were anesthetized and placed on a heating pad. The probe was inserted in the tumor through pre-tunneled tracks (18G IV catheter BD) and fixed to a micromanipulator (model MN151, Narishige International Ltd, London, UK). Tissue  $\text{pO}_2$  was sampled every spatial step of 200  $\mu\text{m}$  for 3 minutes, up to 25 measurements. Data was acquired with a Powerlab/8sp (ADInstruments, Oxford, UK) and plotted using Chart 5.0 software. The hypoxic fraction was calculated as the percentage of measurements with a  $\text{pO}_2 < 5$  mmHg (HP5 (%)).

Interstitial fluid pressure (IFP) was measured at day 25, with a Samba Preclin probe (Samba Sensors, Bioseb, Vitrolles, France) according to the method reported by Ozerdem [144]. The probe was calibrated in air, and inserted in a perforated catheter (22G IV Catheter Insyte-W, Becton Dickinson) filled with gel (Duratears, Alcon). The system was placed in the tumor center through a pre-tunneled track. After acquiring a stable curve, tumor IFP (relative to the atmosphere, mmHg) was recorded during 5 minutes and mean pressures were calculated (Samba 200 SP v1.0.1).



## *IMMUNOHISTOCHEMISTRY (IHC)*

Tumors were excised and divided in half. One part was impregnated with formaldehyde 4%, embedded in paraffin and cut in 5  $\mu\text{m}$  thick sections using a microtome (Microm HM355S, Thermo Scientific, Rockford, IL, USA). Tumor regions were identified and general aspects (necrosis, cell density...) were evaluated on H&E stained slides with a light microscope (ColorView I, BX43F, Olympus, Tokyo, Japan). Standard Ki67 staining was carried (primary rabbit monoclonal anti-human/rat/mouse Ab Anti-Ki67 [SP6] (ab16667) and HRP anti-rabbit secondary Ab, both DAKO K4011). Proliferation indices (fraction of Ki67+ cells/total cells) were calculated by hotspot analysis (6 per slide, magnification 400x) with ImmunoRatio (Institute of Biomedical Technology, University of Tampere, Finland). Additionally, exogenous administered pimonidazole was stained. Sections were deparaffinized in xylene and rehydrated in ethanol. Antigens were unmasked with citrate buffer (pH=6, 20 min, 95 °C). Endogenous peroxidase was blocked with 3% H<sub>2</sub>O<sub>2</sub> in PBS (10 min at RT) and mouse IgG with the Mouse on Mouse (M.O.M.) basic kit (1hour at RT, ref. BMK-2202 Vector Lab.). Then, the primary antibody was applied, Hypoxyprobe anti-pimonidazole mouse IgG1 monoclonal Ab (HP1-100Kit) for 1h at room temperature followed by the secondary antibody from LSAB+ System-AP kit (DAKO K0675(11)) according to manufacturer's protocol. Hypoxic fraction (% pimonidazole+ area/total tumor area) was calculated with ImageJ (NIH).

Furthermore, staining for endothelial cells (CD105, endoglin) was performed. Deparaffination, rehydration, unmasking and blocking (endogenous peroxidase) were performed as described above. Then, proteins were blocked with blocking buffer (from Vectastain kit, AP Goat IgG AK-5005) for 30 min at 37°C. Primary antibody for endoglin (monoclonal goat anti-mouse, CD105 R&D system AF1320) was applied at 1/50 in TBS and blocking buffer, according to the manufacturer's protocol. Secondary antibody was applied from Vectastain kit (AP Goat IgG AK- 5005) for 30 min and streptavidin-AP was applied for 30 min. Detection was performed with fuchsin chromogen for 1min at room temperature (RT) and counterstaining with hematoxylin. Mean vessel density (MVD, number of vessels per area (mm<sup>2</sup>)) was calculated by hotspot analysis (up to 6 hotspots per slide, magnification 200x) with ImageJ (NIH).

In addition, TUNEL staining was performed to detect apoptosis. Deparaffination and rehydration were performed as described above. Antigens were unmasked with citrate buffer (pH=6, 20min, 95°C, + 0.1% Tween 20). Then, the In-Situ Cell Death Detection Kit,

Fluorescein, (Roche 11684795910) was used according to manufacturer's protocol to perform the TUNEL reaction. Counterstaining was performed with Vectashield medium with DAPI. Sections were analyzed with the fluorescence microscope (Zeiss Axiovert 200M, software Axiovision 4.1), 6 random fields with magnification were selected and the percentage of double stained cells (TUNEL+ and DAPI+) on all DAPI+ cells was calculated.

The other part of the tumor was snap frozen (-80°C). Ten  $\mu\text{m}$  cryostat sections were prepared and evaluated for Hoechst staining with fluorescence microscopy. Whole tumor sections were scanned at magnification 400x and the perfusion index (Fraction of perfused area/total tumor area) was calculated using ImageJ (NIH).

## STATISTICAL ANALYSIS

Statistical analysis was performed with GraphPad Prism 6 (Graphpad Software, Inc.: La Jolla, CA, USA). Data were analyzed with non-parametric tests (Kruskal-Wallis and Mann Whitney U test) and summarized as medians. Tumor growth and microvessel permeability were determined by non-linear regression analysis (exponential growth and one-phase association). Results were considered statistically significant when the probability of a type I error was  $\leq 0.05$ .

## **RESULTS**

### EFFECT OF CEDIRANIB AND RT ON TUMOR GROWTH AND PROLIFERATION

Tumor growth was calculated from the measurements of SC tumors. Addition of cediranib to RT led to a significantly increased growth delay compared to RT alone with an increase in tumor doubling time from 13.16 days with RT alone to 27.13 days with combination treatment ( $p < 0.0001$ , Fig. 2A). In addition, cediranib monotherapy and RT monotherapy led to a similar growth inhibition compared to controls.

Addition of cediranib to RT led to moderately higher apoptotic rates compared to RT alone (Fig 2.B, D above). Alternatively, cediranib and RT led to somewhat higher proliferation rates, while the combined treatment led to significantly higher proliferation rate compared to controls ( $p < 0.05$ ) (Fig 2.C, D under). The control group had the densest tumors, with the least necrotic areas. All treatment groups showed diffuse areas with less tumor cell density,

probably due to treatment induced cell death followed by cell loss. The combination treatment group had the least cell-dense tumors.

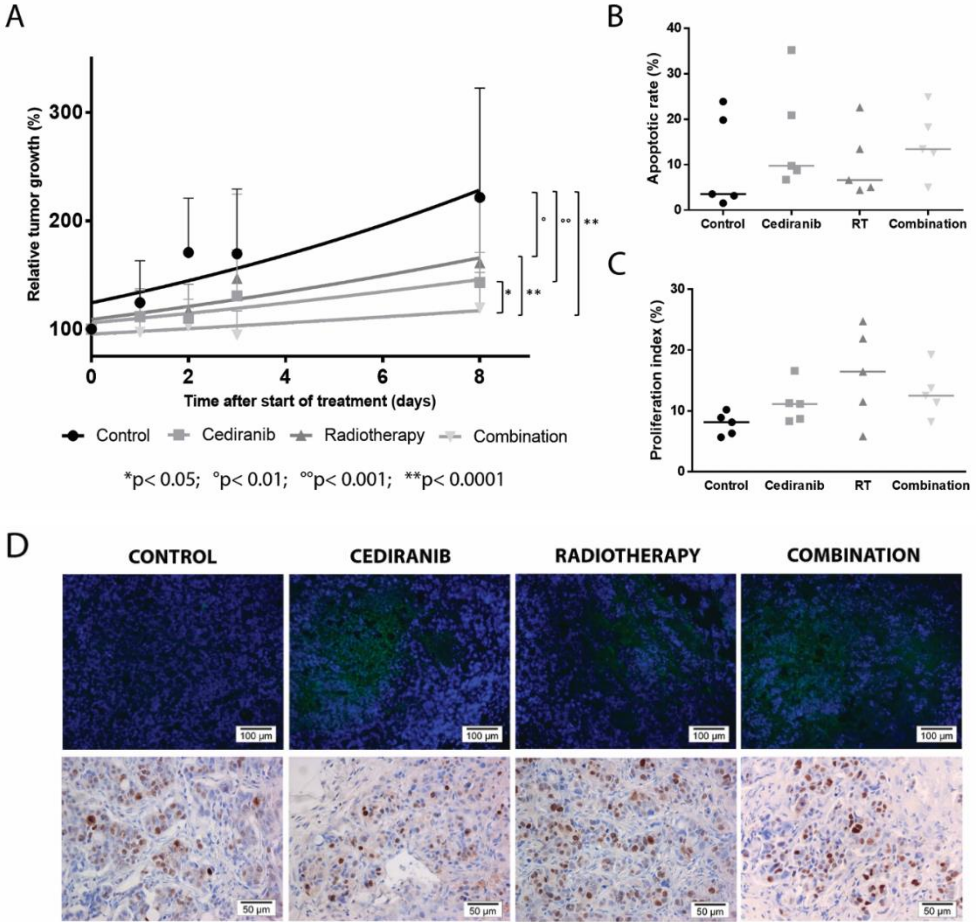


**FIGURE 2: Tumor growth.** (A) Relative tumor growth of subcutaneous HT29 tumors. Exponential growth curves, mean, standard deviation. (B) Apoptotic rates calculated from TUNEL staining. Percentage of TUNEL positive stained cells on the total cell count.  $p = 0.5208$ , single values, median. (C) Proliferation rates calculated from Ki67 staining. Percentage of Ki67 positive stained cells on the total cell count.  $p = 0.0772$ , single values, median. (D) Representative images of TUNEL staining (above) and Ki67 staining (under) of each treatment group. Above: green= TUNEL positive cells, blue= DAPI positive cells. Magnification 200x, scale bar 100 $\mu$ m. Compared to controls, treatment groups show more apoptosis. Under: brown= Ki67 positive cells. Magnification 400x, scale bar 50 $\mu$ m. No difference in Ki67 staining between the groups is seen at first sight. After quantification, the combination treated group shows significant higher proliferation rates than controls ( $p < 0.05$ ).

## EFFECT OF CEDIRANIB AND RT ON TUMOR VASCULATURE

Figure 3 shows representative pictures of a DSWC of each treatment group, illustrating that the cediranib and combination groups (Fig 3.C-D) displayed more linear and less dilated vessels than the control and RT groups (Fig 3.A-B), whereas microvessel density did not differ greatly between the groups.

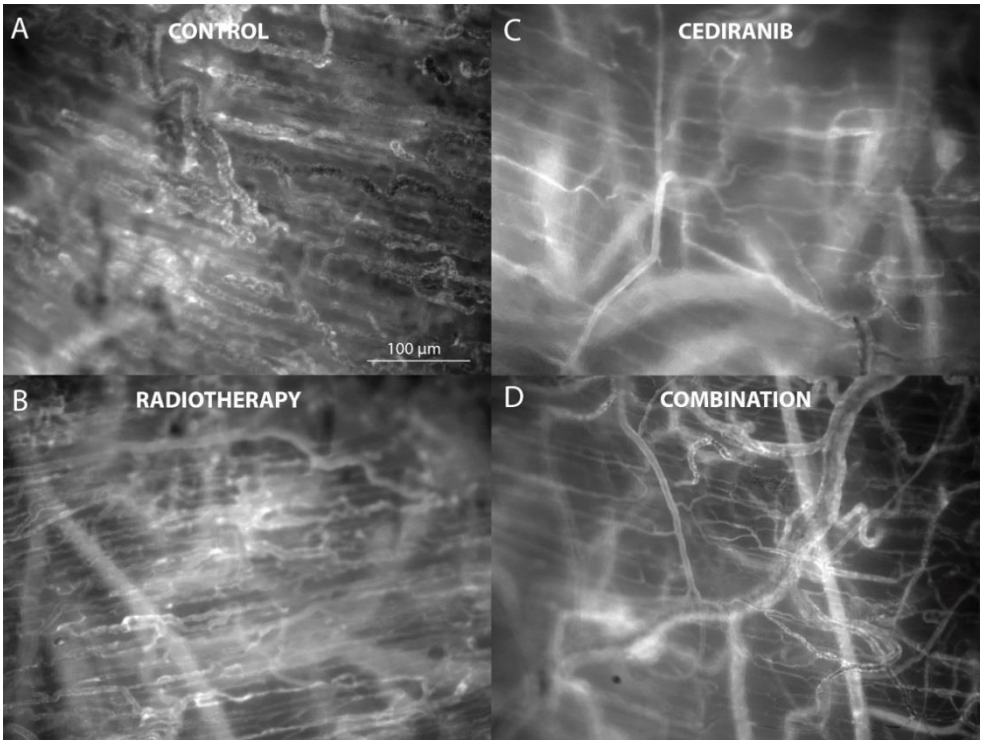


**FIGURE 3: *In vivo* microscopy.** (A-D) DSWC images after 5 days of treatment. Representative images of each treatment group. Magnification 100x, scale bar 100µm. Vessels of the control and radiotherapy group appear to be more tumoral (more tortuous, more dilated) than those of the groups treated with cediranib.

Quantification of these DSWC with the additional histologic and DCE-MRI analyses of the SC xenografts led to the following results on tumor vasculature. Cediranib and RT did not lead to a change in vessel density calculated from the DSWC (N/A, Fig 4.A) or calculated from the endoglin stained sections in the SC xenograft group (MVD, Fig 4.B, E). Further, no difference was seen between the groups in volumetric blood flow (VQ, Fig 4.C) or tumor perfusion (Hoechst, Fig 4.D). Curve analysis of DCE-MRI did not show any differences

100

between the groups for the amount of leaked contrast (AUC, rAUC ttp), the velocity of leakage (MUS) or the velocity of washout of contrast (MWS) (Fig 5. A-D).

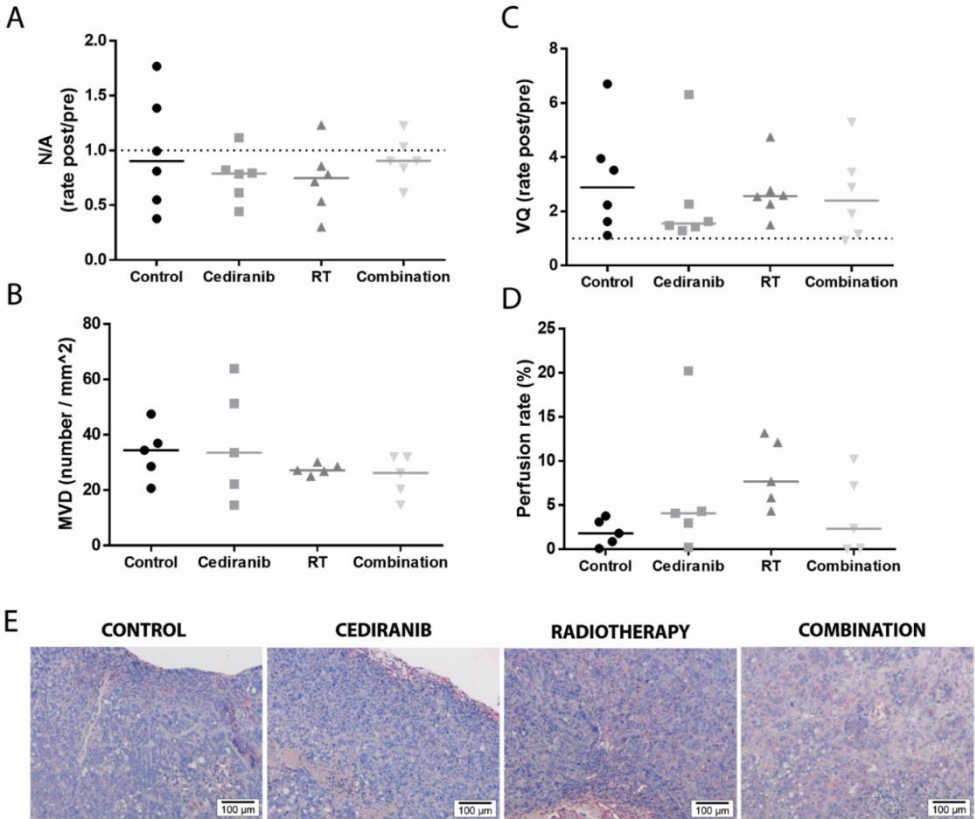


**FIGURE 4: Tumor vessel density and tumor perfusion.** (A) Number of vessels per area (N/A) calculated from IVM images.  $p=0.4563$ , post- to pre-treatment rate, single values, median. (B) Mean vessel density (MVD) calculated from endoglin stained sections of SC tumors. Number of vessels per area ( $\text{mm}^2$ ).  $p=0.4320$ , single values, median. (C) Volumetric blood flow (VQ) calculated from IVM images.  $p=0.6251$ , post- to pre-treatment rate, single values, median. (D) Perfusion rate calculated from Hoechst stained sections of SC tumors. Percentage of Hoechst positive stained area on total tumor area.  $p=0.0637$ , single values, median. (E) Representative images of endoglin staining of each treatment group. Pink= endoglin. Blue= cell nuclei. Magnification 200x, scale bar 100 $\mu\text{m}$ . No difference in number of vessels is seen between the groups.

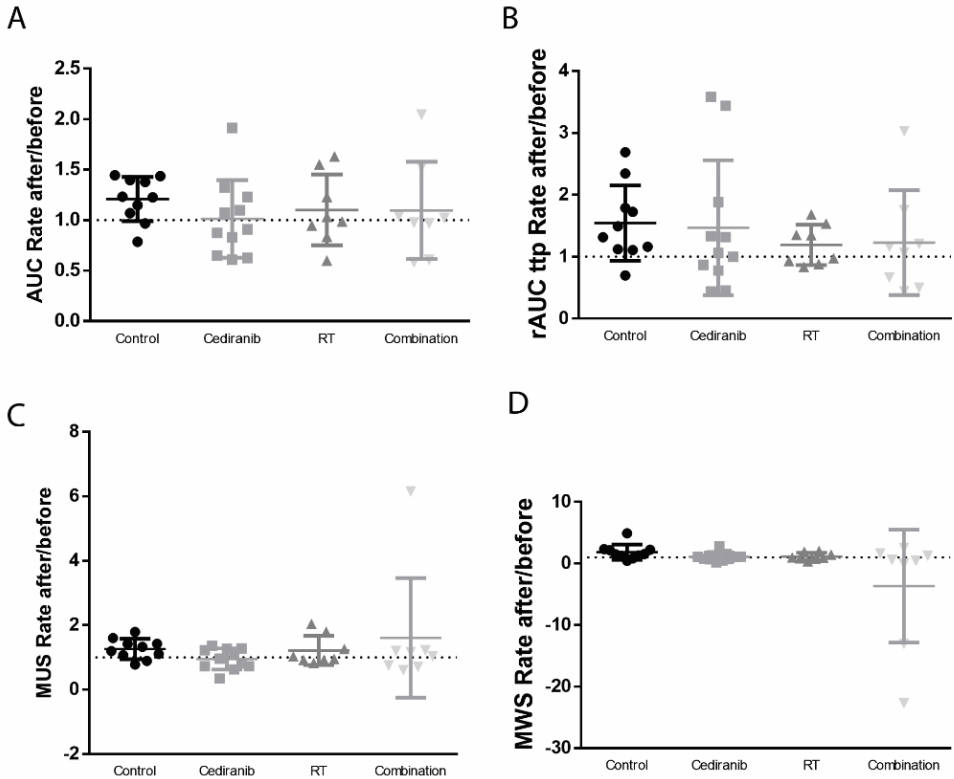


**FIGURE 5: DCE-MRI analyses.** (A) Area under the curve.  $p = 0.6804$ , post- to pre-treatment rate, single values, median. (B) Area under the curve until time to peak.  $p = 0.5190$ , post- to pre-treatment rate, single values, median. (C) Maximum uptake slope.  $p = 0.3119$ , post- to pre-treatment rate, single values, median. (D) Maximum washout slope.  $p = 0.1180$ , post- to pre-treatment rate, single values, median.

However, cediranib led to a significant decrease in vessel permeability compared to the control or RT group ( $p < 0.0001$ ) calculated from the DSWC imaging data ( $MFI_{inter}$ , Fig 6). As can be seen in Fig 6, there was a relatively fast accumulation of contrast agent (CA) in the interstitial space during the first time interval (0'' – 30''), reaching a plateau phase at the second time interval (1'30''–2'00'') that persisted at the 2 latest time points (4'30'' and 15'00''). The washout phase was not observed.

Moreover, cediranib led to a significant decrease in microvessel tortuosity (T, Fig 7.A) ( $p < 0.01$ ) and cediranib inhibited, although moderately, dilatation of microvessels compared to the control group (Fig 7.B).

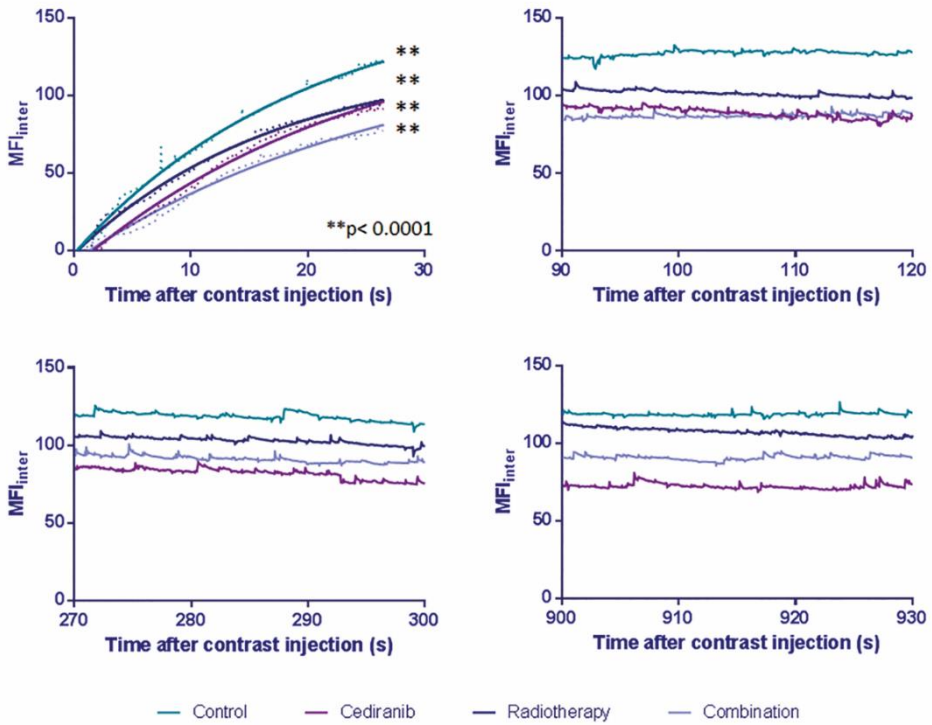


**FIGURE 6: Tumor vessel permeability.** Mean interstitial fluorescence intensity at 4 time intervals: immediately after contrast injection, 90', 270' and 900' after contrast injection.

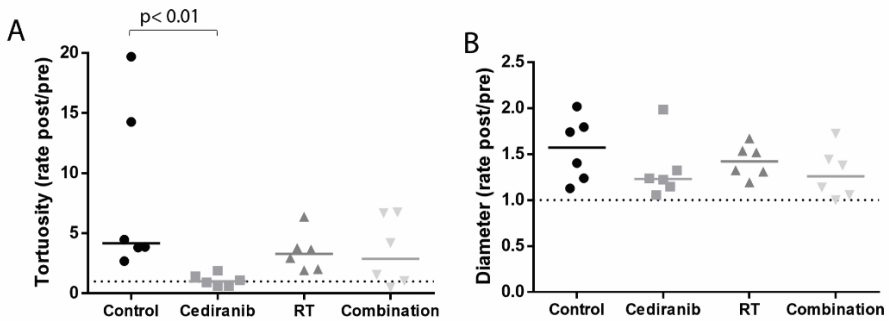


**FIGURE 7: Tumor vessel tortuosity and diameter.** (A) Tumor vessel tortuosity calculated from IVM images.  $p < 0.05$ , post- to pre-treatment rate, single values, median. (B) Tumor vessel diameter calculated from IVM images.  $p = 0.3551$ , post- to pre-treatment rate, single values, median.

## EFFECT OF CEDIRANIB AND RT ON TUMOR MICROENVIRONMENT

Lower tumor hypoxia rates were observed in the cediranib and combination groups compared to the control and RT groups (HP5%, Fig 8.A). Furthermore, addition of cediranib to RT led to a significant decrease in tumor hypoxia ( $p < 0.05$ ) (pimonidazole, Fig 8.B).

Surprisingly, cediranib led to a significant increase in IFP compared to RT ( $p < 0.05$ ) while RT decreased IFP in comparison to the controls (Fig 8.C).

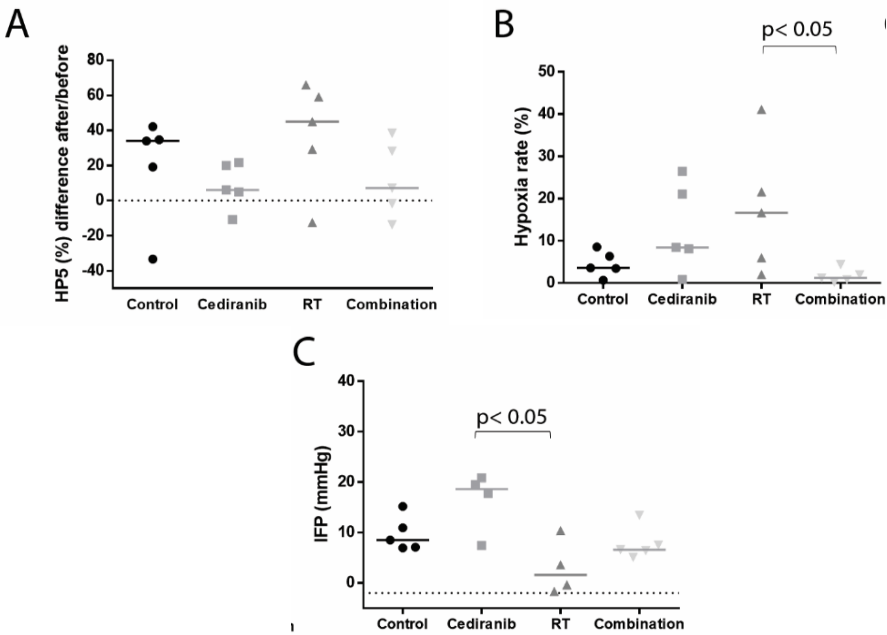


**FIGURE 8: Tumor microenvironment.** (A) Tumor hypoxia calculated from OxyLite probe measurements of SC tumors. Hypoxic fraction ( $\% < 5 \text{ mmHg pO}_2$ ).  $p = 0.2418$ , difference after-before, single values, median. (B) Tumor hypoxia calculated from pimonidazole stained sections of SC tumors. Percentage of hypoxic area on total tumor area.  $p < 0.05$ , single values, median. (C) Tumor interstitial fluid pressure calculated from Samba Preclin probe measurements of SC tumors.  $p < 0.05$ , single values, median.



## **DISCUSSION**

This study investigated the effect of combining fractionated RT with cediranib, a pan-VEGF-receptor tyrosine kinase inhibitor, in a human CRC mouse model. For the first time, the underlying microvascular changes of this combined treatment in CRC were evaluated *in vivo*.

Cediranib was shown to successfully enhance tumor growth inhibition of RT ( $p < 0.0001$ ) and to increase, although moderately, tumor cell apoptosis. Only one previous study was performed on the combined effect of RT and cediranib in CRC [139]. Mice with SC xenografts (human LoVo cell line) were treated with RT (2Gy/ day, for 5 days) and cediranib (6mg/kg, continued for 28 days in total). Similar to our study, improved tumor growth inhibition was seen during combined treatment and continued cediranib treatment. Unfortunately, underlying microvascular changes were not investigated.

One proposed and frequently debated mechanism is the one of microvessel normalization [41]. Inhibition of VEGF-signaling may induce 'normalization' of tumor microvessels, which could lead to better perfusion and oxygenation of tumor tissue. Because oxygen is important for the generation of free radicals and DNA damage, oxygenated tumor tissue reacts 2- 3 times better to RT than hypoxic tumor tissue [25, 145]. As such, microvessel normalization might sensitize tumors for RT. This study focused on the *in vivo* imaging of these vascular changes and normalization. First, microvessels were shown to be significantly less tortuous ( $p = 0.0066$ ) after cediranib treatment. Second, microvessels had moderately smaller diameters after cediranib treatment and third, cediranib decreased vessel permeability ( $p < 0.0001$ ). As previously proposed in other xenograft studies [134, 139, 146, 147], this suggests cediranib induces clear changes in microvessel structure and leads to a normalization of the microvessel wall. For the first time, these changes were imaged *in vivo* with DSWC in CRC.

Single high dose RT (10-30 Gy) is known to have anti- angiogenic effects with disappearance of small tumor vessels in the acute phase and stimulation of tumor angiogenesis at long-term (after 14 days) [148]. Yet, nothing is known about the effect of fractionated RT and cediranib on tumor microvasculature in CRC. Our results suggest that fractionated radiation (5 x 1.8 Gy) has no immediate anti-angiogenic effects like single high dose RT. This is illustrated in figure 3 where the control and RT treated tumors clearly show tumor vessel structures, in contrast to the cediranib and combination treated group, that appear to have a more normal vessel structure. The underlying pathways were not

investigated but are suggested to be divergent. VEGF-inhibition with cediranib inhibited these pro-angiogenic effects only partially. A new study will be started in the near future to investigate microvasculature after single high dose RT versus fractionated RT.

These observed microvascular changes are thought to lead to changes in tumor microenvironment. Indeed, cediranib decreased tumor hypoxia, which explains the lower radioresistance and the enhanced tumor growth delay. The fact that addition of cediranib to RT led to a decrease in tumor hypoxia compared to RT alone could be due to a better response to RT (higher apoptotic rate in combination treated group) followed by a decrease in oxygen consumption. The increased proliferation rates of tumors in the combined treatment group could be due to the same mechanism of a proportional increased proliferative potential of tumor cells that survived treatment. The effect of this proportional increased proliferation remains to be investigated in future studies with longer follow-up.

With respect to the interstitial fluid pressure, it is known that most solid tumors show an increased IFP (normal tissue: IFP= -1 to -3mm Hg [149, 150]) due to vessel abnormalities, fibrosis and contraction of the interstitial matrix [151]. Certain VEGF signaling pathway inhibitors, such as bevacizumab, lead to normalization of this raised IFP [152]. This was the first study to investigate the effect of cediranib on IFP. Surprisingly, cediranib led to a significant increase in IFP compared to RT. This might be due to the inhibitory effect of cediranib on lymphangiogenesis through VEGFR-3 inhibition. Indeed, it has been shown previously that stimulation of VEGFR-3 through VEGF-C decreases IFP [153].

Remarkably, 3 days after cessation of therapy, the reduction in vessel permeability was not visible anymore (DCE-MRI). A similar study, where DCE-MRI was performed immediately after administration of cediranib (2h), could demonstrate a reduction of 70% in permeability surface area product per unit volume of tissue (parameter for permeability) [147]. These findings support the fact that cediranib leads to rapid changes in microvasculature, described as a 'window of normalization' [8], which disappear after cessation of therapy. These fast changes underscore the importance of treatment timing and *in vivo* measurements of treatment effects.

This study emphasizes the potential benefits of further investigating the role of cediranib in a neoadjuvant setting in locally advanced rectal cancer, combined with RT. Several phase II trials with bevacizumab and neoadjuvant radiochemotherapy have been performed in LARC [154, 155]. So far, results were not very promising with increased toxicities and

increased post- operative morbidity as major obstacles. Whether cediranib will do better, is to be investigated.

## **CONCLUSION**

We showed that the combination of fractionated RT with the VEGFR- inhibitor cediranib enhances tumor control in a colorectal xenograft model. In addition, the imaged structural and functional vascular changes suggest that cediranib has a stabilizing effect on the vessel wall leading to vascular normalization.



**CHAPTER 7**  
**GENERAL DISCUSSION AND**  
**CONCLUSION**



## **CHAPTER 7: GENERAL DISCUSSION AND CONCLUSION**

Our objective was to study hypoxia in solid tumors and use it as a biomarker and target for individualized therapy.

We started by describing the development of an EAC tumor model in chapter 3. Two generally available EAC cell lines were used, OE33 and OACM5 1.C and injected at an ectopic (subcutaneous, hind legs) or orthotopic site (distal esophageal wall through midline laparotomy). We also evaluated different *in vitro* functional cell line characteristics such as invasiveness or cell-cell adherence. We could conclude that the OE33 cell line has high subcutaneous and orthotopic tumor take rates, but that tumors grew extremely slow. Further, the OACM5 1.C cell line was not appropriate for tumor development in our tumor model. However, we succeeded to develop a daughter cell line of OACM5 1.C through an *in vivo* selection technique, that was named OACM5 1.C SC1, which had improved tumor take rates and faster growing tumors. Taken these results together, we had a reliable orthotopic and subcutaneous EAC tumor model to perform further preclinical research on.

The use of a xenograft model could be a point of criticism. This choice was based on a careful study of literature on esophageal carcinoma tumor models and after weighing pros and cons. A diversity of esophageal tumor models in a diversity of laboratory animals (rat, mouse, rabbit...) exist. The number of ESCC models overshadows the limited number of EAC models and no ideal EAC model has been developed yet [88, 156].

On the one hand, a syngeneic EAC model could be used. These use immunocompetent animals and might more closely mimic carcinogenesis with its tumor-host immune interactions. With respect to EAC, no syngeneic cell line is available for laboratory animals, but a transgenic model is available in mice (GEMM genetically engineered mouse model [107]) and different reflux models [157, 158] and carcinogen or diet-induced models (e.g. caustic agents to cause inflammation of the esophagus) have been described. Disadvantages of these syngeneic models are that tumor development is unpredictable and seen in a late stage (time-consuming), and that no human tissues are investigated which can impede translation of the results to the clinical setting.

On the other hand, xenograft models can be used where human cancer material is injected/implanted in immunodeficient animals (orthotopic or ectopic). More and more

interest is growing for patient derived xenografts (PDX), because tumor heterogeneity is better preserved and because they retain the structure and stromal components of the original tumor better compared to continuous human cancer cell lines [159]. Xenograft models are easy and the timing of tumor development can be approximately predicted. The major disadvantage is the use of immunodeficient animals with loss of tumor-host immune interactions.

Taking into account all these aspects, we can support our choice to use a xenograft setting, where tumor development is consistent and can be more or less predicted.

The next step was to test the feasibility of the hypoxia tracer  $^{18}\text{F}$ -FAZA in both tumor models, which was described in chapter 4. We encountered a problem of diffuse background activity in the liver and intestines which compromised accurate visualization of tumors in those regions (EAC at the distal site of the esophagus and gastro-esophageal junction). Background activity was also seen in the urinary bladder and gall bladder, but this was of lesser importance for our model. As was already mentioned previously, this is due to the tracer characteristics.  $^{18}\text{F}$ -FAZA is metabolized hepatically and excreted via the intestines and kidneys [62]. One could question why not switch to another tracer. Table 1 gives an overview of the principal radiopharmaceuticals applied in hypoxia PET imaging with its applications, advantages and disadvantages. As can be seen, a range of tracers has been developed in the search for the most specific hypoxia tracer with the highest tumor-to-background rates. Four big families, based on 4 uptake mechanisms can be identified. The first family of tracers is  $^{18}\text{F}$ -FDG, where uptake is based on the Pasteur effect, with low hypoxia specificity. The second family are the nitroimidazoles which were discussed in the introduction of this thesis. These have been studied extensively and already reached clinical evidence. However, these face the problem of having to cross the phospholipid bilayer and at the same time the need to be hydrophilic, as to rapidly clear from background tissues. The third family are the ones based on reduction of Cu-ATSM, but some doubt exists for the hypoxia specificity [52]. And as last, the recognizers of CA9, a transmembrane protein in hypoxic conditions, which have not been studied much, but seem promising because no crossing of the phospholipid bilayer is needed. In this field of hypoxia tracers, FAZA is the second most studied one, after FMISO, and has proven to be superior to FMISO concerning tumor-to-background rates. Taken together this information, we believe FAZA is one of the leading contenders in reaching a clinical applicability for hypoxia imaging and believe



research should continue to confirm this. We expect that the delineation of distal esophageal tumors would be easier in the clinical setting than in mice because of the larger structures and better soft tissue resolution on clinical applications. Therefore, we continued in the following chapter with the evaluation of  $^{18}\text{F}$ -FAZA as a predictor for radiation response in the subcutaneous EAC model.

Uptake mechanism	Tracer	Tumors imaged
Pasteur effect (anaerobic glycolysis) [25]	<sup>18</sup> F-FDG ( <sup>18</sup> F-fluorodeoxyglucose)	NSCLC [23, 27, 32, 37] Head and neck tumors [31] Oral squamous cell carcinoma [40, 41] Gastric cancer [39]
Nitroimidazole-like uptake: reduction into RNO <sub>2</sub> radicals and RNHOH compounds in hypoxic conditions. Then covalent binding to macromolecules [21, 59]	<sup>18</sup> F-MISO ( <sup>18</sup> F-fluoromisonidazole)	Head and neck tumors [35, 42-45] Locally advanced HNSCC [35, 46] Glioblastoma multiforme (GBM) [37, 47, 48] Breast cancer [49] NSCLC [32, 33, 50] Renal cell carcinoma [51]
	<sup>18</sup> F-FAZA ( <sup>18</sup> F-fluoroazomycin-arabinozide)	Head and neck tumors [52, 53] Cervical cancer [54] Prostate cancer [55] NSCLC [56, 57] Rectal cancer [58]
	<sup>18</sup> F-FETNIM ( <sup>18</sup> F-fluoroerythronitroimidazole)	NSCLC [60] Esophageal cancer [61]
	<sup>18</sup> F-EF5 ( <sup>18</sup> F-2-nitroimidazol-pentafluoropropyl acetamide)	Brain tumors [62] Soft tissue sarcoma [63] Head and neck tumors [64]
	<sup>18</sup> F-EF3 ( <sup>18</sup> F-2-nitroimidazol-trifluoropropyl acetamide)	Rats bearing syngeneic rhabdomyosarcoma tumours [65] Head and neck tumors [66]
	<sup>18</sup> F-FETA ( <sup>18</sup> F-fluoroetanidazole)	Mice bearing MCF-7, RIF-1, EMT6, HT1080/26.6, and HT1080/1-3C xenografts [67, 68]
	<sup>124</sup> I-IAZG ( <sup>124</sup> I-iodoazomycin galactopyranoside)	Hepatocellular carcinoma [69]
	<sup>68</sup> Ga-labeled nitroimidazole analogs ( <sup>68</sup> Ga-NOTA-nitroimidazole, <sup>68</sup> Ga-DOTA-nitroimidazole, <sup>68</sup> Ga-SCN-NOTA-nitroimidazole)	Tumor xenografted mice [70, 71]
Reduction of Cu(II)-ATSM complex into Cu(I)-ATSM and dissociation of Cu(I) in hypoxic conditions: then Cu(I) nuclide binding to intracellular proteins [77]	<sup>60,61,62,64</sup> Cu-ATSM ( <sup>60,61,62,64</sup> Cu-diacetyl-bis(N4-methylthiosemicarbazone)	Tumor xenografted rats/mice (a,b,c) Lung cancer (d,e,f) Head and neck cancer (g,h,i) Esophageal cancer (j) Pancreatic cancer (j)
	<sup>60,61,62,64</sup> Cu-ATSM ( <sup>60,61,62,64</sup> Cu-diacetyl-bis(N4-methylthiosemicarbazone)	NSCLC [34] Head and neck tumors [72, 73] Cervical cancer [74, 75] Rectal cancer [76] Brain tumors [78]
Recognizes carbonic anhydrase IX (CA IX) [80]	<sup>124</sup> I-cG250 ( <sup>124</sup> I-chimeric mAb G250)	Renal cell carcinoma [79]
	<sup>89</sup> Zr-cG250-F(ab') <sub>2</sub> ( <sup>89</sup> Zr-chimeric G250 F(ab') <sub>2</sub> )	Head and neck tumors [81]

**TABLE 1: Principal radiopharmaceuticals applied in PET imaging of tumor hypoxia.** Adapted from [54] with the addition of <sup>18</sup>F-HX4.

Benefits	Limitations
Good correlation with tumor aggressiveness and prognosis Easily reproducible and broad availability	Overlap between uptake in normoxic (Warburg effect) [26] and hypoxia tumor tissue
Broadest evidence of value as a hypoxia tracer. Good correlation with immunohistochemistry and prognosis in most cases. Good availability	Lack of correlation in all tumors Low tumor-to-background ratio Variable reproducibility
Good correlation with immunohistochemistry and prognosis in most cases. Faster diffusion and clearance with slightly higher tumor-to-background ratio than $^{18}\text{F}$ -MISO.	More limited evidence compared to $^{18}\text{F}$ -MISO.
Promising tracer with possible correlation with outcome. Slightly higher tumor-to-background ratio than $^{18}\text{F}$ -MISO.	Limited evidence compared to $^{18}\text{F}$ -MISO.
Promising tracer with possible correlation with outcome	Limited evidence.
Promising tracer.	Very limited evidence, mostly preclinical.
Promising tracer with better biodistribution than $^{18}\text{F}$ -MISO.	Preclinical evidence
Promising tracer	Preclinical evidence
Promising tracer	Preclinical evidence
More hydrophilic than $^{18}\text{F}$ -FMISO Good correlation with immunohistochemistry	More limited evidence compared to $^{18}\text{F}$ -FMISO and $^{18}\text{F}$ -FAZA.
Good correlation with immunohistochemistry and prognosis. Early uptake of the tracer with high tumor-to-background ratio. Possibility for late acquisition with $^{64}\text{Cu}$ -ATSM. Possibility for radionuclide therapy with $^{64}\text{Cu}$ -ATSM.	Evidence more limited compared to $^{18}\text{F}$ -MISO. Less clear mechanism of uptake in tumor hypoxia compared to nitroimidazole-like compounds.
Promising tracer	Preclinical evidence
Promising tracer	Preclinical evidence

In chapter 5 we used hypoxia as a biomarker and target for individualized treatment in EAC. By using  $^{18}\text{F}$ -FAZA PET/CT we evaluated the effect of hypoxia on radiation response in a mouse model with subcutaneous human EAC tumors. In a subset of animals, hypoxia imaging was performed also after treatment to evaluate the influence of treatment on hypoxia status. Further, we evaluated if hypoxic radioresistance could be decreased by pretreatment with the radiosensitizer nimorazole. We found that tumors with high  $^{18}\text{F}$ -FAZA activity, were less inhibited by radiotherapy than tumors with less  $^{18}\text{F}$ -FAZA activity with respect to tumor growth. ROC analysis showed that a cut-off of 3.59 for tumor to background ratio could predict treatment response with good sensitivity (92.3%) and specificity (71.4%). We further showed on histology of the xenografts and with an *in vitro* cell viability assay (MTS) that hypoxia indeed caused radioresistance. Hereby we confirmed that hypoxia is a negative predictive factor in our xenograft model and that pretreatment  $^{18}\text{F}$ -FAZA PET/CT could identify tumors that will react worse to radiotherapy. In our model  $^{18}\text{F}$ -FAZA activity in the tumor was quantified as the ratio of mean tumor uptake to mean background uptake. Mean tumor uptake was calculated in the >40% isocontour volume according to Tran et al [123]. Mean background uptake was the mean  $^{18}\text{F}$ -FAZA activity in a sphere with radius 1.5 mm in the foreleg muscle. This parameter was used because it delivered the most accurate cut-off to predict treatment response. Other research groups describe the use of maximum tumor uptakes [110] or mean tumor uptake of the whole tumor [160] and lung [62], pelvic muscle [160] or blood (heart [66])... as background tissues. The cut-off value and the T/B parameter that were used our study, were valuable in the xenograft subcutaneous model, but will need to be revised when translating it to the clinical setting where tumor growth is more variable, and neoadjuvant treatment differs. With respect to the quantification method of  $^{18}\text{F}$ -FAZA, it is not known which parameter is the most valuable. Most clinical studies use their own quantification method, but almost always reflect the most hypoxic areas in the tumor by using  $\text{SUV}_{\text{max}}$  or a kind of > x% isocontour method, and mostly compare this to a reference tissue (muscle, spleen...) [161-163]. A future clinical study should determine a spectrum of different parameters, and determine the most valuable one. Further, to target hypoxia based on  $^{18}\text{F}$ -FAZA PET/CT scan, the method of modification will influence the quantification method of  $^{18}\text{F}$ -FAZA. For dose-painting, a 3D-map of  $^{18}\text{F}$ -FAZA uptake is needed, and repeated  $^{18}\text{F}$ -FAZA scans are needed to offer an up-to-date identification of high hypoxic areas. For radiosensitizers such

as nimorazole, a cut-off can be more valuable than a 3D distribution map, to know if the modifier will be worth it or not.

With respect to nimorazole, we found a clear *in vitro* evidence of radiosensitization under hypoxic conditions, but nimorazole was not able to fully revert the resistance. This is in line with other preclinical studies where a sensitizer enhancement ratio of about 1.4 is reported with single dose irradiation [164, 165], which is indeed smaller than the oxygen enhancement ratio of 2 - 3 that is usually referred to [24, 25]. Further, the benefit of nimorazole was less obvious in the xenografts. When evaluating all xenografts, no benefit is seen, but when evaluating only hypoxic tumors (based on <sup>18</sup>F-FAZA) or hypoxic tumor areas (based on pimonidazole staining), there seems to be a trend of radiosensitization by nimorazole. This less pronounced effect could be due to the different radiation schedule that was used *in vitro* (single dose irradiation) and *in vivo* (hypofractionated). Indeed, a reduction in sensitizer enhancement ratio from 1.4 to 1.3 when combined with fractionated irradiation instead of single dose irradiation has been reported [165]. The Danish Head and Neck Cancer group (DAHANCA) performed substantial research on combination treatment of nimorazole with radiotherapy in patients with head and neck carcinomas (DAHANCA trials). Nimorazole was proven to enhance loco-regional control in HNSCC with a fractionated RT regimen (62- 68 Gy, 2 Gy per fraction) [35] and is part of daily practice in Denmark. In our EAC tumor model, nimorazole does not seem to be the ideal radiosensitizer to cope with hypoxic radioresistance. It remains to be investigated whether nimorazole has a sensitizing effect in the clinical setting, where a fully fractionated schedule is used. Such clinical study has to include hypoxia detection methods to identify patient that could benefit from nimorazole, because nimorazole has no effect in normoxic conditions.

In the previous chapter, we investigated the effect of hypoxia on radiation response, and how we could target this hypoxic resistance by replacing oxygen by an oxygen mimicker in the radiobiological process. We also wanted to investigate the underlying cause of hypoxia, to maybe intervene at that stage and enhance radiation efficacy. In the introduction, we already discussed the multiple etiologies of hypoxia where the immature tumor vascular network plays an important role. In the last chapter (6) we focused on this tumor angiogenesis as cause of hypoxia and performed an integrated study on the effect of irradiation and antiangiogenic therapy on tumor vasculature, tumor microenvironment (e.g. hypoxia) and tumor growth in a xenograft colorectal cancer mouse model. This model was

chosen because anti-angiogenic agents have already proven their benefits in metastatic colorectal cancer patients. On the one hand, we investigated the hypoxia status of subcutaneous xenografts with an OxyLite probe and immunohistochemistry (exogenous marker pimonidazole) and on the other hand, the underlying vascular changes were investigated with *in vivo* fluorescence microscopy in dorsal skinfold window chambers (DSWC), with DCE-MRI of subcutaneous xenografts and with immunohistochemistry (endoglin) of xenografts. We aimed to link the vascular changes of IVM (DSWC tumor model) with changes in DCE-MRI parameters (subcutaneous tumor model), so in the future, DCE-MRI might be used to analyze the vascular status of tumors. Our results showed that all tumors were highly hypoxic before treatment as was measured with OxyLite probes. Despite this hypoxia, radiotherapy managed to inhibit tumor growth control partially, but as expected, cediranib further increased radiation induced growth control. We showed that after cediranib treatment (pan-VEGFR-inhibitor), a window of normalization arises where vessels are less tortuous, less permeable and less dilated and where hypoxia is decreased. If radiotherapy is applied during the normalization period, as in our study, cediranib acts as a radiosensitizer and leads to increased tumor control. Unfortunately, we could not link the observed vascular changes of *in vivo* fluorescence microscopy with parameters calculated from DCE-MRI that was performed 3 days after cessation of cediranib administration, because VEGF-stimulated tumor angiogenesis had probably relapsed at that time point.

We would like to also indicate limitations of this thesis.

First, the use of two tumor types could be seen as a limiting factor. Our first focus was esophageal cancer, as there is an existing clinical need for predictive biomarkers and patient stratification. To investigate tumor angiogenesis as underlying mechanism, we opted for a CRC tumor model, because evidence exists for cediranib efficacy in colorectal cancer (metastatic setting). This difference in tumor types causes a certain incoherence between the two research questions, but it does not limit possible translation to the clinic, for <sup>18</sup>F-FAZA PET/CT and nimorazole in locally advanced esophageal and for cediranib in locally advanced rectal cancer.

Second, a variety of techniques were used across the different experiments. In chapter 5, <sup>18</sup>F-FAZA PET/CT and IHC with pimonidazole were used, while in chapter 6, OxyLite probe, DCE-MRI, *in-vivo* microscopy, IHC pimonidazole/Hoechst and Samba Preclin probe. It would have been interesting to integrate these techniques in one project, to validate

measurements and make stronger conclusions on cause-effect. For example, including  $^{18}\text{F}$ -FAZA PET/CT in chapter 6 could maybe select tumors that would benefit from cediranib treatment and would provide an added value to the experiments.

As last, no clinical data were included, limiting conclusions to the preclinical setting. Predictions about possible clinical applicability and future clinical studies are described in the next chapter.

In conclusion, this thesis emphasized the importance of tumor hypoxia as predictive biomarker and target for treatment. For the first time, it was shown that  $^{18}\text{F}$ -FAZA PET/CT can predict radiation response with high sensitivity and specificity in an EAC mouse model, and that repeated imaging contributes to the evaluation of treatment-induced changes in hypoxia. We further showed that hypoxia-induced radioresistance can be decreased by replacement of oxygen in the radiochemical process with nimorazole. As last, tumor angiogenesis was investigated as underlying mechanism of hypoxia. We supported its importance and showed that cediranib (pan-VEGFR inhibitor) increases radiation efficacy through a transient normalization of tumor vessels and subsequent decrease of hypoxia in a CRC mouse model.





**CHAPTER 8**  
**GENERAL RELEVANCE AND FUTURE**  
**PERSPECTIVES**



## **CHAPTER 8: GENERAL RELEVANCE AND FUTURE PERSPECTIVES**

Cancer remains one of the most important causes of death worldwide [1]. Treatment mostly consists of a combination of chemotherapy, radiotherapy and/or surgery and is based on the TNM classification (UICC) of the tumor. This classification is determined by the size and extent of the primary tumor, number of nearby lymph nodes and whether the cancer has metastasized. However, it has been observed that tumors with the same TNM stage and treated with the same therapy, can have a completely different response to treatment. This suggests that tumors are more diverse than the factors described by the TNM stage. Indeed, tumors differ strongly from one another with respect to genetics, epigenetics and microenvironmental characteristics. In the future, it will be critical to include these individual tumor characteristics in cancer staging and treatment, to offer a more tumor and patient-specific approach.

In an era where medicine is evolving to a more patient-tailored and individualized approach, biomarkers are highly important. The world health organization defines them as ‘any substance, structure or process that can be measured in the body or its products and influence or predict the incidence of outcome or disease’. The most known and widespread biomarker is Her2/neu (human epidermal growth factor receptor 2) and is a good example of how biomarkers can influence clinical decision making and improve patient’s outcomes. Her2/neu is overexpressed in different tumor types (breast cancer, gastric cancer) and has been correlated with worse prognosis [166, 167]. The discovery of the targeted agent trastuzumab (Herceptin), a monoclonal antibody to the Her2-receptor, brought change to his. Trastuzumab showed to increase overall survival of patients with Her2/neu overexpressed breast cancers and is now used in the daily work-up of breast cancer patients [168].

This thesis is part of the quest for biomarkers to offer cancer patients a more tumor specific and individualized therapy. We focused on tumor hypoxia for several reasons. First, it is a microenvironmental characteristic that is present in almost all solid tumors so the potential applicability is wide. Second, preclinical as well as clinical evidence exists that tumor hypoxia is correlated with worse outcomes in different solid tumors. Third, tumor hypoxia

can be measured through non-invasive techniques, which is attractive for the translation to patients. Fourth, numerous targeting methods have been described, for example hypoxia activated prodrugs or intensity modulated radiotherapy (IMRT), which ensures the potential influence on daily clinical decision making.

This thesis showed that  $^{18}\text{F}$ -FAZA PET/CT predicts radiation response in an EAC tumor model, which suggests that  $^{18}\text{F}$ -FAZA PET/CT could play a role in predicting treatment response of EAC patients. This could have several advantages.

First, outcomes of esophageal cancer patients could be improved. Esophageal cancer remains a difficult disease to treat. Treatment has evolved from a surgical approach only, to a more multimodal therapy with chemo- and radiotherapy. The MAGIC and recent CROSS trial have confirmed that addition of neoadjuvant treatment is superior to surgery alone in patients with locally advanced disease [82, 169]. Further, two biological agents have been FDA-approved. Trastuzumab, targeting Her2/neu, and ramucirumab, targeting VEGFR2, showed to improve overall survival in randomized phase III trials in unresectable or metastatic gastro-esophageal junction tumors (ToGa trial [170], REGARD and RAINBOW trial [171, 172]). However, about 70% of esophageal cancer patients show residual disease after neoadjuvant chemoradiation [116]. If these partial responders could be identified with  $^{18}\text{F}$ -FAZA PET/CT before treatment, their outcomes could be improved by methods of hypoxia targeting (e.g. nimorazole or IMRT).

Second,  $^{18}\text{F}$ -FAZA PET/CT is a non-invasive technique that has already been used in patients in clinical trials [161, 163, 173]. Besides the exposure to irradiation,  $^{18}\text{F}$ -FAZA PET/CT seems to have no major disadvantages for the patient.

Third, the imaging can be performed on a standard PET/CT scanner that is routinely used for  $^{18}\text{F}$ -FDG PET/CT imaging. If the radionuclide department of the hospital has the permission to produce  $^{18}\text{F}$ -FAZA, all technical necessities are available to start a trial.

Future work of our team will include a clinical study where  $^{18}\text{F}$ -FAZA PET/CT will be introduced for locally advanced esophageal adenocarcinoma patients requiring nCRT. First, a pilot study should be performed to determine a clinical cut-off of FAZA-tumor uptake that is predictive for therapy response. Patients need to be divided in responder and non-responders which can be done based on the pathological characteristics of the resection specimen (e.g. Mandard regression score). If a correlation between pretreatment  $^{18}\text{F}$ -FAZA

uptake and treatment response can be confirmed, treatment modifications can be considered to improve patient outcomes.

If a modifier like nimorazole would be used, it seems useful to repeat  $^{18}\text{F}$ -FAZA PET/CT during neoadjuvant treatment to reassess hypoxia status of tumors. As was seen in our study, most of the tumors reoxygenated upon treatment. If reoxygenation is found, the modifier might be discontinued.

Also for dose-painting, repeating the  $^{18}\text{F}$ -FAZA PET/CT scan is important because the hypoxia distribution changes over time, so the irradiation mapping at the beginning of treatment will not be useful during the full treatment. Whether an  $^{18}\text{F}$ -FAZA PET/CT after ending nCRT, so before surgery, would be interesting is arguable. We found no evidence that reoxygenation of tumors is linked to treatment response in our model. Further,  $^{18}\text{F}$ -FDG PET is known to be correlated with treatment response, so it would be more useful to perform an  $^{18}\text{F}$ -FDG PET.

Additionally, patient survival data and relapse data will be monitored to also correlate pretreatment  $^{18}\text{F}$ -FAZA PET/CT with prognosis. Later, this could be extended to other tumor types (e.g. rectal cancer, lung cancer...).

Further, this thesis showed how anti-angiogenic therapy with cediranib normalizes tumor vasculature, reduces tumor hypoxia and enhances radiotherapy efficacy in a CRC tumor model. This stresses the importance of hypoxia in CRC and the potential role of cediranib in addition to radiotherapy. At present, patients with locally advanced rectal cancer are treated with neoadjuvant chemoradiation followed by surgery [174]. Addition of targeted agents such as bevacizumab (targeting VEGF-A) or cetuximab (targeting EGFR) have been examined, but provided conflicting results [154, 155, 175]. Whether cediranib will improve patients' outcomes in the neoadjuvant setting, with acceptable toxicities, is to be investigated.

In conclusion, tumor hypoxia is a long-known problem within oncology with little impact in the daily clinic. This is partially because hypoxia detection methods have not reached the routine clinical work-up of cancer patients. To continue enhancing patients' outcomes and minimizing useless treatments, we are convinced a patient-tailored approach is required where tumor hypoxia will be one of the guiding biomarkers.



## **CHAPTER 9**

### **SUMMARY/SAMENVATTING**





## **CHAPTER 9: SUMMARY**

In a time of continuous development of new approaches in cancer treatment, combined with the heterogeneous aspects of tumors, the search for biomarkers to predict treatment response and prognosis is extensive. Tumor hypoxia as a biomarker, is a very interesting research area, because it has been proven to be a negative predictive and prognostic marker in certain solid tumors. After decades of research to target hypoxia, little have reached the clinical setting. Mostly because no patient identification was performed and as such, they failed to improve outcomes. In this thesis, we present an integrated study on hypoxia in solid tumors and investigate its role as biomarker and target for individualized therapy.

The first part of this thesis (chapter 3-5) focused on esophageal adenocarcinoma, an aggressive disease with poor survival rates and unpredictable response to neoadjuvant therapy. Our aim was to investigate the predictive value of  $^{18}\text{F}$ -FAZA PET/CT, a non-invasive hypoxia imaging method, to radiation response in an EAC tumor model and to study the radiosensitizing effect of nimorazole, a promising hypoxia targeting molecule.

We first described the development of an orthotopic and subcutaneous EAC xenograft model in nude mice in **chapter 3**. Two different human EAC cell lines were used to induce xenografts. The first, OE33, is derived from a stage IIA adenocarcinoma of the lower esophagus with poor differentiation. The second was OACM5 1.C and is derived from a metastatic lymph node of a distal esophageal adenocarcinoma. After injection of the cell lines at an orthotopic and ectopic (subcutaneous) site, *in vivo* tumor growth was evaluated. Additionally, functional cell line characteristics were examined through *in vitro* assays for collagen invasion, cell-cell adherence and clonogenicity. OE33 was found to induce orthotopic and subcutaneous small, slow growing tumors and was thus not ideal to investigate the predictive value of  $^{18}\text{F}$ -FAZA PET/CT for radiation response. The second cell line, OACM5 1.C had no tumor take orthotopically and only 50% tumor take subcutaneously. However, through *in vivo* selection, a daughter cell line of OACM5 1.C was developed, named OACM5 1.C SC1, with enhanced tumor take rates, and most importantly, leading to larger and faster growing tumors that could be used to study radiation response and predictive value of  $^{18}\text{F}$ -FAZA PET/CT.

Subsequently, the feasibility of  $^{18}\text{F}$ -FAZA PET/CT in both the orthotopic and subcutaneous EAC tumor model was tested and described in **chapter 4**. A problem of intense background activity in the gastro-intestinal tract was encountered due to metabolization of the tracer.

Because of this, orthotopic tumors could not be delineated. This is an unavoidable aspect of nitroimidazole hypoxia tracers, but will probably not cause such a problem in patients because of larger structures and better soft tissue resolution on CT. Therefore, we decided to continue with the subcutaneous model in which  $^{18}\text{F}$ -FAZA PET/CT enabled clear visualization of tumor hypoxia distribution and hypoxia quantification.

In **chapter 5**, we evaluated the predictive value of  $^{18}\text{F}$ -FAZA PET/CT for radiation response in subcutaneous EAC xenografts and found that a tumor-to-background ratio of 3.59 or higher could identify tumors that responded worse to radiotherapy. We then examined whether nimorazole, a hypoxic radiosensitizer, could increase radiotherapy efficacy in hypoxic conditions. Nimorazole significantly increased *in vitro* radiotherapy efficacy in hypoxic conditions. In the EAC xenografts, a trend was seen to better inhibition of tumor cell proliferation, but results on tumor growth control were limited. FAZA uptake after treatment was also evaluated, but no link was found between treatment response and normalization of hypoxia status. We did see a reoxygenation in almost all tumors after treatment. These results suggest that  $^{18}\text{F}$ -FAZA PET/CT could play an important role in predicting treatment response in EAC patients and that nimorazole might decrease hypoxia induced radioresistance.

In the second section of this thesis, the focus was shifted to tumor angiogenesis as one of the underlying mechanisms of tumor hypoxia, and was described in **chapter 6**. This chapter focused on colorectal cancer, one of the most common tumor types worldwide. An integrated study on tumor vasculature and microenvironment (e.g. hypoxia) was performed, in response to radiotherapy and anti-angiogenic therapy. CRC xenografts were induced in dorsal skinfold window chambers and subcutaneously in the hind legs of nude mice. *In vivo* fluorescence microscopy of the DSWC was performed and immunohistochemistry,  $\text{pO}_2$  and IFP measurements and DCE-MRI were performed in the subcutaneous xenografts. The pan-VEGFR inhibitor cediranib was investigated as anti-angiogenic drug. We showed that all tumors expressed a significant amount of tumor hypoxia and that cediranib normalized tumor vasculature and decreased tumor hypoxia, leading to an enhanced effect of radiotherapy.

In conclusion, this thesis emphasizes the importance of tumor hypoxia in solid tumors. Hypoxia imaging with  $^{18}\text{F}$ -FAZA PET/CT is a useful detection and quantification method

and is predictive for radiation response in an EAC xenograft model. Further we showed that targeting hypoxia, by nimorazole and by cediranib, increases radiation response, which underscores the applicability of hypoxia as targetable biomarker in patients.



## **SAMENVATTING**

In een tijd waar de ontwikkelingen binnen de oncologie niet stilstaan, gecombineerd met de grote heterogeniteit van tumoren, is de zoektocht naar biomerkers om therapierespons en prognose te voorspellen enorm. In bepaalde solide tumoren werd reeds aangetoond dat tumorhypoxie gecorreleerd is met een slechtere therapierespons en prognose. Tumorhypoxie zou dus een zeer interessante biomarker kunnen zijn en vormt een belangrijk onderzoeksdomein in de oncologie. Na tientallen jaren onderzoek naar mogelijkheden om tumorhypoxie aan te pakken, zijn er slecht weinig geïmplementeerd in de kliniek. Er werd meestal geen identificatie verricht van hypoxische versus niet-hypoxische tumoren, waardoor de therapieën gericht op hypoxie, er niet in slaagden de outcomes te verbeteren. Deze thesis is een geïntegreerde studie over hypoxie in solide tumoren, waar hypoxie wordt onderzocht als mogelijke biomarker en als doelwit voor geïndividualiseerde behandeling.

Het eerste deel van deze thesis (hoofdstuk 3-5) richtte zich op slokdarmkanker van het type adenocarcinoom. Deze agressieve ziekte heeft slechte overlevingscijfers en reageert onvoorspelbaar op neoadjuvante therapie. Ons doel was om de voorspellende waarde van  $^{18}\text{F}$ -FAZA PET/CT, een niet-invasieve manier om hypoxie te beeldvormen, voor respons op radiotherapie te onderzoeken in een preklinische studie en om het radiosensitizerend effect van nimorazole, een veelbelovende therapie gericht op hypoxie, te bestuderen.

We zijn gestart met het beschrijven van de ontwikkeling van een orthotoop en subcutaan slokdarm adenocarcinoom model in naakte muizen (**hoofdstuk 3**). Hierbij werden 2 verschillende humane cellijnen gebruikt om xenografts te induceren. De eerste, OE33, stamt af van een stadium IIA adenocarcinoom van de distale slokdarm, met slechte differentiatie. De tweede, OACM5 1.C stamt af van een metastatische lymfeknoop van een adenocarcinoom van de distale slokdarm. Na injectie van de cellen op een orthotope (distale slokdarm) of ectopische (subcutaan in de dijen) plaats werd *in vivo* tumorgroei geëvalueerd. Verder werden met verschillende *in vitro* testen functionele eigenschappen van de cellen onderzocht met betrekking op cel-cel adherentie, invasiviteit en clonogeniciteit. OE33 leidde tot de ontwikkeling van kleine, traag groeiende tumoren, zowel orthotoop als ectopisch, en was dus niet geschikt om de voorspellende waarde van  $^{18}\text{F}$  FAZA PET/CT voor respons op radiotherapie te onderzoeken. Met de tweede cellijn, OACM5 1.C, konden geen orthotope tumoren ontwikkeld worden, en leidde slechts 50% van de subcutane injecties tot ontwikkeling van tumoren. Echter, we slaagden erin om met een *in vivo* selectie

techniek een dochtercellijn te ontwikkelen, OACM5 1.C SC1, die tot procentueel meer tumorontwikkeling leidde en belangrijker, resulteerde in grotere en sneller groeiende tumoren. Deze *in vivo* geselecteerde cellijn kan in een toekomstige studie gebruikt worden om de voorspellende waarde van  $^{18}\text{F}$  FAZA PET/CT voor respons op radiotherapie te onderzoeken.

Vervolgens werd de uitvoerbaarheid van  $^{18}\text{F}$ -FAZA PET/CT beeldvorming in beide tumor modellen (orthotoop en subcutaan) onderzocht en beschreven in **hoofdstuk 4**. Daar botsten we op een probleem van intense achtergrondactiviteit van de tracer ter hoogte van de lever en het maagdarmsstelsel, door afbraak en excretie van de tracer aldaar. Hierdoor konden de tumoren in de distale slokdarm niet gevisualiseerd en afgelijnd worden op de PET/CT scan. Dit is een onvermijdbaar aspect van nitroimidazole tracers, maar zal bij patiënten waarschijnlijk niet zo'n probleem vormen gezien de structuren groter zijn en de CT resolutie voor zachte weefsels beter is. Daarom besloten we verder te gaan met het subcutane model, waar de distributie van tumorhypoxie duidelijk gevisualiseerd en afgelijnd kon worden met  $^{18}\text{F}$ -FAZA PET/CT.

In **hoofdstuk 5** evalueerden we de voorspellende waarde van  $^{18}\text{F}$ -FAZA PET/CT voor respons op radiotherapie in subcutane slokdarmadenocarcinoma xenografts. We toonden aan dat een tumor-to-background ratio van 3.59, met goede sensitiviteit en specificiteit, tumoren kon identificeren die slechter zouden reageren op radiotherapie. Daarnaast onderzochten we of nimorazole, een radiosensitiseerder gericht op hypoxie, het effect van radiotherapie in hypoxische omstandigheden kon verbeteren. Nimorazole verbeterde significant het effect van radiotherapie in hypoxische omstandigheden in de *in vitro* setting, en er werd een trend gezien in de xenografts tot betere inhibitie van kankercel proliferatie. Het effect op tumorgroei was eerder beperkt. We evalueerde ook  $^{18}\text{F}$ -FAZA-opname na therapie, maar vonden geen correlatie tussen therapierespons en normalisatie van de hypoxie status. Wel zagen we een reoxygenatie in bijna alle tumoren na therapie. Deze resultaten tonen aan dat  $^{18}\text{F}$ -FAZA PET/CT een belangrijke rol zou kunnen spelen in het voorspellen van therapierespons in slokdarmadenocarcinoma patiënten en dat nimorazole de hypoxie geïnduceerde radioresistentie zou kunnen verminderen.

Het tweede deel van de thesis richtte zich op tumor angiogenese als onderliggende oorzaak van tumorhypoxie (**hoofdstuk 6**). Hiervoor richtten we ons op colorectaal kanker, een van de meest voorkomende kankers wereldwijd, waarvoor reeds bewezen is dat angiogenese

remmende therapie een effect heeft bovenop de bestaande modaliteiten. Een geïntegreerde studie over de structuur en functie van tumorale bloedvaten, en de tumor micro-omgeving (waaronder hypoxie), werd verricht. Het effect van radiotherapie en anti-angiogene behandeling met de pan-VEGR inhibitor cediranib werd onderzocht. Hiervoor gebruikten we colorectale xenografts in *dorsal skinfold window chambers* en subcutaan in de dijen, in naakte muizen. *In vivo* fluorescentie microscopie van de DSWC werd verricht en immunohistochemische kleuringen, pO<sub>2</sub> en IFP probe metingen en DCE-MRI werden verricht van de subcutane xenografts. We toonden aan dat alle tumoren een aanzienlijke hoeveelheid tumorhypoxie bezaten en dat cediranib de tumorale vaten normaliseerde, tumorhypoxie verminderde en het effect van radiotherapie verbeterde.

Deze thesis benadrukt het belang van tumorhypoxie in solide tumoren. We besluiten dat <sup>18</sup>F-FAZA PET/CT een bruikbare techniek is om hypoxie te meten en dat het de respons op radiotherapie in een slokdarmadenocarcinoma xenograft model kan voorspellen. Verder toonden we aan dat hypoxiegerichte therapie, met nimorazole en cediranib, de respons op radiotherapie verbetert, wat de toepasbaarheid van hypoxie als biomarker en doelwit van therapie in de kliniek verzekert.





## **REFERENCES**

- [1] WHO. World Health Organization: Fact sheets. <http://www.who.int/mediacentre/factsheets/fs297/en/>. Last updated February 2017;(Accessed February 11th 2017).
- [2] Hanahan D, Weinberg RA. Hallmarks of cancer: the next generation. *Cell*. 2011;144(5):646-74.
- [3] Hanahan D, Weinberg RA. The hallmarks of cancer. *Cell*. 2000;100(1):57-70.
- [4] Hockel M, Vaupel P. Tumor hypoxia: definitions and current clinical, biologic, and molecular aspects. *J Natl Cancer Inst*. 2001;93(4):266-76.
- [5] Warburg O. On the origin of cancer cells. *Science*. 1956;123(3191):309-14.
- [6] Vaupel P, Mayer A. Hypoxia in cancer: significance and impact on clinical outcome. *Cancer Metastasis Rev*. 2007;26(2):225-39.
- [7] Kufe D, Pollock R, Weichselbaum R, et al. *Biologic Basis of Radiation Therapy*. In: Inc. BD, editor. *Holland-Frei Cancer Medicine 6th edition*2003.
- [8] Jain RK. Normalizing tumor microenvironment to treat cancer: bench to bedside to biomarkers. *J Clin Oncol*. 2013;31(17):2205-18.
- [9] Michiels C, Tellier C, Feron O. Cycling hypoxia: A key feature of the tumor microenvironment. *Biochim Biophys Acta*. 2016;1866(1):76-86.
- [10] Rey S, Schito L, Koritzinsky M, Wouters BG. Molecular targeting of hypoxia in radiotherapy. *Adv Drug Deliv Rev*. 2016.
- [11] Patel A, Sant S. Hypoxic tumor microenvironment: Opportunities to develop targeted therapies. *Biotechnol Adv*. 2016;34(5):803-12.
- [12] Wouters BG, Koritzinsky M. Hypoxia signalling through mTOR and the unfolded protein response in cancer. *Nature Reviews Cancer*. 2008;8(11):851-64.
- [13] Hay N, Sonenberg N. Upstream and downstream of mTOR. *Genes Dev*. 2004;18(16):1926-45.
- [14] Semenza GL. HIF-1: using two hands to flip the angiogenic switch. *Cancer Metastasis Rev*. 2000;19(1-2):59-65.
- [15] Chang Q, Jurisica I, Do T, Hedley DW. Hypoxia predicts aggressive growth and spontaneous metastasis formation from orthotopically grown primary xenografts of human pancreatic cancer. *Cancer Res*. 2011;71(8):3110-20.
- [16] Pennacchietti S, Michieli P, Galluzzo M, Mazzone M, Giordano S, Comoglio PM. Hypoxia promotes invasive growth by transcriptional activation of the met protooncogene. *Cancer Cell*. 2003;3(4):347-61.
- [17] Erler JT, Cawthorne CJ, Williams KJ, et al. Hypoxia-mediated down-regulation of Bid and Bax in tumors occurs via hypoxia-inducible factor 1-dependent and -independent mechanisms and contributes to drug resistance. *Mol Cell Biol*. 2004;24(7):2875-89.
- [18] Yotnda P, Wu D, Swanson AM. Hypoxic tumors and their effect on immune cells and cancer therapy. *Methods Mol Biol*. 2010;651:1-29.
- [19] Moskwa P, Buffa FM, Pan Y, et al. miR-182-mediated downregulation of BRCA1 impacts DNA repair and sensitivity to PARP inhibitors. *Mol Cell*. 2011;41(2):210-20.
- [20] Bristow RG, Hill RP. Hypoxia and metabolism. Hypoxia, DNA repair and genetic instability. *Nat Rev Cancer*. 2008;8(3):180-92.
- [21] Harris AL. Hypoxia--a key regulatory factor in tumour growth. *Nat Rev Cancer*. 2002;2(1):38-47.
- [22] Nordmark M, Overgaard J. Tumor hypoxia is independent of hemoglobin and prognostic for loco-regional tumor control after primary radiotherapy in advanced head and neck cancer. *Acta Oncol*. 2004;43(4):396-403.

- [23] Hockel M, Schlenger K, Aral B, Mitze M, Schaffer U, Vaupel P. Association between tumor hypoxia and malignant progression in advanced cancer of the uterine cervix. *Cancer Res.* 1996;56(19):4509-15.
- [24] Rockwell S, Dobrucki IT, Kim EY, Marrison ST, Vu VT. Hypoxia and Radiation Therapy: Past History, Ongoing Research, and Future Promise. *Curr Mol Med.* 2009;9(4):442-58.
- [25] Rockwell S. *Manual de Radiotherapia Oncologia, Principios de radiobiologia.* Yale University, New Haven CT1989.
- [26] Wilson WR, Hay MP. Targeting hypoxia in cancer therapy. *Nature Reviews Cancer.* 2011;11(6):393-410.
- [27] Kaanders JH, Bussink J, van der Kogel AJ. Clinical studies of hypoxia modification in radiotherapy. *Semin Radiat Oncol.* 2004;14(3):233-40.
- [28] Bennett M, Feldmeier J, Smee R, Milross C. Hyperbaric oxygenation for tumour sensitisation to radiotherapy. *Cochrane Database Syst Rev.* 2005(4):CD005007.
- [29] Kaanders JH, Bussink J, van der Kogel AJ. ARCON: a novel biology-based approach in radiotherapy. *Lancet Oncol.* 2002;3(12):728-37.
- [30] Yeh JJ, Kim WY. Targeting tumor hypoxia with hypoxia-activated prodrugs. *J Clin Oncol.* 2015;33(13):1505-8.
- [31] Krohn KA, Link JM, Mason RP. Molecular imaging of hypoxia. *J Nucl Med.* 2008;49:129s-48s.
- [32] Wardman P. Chemical radiosensitizers for use in radiotherapy. *Clin Oncol.* 2007;19(6):397-417.
- [33] Urtasun RC, Chapman JD, Feldstein ML, et al. Peripheral neuropathy related to misonidazole: incidence and pathology. *Br J Cancer Suppl.* 1978;3:271-5.
- [34] Saunders M, Dische S. Clinical results of hypoxic cell radiosensitisation from hyperbaric oxygen to accelerated radiotherapy, carbogen and nicotinamide. *Br J Cancer Suppl.* 1996;27:S271-8.
- [35] Overgaard J, Hansen HS, Overgaard M, et al. A randomized double-blind phase III study of nimorazole as a hypoxic radiosensitizer of primary radiotherapy in supraglottic larynx and pharynx carcinoma, results of the Danish Head and Neck Cancer Study (DAHANCA) protocol 5-85. *Radiother Oncol.* 1998;46(2):135-46.
- [36] Wigerup C, Pahlman S, Bexell D. Therapeutic targeting of hypoxia and hypoxia-inducible factors in cancer. *Pharmacol Ther.* 2016;164:152-69.
- [37] Fukumura D, Duda DG, Munn LL, Jain RK. Tumor Microvasculature and Microenvironment: Novel Insights Through Intravital Imaging in Pre-Clinical Models. *Microcirculation.* 2010;17(3):206-25.
- [38] Folkman J. Tumor angiogenesis: therapeutic implications. *N Engl J Med.* 1971;285(21):1182-6.
- [39] Hurwitz H, Fehrenbacher L, Novotny W, et al. Bevacizumab plus irinotecan, fluorouracil, and leucovorin for metastatic colorectal cancer. *N Engl J Med.* 2004;350(23):2335-42.
- [40] Goel S, Duda DG, Xu L, et al. Normalization of the vasculature for treatment of cancer and other diseases. *Physiol Rev.* 2011;91(3):1071-121.
- [41] Jain RK. Normalization of tumor vasculature: An emerging concept in antiangiogenic therapy. *Science.* 2005;307(5706):58-62.
- [42] Bache M, Kappler M, Said HM, Staab A, Vordermark D. Detection and specific targeting of hypoxic regions within solid tumors: Current preclinical and clinical strategies. *Curr Med Chem.* 2008;15(4):322-38.

- [43] Chitneni SK, Palmer GM, Zalutsky MR, Dewhirst MW. Molecular Imaging of Hypoxia. *J Nucl Med.* 2011;52(2):165-8.
- [44] Vikram DS, Zweier JL, Kuppusamy P. Methods for noninvasive imaging of tissue hypoxia. *Antioxid Redox Signal.* 2007;9(10):1745-56.
- [45] Brown JM, Wilson WR. Exploiting tumour hypoxia in cancer treatment. *Nat Rev Cancer.* 2004;4(6):437-47.
- [46] Kanwisher J. Polarographic Oxygen Electrode. *Limnol Oceanogr.* 1959;4(2):210-7.
- [47] Hockel M, Knoop C, Schlenger K, et al. Intratumoral pO<sub>2</sub> predicts survival in advanced cancer of the uterine cervix. *Radiother Oncol.* 1993;26(1):45-50.
- [48] Nordmark M, Alsner J, Keller J, et al. Hypoxia in human soft tissue sarcomas: adverse impact on survival and no association with p53 mutations. *Br J Cancer.* 2001;84(8):1070-5.
- [49] Nordmark M, Overgaard J. A confirmatory prognostic study on oxygenation status and loco-regional control in advanced head and neck squamous cell carcinoma treated by radiation therapy. *Radiother Oncol.* 2000;57(1):39-43.
- [50] <http://www.oxford-optronix.com/oxylyte#tab7-tab>. Last updated 2016:(Accessed February 27th 2017).
- [51] Russell J, Carlin S, Burke SA, Wen B, Yang KM, Ling CC. Immunohistochemical Detection of Changes in Tumor Hypoxia. *Int J Radiat Oncol.* 2009;73(4):1177-86.
- [52] Carlin S, Zhang HW, Reese M, Ramos NN, Chen Q, Ricketts SA. A Comparison of the Imaging Characteristics and Microregional Distribution of 4 Hypoxia PET Tracers. *J Nucl Med.* 2014;55(3):515-21.
- [53] Harris BH, Barberis A, West CM, Buffa FM. Gene Expression Signatures as Biomarkers of Tumour Hypoxia. *Clin Oncol (R Coll Radiol).* 2015;27(10):547-60.
- [54] Lopci E, Grassi I, Chiti A, et al. PET radiopharmaceuticals for imaging of tumor hypoxia: a review of the evidence. *Am J Nucl Med Mol Imaging.* 2014;4(4):365-84.
- [55] Evans CE, Mattock K, Humphries J, et al. Techniques of assessing hypoxia at the bench and bedside. *Angiogenesis.* 2011;14(2):119-24.
- [56] Sorg BS, Moeller BJ, Donovan O, Cao Y, Dewhirst MW. Hyperspectral imaging of hemoglobin saturation in tumor microvasculature and tumor hypoxia development. *J Biomed Opt.* 2005;10(4):44004.
- [57] <https://commons.wikimedia.org/w/index.php?curid=3447869>. Last updated February 2017:(Accessed February 27th 2017).
- [58] Egeland TA, Gulliksrud K, Gaustad JV, Mathiesen B, Rofstad EK. Dynamic contrast-enhanced-MRI of tumor hypoxia. *Magn Reson Med.* 2012;67(2):519-30.
- [59] Wang W, Lee NY, Georgi JC, et al. Pharmacokinetic analysis of hypoxia (18)F-fluoromisonidazole dynamic PET in head and neck cancer. *J Nucl Med.* 2010;51(1):37-45.
- [60] Price JM, Robinson SP, Koh DM. Imaging hypoxia in tumours with advanced MRI. *Q J Nucl Med Mol Imaging.* 2013;57(3):257-70.
- [61] Mees G, Dierckx R, Vangestel C, Van de Wiele C. Molecular imaging of hypoxia with radiolabelled agents. *Eur J Nucl Med Mol Imaging.* 2009;36(10):1674-86.
- [62] Piert M, Machulla HJ, Picchio M, et al. Hypoxia-specific tumor imaging with F-18-fluoroazomycin arabinoside. *J Nucl Med.* 2005;46(1):106-13.
- [63] Kumar P, Stypinski D, Xia H, McEwan AJB, Machulla HJ, Wiebe LI. Fluoroazomycin arabinoside (FAZA): Synthesis, H-2 and H-3-labelling and preliminary biological evaluation of a novel 2-nitroimidazole marker of tissue hypoxia. *J Labelled Compd Rad.* 1999;42(1):3-16.

- [64] Reischl G, Dorow DS, Cullinane C, et al. Imaging of tumor hypoxia with [I-124] IAZA in comparison with [F-18] FMISO and [F-18]FAZA - first small animal PET results. *Journal of Pharmacy and Pharmaceutical Sciences*. 2007;10(2):203-11.
- [65] Dubois LJ, Lieuwes NG, Janssen MHM, et al. Preclinical evaluation and validation of [F-18]HX4, a promising hypoxia marker for PET imaging. *Proc Natl Acad Sci U S A*. 2011;108(35):14620-5.
- [66] Peeters SG, Zegers CM, Lieuwes NG, et al. A comparative study of the hypoxia PET tracers [(1)(8)F]HX4, [(1)(8)F]FAZA, and [(1)(8)F]FMISO in a preclinical tumor model. *Int J Radiat Oncol Biol Phys*. 2015;91(2):351-9.
- [67] Zegers CML, van Elmpt W, Reymen B, et al. In Vivo Quantification of Hypoxic and Metabolic Status of NSCLC Tumors Using [F-18]HX4 and [F-18]FDG-PET/CT Imaging. *Clin Cancer Res*. 2014;20(24):6389-97.
- [68] Zegers CML, van Elmpt W, Szardenings K, et al. Repeatability of hypoxia PET imaging using [F-18]HX4 in lung and head and neck cancer patients: a prospective multicenter trial. *Eur J Nucl Med Mol Imaging*. 2015;42(12):1840-9.
- [69] Verwer EE, Zegers CM, van Elmpt W, et al. Pharmacokinetic modeling of a novel hypoxia PET tracer [18F]HX4 in patients with non-small cell lung cancer. *EJNMMI Phys*. 2016;3(1):30.
- [70] Chen LM, Zhang ZW, Kolb HC, Walsh JC, Zhang J, Guan YH. F-18-HX4 hypoxia imaging with PET/CT in head and neck cancer: a comparison with F-18-FMISO. *Nucl Med Commun*. 2012;33(10):1096-102.
- [71] Zegers CML, Hoebbers FJP, van Elmpt W, et al. Evaluation of tumour hypoxia during radiotherapy using [F-18]HX4 PET imaging and blood biomarkers in patients with head and neck cancer. *Eur J Nucl Med Mol Imaging*. 2016;43(12):2139-46.
- [72] Klaassen R, Bennink RJ, van Tienhoven G, et al. Feasibility and repeatability of PET with the hypoxia tracer [F-18]HX4 in oesophageal and pancreatic cancer. *Radiother Oncol*. 2015;116(1):94-9.
- [73] Doss M, Zhang JJ, Belanger MJ, et al. Biodistribution and radiation dosimetry of the hypoxia marker F-18-HX4 in monkeys and humans determined by using whole-body PET/CT. *Nucl Med Commun*. 2010;31(12):1016-24.
- [74] Yang DJ, Wallace S, Cherif A, et al. Development of F-18 Labeled Fluoroerythronitroimidazole as a Pet Agent for Imaging Tumor Hypoxia. *Radiology*. 1995;194(3):795-800.
- [75] Dolbier WR, Jr., Li AR, Koch CJ, Shiue CY, Kachur AV. [18F]-EF5, a marker for PET detection of hypoxia: synthesis of precursor and a new fluorination procedure. *Appl Radiat Isot*. 2001;54(1):73-80.
- [76] Halmos GB, de Bruin LB, Langendijk JA, van der Laan BFAM, Pruijm J, Steenbakkers RJHM. Head and Neck Tumor Hypoxia Imaging by F-18-Fluoroazomycin-araboside (F-18-FAZA)-PET A Review. *Clin Nucl Med*. 2014;39(1):44-8.
- [77] Peeters SG, Zegers CM, Yaromina A, Van Elmpt W, Dubois L, Lambin P. Current preclinical and clinical applications of hypoxia PET imaging using 2-nitroimidazoles. *Q J Nucl Med Mol Imaging*. 2015;59(1):39-57.
- [78] Tran LB, Bol A, Labar D, et al. Predictive value of (18)F-FAZA PET imaging for guiding the association of radiotherapy with nimorazole: A preclinical study. *Radiother Oncol*. 2015;114(2):189-94.
- [79] Mortensen LS, Busk M, Nordmark M, et al. Accessing radiation response using hypoxia PET imaging and oxygen sensitive electrodes: A preclinical study. *Radiother Oncol*. 2011;99(3):418-23.

- [80] Saga T, Inubushi M, Koizumi M, et al. Prognostic value of PET/CT with F-18-fluoroazomycin arabinoside for patients with head and neck squamous cell carcinomas receiving chemoradiotherapy. *Ann Nucl Med.* 2016;30(3):217-24.
- [81] Saga T, Inubushi M, Koizumi M, et al. Prognostic value of F-18-fluoroazomycin arabinoside PET/CT in patients with advanced non-small-cell lung cancer. *Cancer Sci.* 2015;106(11):1554-60.
- [82] Shapiro J, van Lanschot JJ, Hulshof MC, et al. Neoadjuvant chemoradiotherapy plus surgery versus surgery alone for oesophageal or junctional cancer (CROSS): long-term results of a randomised controlled trial. *Lancet Oncol.* 2015;16(9):1090-8.
- [83] Driessen A, Landuyt W, Pastorekova S, et al. Expression of carbonic anhydrase IX (CA IX), a hypoxia-related protein, rather than vascular-endothelial growth factor (VEGF), a pro-angiogenic factor, correlates with an extremely poor prognosis in esophageal and gastric adenocarcinomas. *Ann Surg.* 2006;243(3):334-40.
- [84] Ogawa K, Chiba I, Morioka T, et al. Clinical Significance of HIF-1 alpha Expression in Patients with Esophageal Cancer Treated with Concurrent Chemoradiotherapy. *Anticancer Res.* 2011;31(6):2351-9.
- [85] Napier KJ, Scheerer M, Misra S. Esophageal cancer: A Review of epidemiology, pathogenesis, staging workup and treatment modalities. *World J Gastrointest Oncol.* 2014;6(5):112-20.
- [86] Stahl M, Mariette C, Haustermans K, Cervantes A, Arnold D, Group EGW. Oesophageal cancer: ESMO Clinical Practice Guidelines for diagnosis, treatment and follow-up. *Ann Oncol.* 2013;24 Suppl 6:vi51-6.
- [87] Gavin AT, Francisci S, Foschi R, et al. Oesophageal cancer survival in Europe: A EURO CARE-4 study. *Cancer Epidemiol.* 2012;36(6):505-12.
- [88] Tetreault MP. Esophageal Cancer: Insights From Mouse Models. *Cancer Growth Metastasis.* 2015;8(Suppl 1):37-46.
- [89] Bibby MC. Orthotopic models of cancer for preclinical drug evaluation: advantages and disadvantages. *Eur J Cancer.* 2004;40(6):852-7.
- [90] Kuroda S, Kubota T, Aoyama K, et al. Establishment of a Non-Invasive Semi-Quantitative Bioluminescent Imaging Method for Monitoring of an Orthotopic Esophageal Cancer Mouse Model. *PLoS One.* 2014;9(12):e114562.
- [91] Song S, Chang D, Cui Y, et al. New orthotopic implantation model of human esophageal squamous cell carcinoma in athymic nude mice. *Thoracic Cancer.* 2014;5(5):417-24.
- [92] Habibollahi P, Figueiredo JL, Heidari P, et al. Optical Imaging with a Cathepsin B Activated Probe for the Enhanced Detection of Esophageal Adenocarcinoma by Dual Channel Fluorescent Upper GI Endoscopy. *Theranostics.* 2012;2(2):227-34.
- [93] Gros SJ, Dohrmann T, Peldschus K, et al. Complementary use of fluorescence and magnetic resonance imaging of metastatic esophageal cancer in a novel orthotopic mouse model. *Int J Cancer.* 2010;126(11):2671-81.
- [94] Drenckhan A, Kurschat N, Dohrmann T, et al. Effective inhibition of metastases and primary tumor growth with CTCE-9908 in esophageal cancer. *J Surg Res.* 2013;182(2):250-6.
- [95] Kuroda S, Fujiwara T, Shirakawa Y, et al. Telomerase-Dependent Oncolytic Adenovirus Sensitizes Human Cancer Cells to Ionizing Radiation via Inhibition of DNA Repair Machinery. *Cancer Res.* 2010;70(22):9339-48.
- [96] Furihata T, Sakai T, Kawamata H, et al. A new in vivo model for studying invasion and metastasis of esophageal squamous cell carcinoma. *Int J Oncol.* 2001;19(5):903-7.

- [97] Ip JC, Ko JM, Yu VZ, et al. A versatile orthotopic nude mouse model for study of esophageal squamous cell carcinoma. *Biomed Res Int.* 2015;2015:910715.
- [98] Ohara T, Takaoka M, Sakurama K, et al. The establishment of a new mouse model with orthotopic esophageal cancer showing the esophageal stricture. *Cancer Lett.* 2010;293(2):207-12.
- [99] Hori T, Yamashita Y, Ohira M, Matsumura Y, Muguruma K, Hirakawa K. A novel orthotopic implantation model of human esophageal carcinoma in nude rats: CD44H mediates cancer cell invasion in vitro and in vivo. *Int J Cancer.* 2001;92(4):489-96.
- [100] Gros SJ, Kurschat N, Drenckhan A, et al. Involvement of CXCR4 Chemokine Receptor in Metastatic HER2-Positive Esophageal Cancer. *PLoS One.* 2012;7(10).
- [101] Gros SJ, Kurschat N, Dohrmann T, et al. Effective Therapeutic Targeting of the Overexpressed HER-2 Receptor in a Highly Metastatic Orthotopic Model of Esophageal Carcinoma. *Mol Cancer Ther.* 2010;9(7):2037-45.
- [102] Gros SJ, Dohrmann T, Rawnaq T, et al. Orthotopic Fluorescent Peritoneal Carcinomatosis Model of Esophageal Cancer. *Anticancer Res.* 2010;30(10):3933-8.
- [103] Castro C, Bosetti C, Malvezzi M, et al. Patterns and trends in esophageal cancer mortality and incidence in Europe (1980-2011) and predictions to 2015. *Ann Oncol.* 2014;25(1):283-90.
- [104] Almhanna K, Meredith KL, Hoffe SE, Shridhar R, Coppola D. Targeting the Human Epidermal Growth Factor Receptor 2 in Esophageal Cancer. *Cancer Control.* 2013;20(2):111-6.
- [105] De Wever O, Hendrix A, De Boeck A, et al. Modeling and quantification of cancer cell invasion through collagen type I matrices. *Int J Dev Biol.* 2010;54(5):887-96.
- [106] Raggi M, Langer R, Feith M, Friess H, Schauer M, Theisen J. Successful evaluation of a new animal model using mice for esophageal adenocarcinoma. *Langenbecks Arch Surg.* 2010;395(4):347-50.
- [107] Quante M, Bhagat G, Abrams JA, et al. Bile acid and inflammation activate gastric cardia stem cells in a mouse model of Barrett-like metaplasia. *Cancer Cell.* 2012;21(1):36-51.
- [108] De Vlieghere E, Carlier C, Ceelen W, Bracke M, De Wever O. Data on in vivo selection of SK-OV-3 Luc ovarian cancer cells and intraperitoneal tumor formation with low inoculation numbers. *Data in Brief.* 2016;6:542-9.
- [109] Minn AJ, Gupta GP, Siegel PM, et al. Genes that mediate breast cancer metastasis to lung. *Nature.* 2005;436(7050):518-24.
- [110] Solomon B, Binns D, Roselt P, et al. Modulation of intratumoral hypoxia by the epidermal growth factor receptor inhibitor gefitinib detected using small animal PET imaging. *Mol Cancer Ther.* 2005;4(9):1417-22.
- [111] Busk M, Jakobsen S, Horsman MR, et al. PET imaging of tumor hypoxia using F-18-labeled pimonidazole. *Acta Oncol.* 2013;52(7):1300-7.
- [112] *Applied Radiation and Isotopes* 2005;62:897-901.
- [113] *Applied Radiation and Isotopes.* 2011;69:1007-13.
- [114] Loening AM, Gambhir SS. AMIDE: a free software tool for multimodality medical image analysis. *Mol Imaging.* 2003;2(3):131-7.
- [115] Siewert JR, Stein HJ, Feith M, Bruecher BL, Bartels H, Fink U. Histologic tumor type is an independent prognostic parameter in esophageal cancer: lessons from more than 1,000 consecutive resections at a single center in the Western world. *Ann Surg.* 2001;234(3):360-7; discussion 8-9.

- [116] Staal EFWC, Aleman BMP, Boot H, van Velthuysen MLF, van Tinteren H, van Sandick JW. Systematic review of the benefits and risks of neoadjuvant chemoradiation for oesophageal cancer. *Br J Surg*. 2010;97(10):1482-96.
- [117] Ping W, Sun W, Zu YK, Chen WS, Fu XN. Clinicopathological and prognostic significance of hypoxia-inducible factor-1 alpha in esophageal squamous cell carcinoma: a meta-analysis. *Tumor Biol*. 2014;35(5):4401-9.
- [118] Yue J, Yang Y, Cabrera AR, et al. Measuring tumor hypoxia with 18F-FETNIM PET in esophageal squamous cell carcinoma: a pilot clinical study. *Dis Esophagus*. 2012;25(1):54-61.
- [119] Melsens E, De Vlieghere E, Descamps B, et al. Improved xenograft efficiency of esophageal adenocarcinoma cell lines through in vivo selection. *Oncol Rep*. 2017.
- [120] Overgaard J, Overgaard M, Nielsen OS, Pedersen AK, Timothy AR. A comparative investigation of nimorazole and misonidazole as hypoxic radiosensitizers in a C3H mammary carcinoma in vivo. *Br J Cancer*. 1982;46(6):904-11.
- [121] Reischl G, Ehrlichmann W, Bieg C, et al. Preparation of the hypoxia imaging PET tracer [18F]FAZA: reaction parameters and automation. *Appl Radiat Isot*. 2005;62(6):897-901.
- [122] Hayashi K, Furutsuka K, Takei M, et al. High-yield automated synthesis of [18F]fluoroazomycin arabinoside ([18F]FAZA) for hypoxia-specific tumor imaging. *Appl Radiat Isot*. 2011;69(7):1007-13.
- [123] Tran LB, Bol A, Labar D, et al. Potential role of hypoxia imaging using (18)F-FAZA PET to guide hypoxia-driven interventions (carbogen breathing or dose escalation) in radiation therapy. *Radiother Oncol*. 2014;113(2):204-9.
- [124] Maier FC, Kneilling M, Reischl G, et al. Significant impact of different oxygen breathing conditions on noninvasive in vivo tumor-hypoxia imaging using [(1)(8)F]-fluoroazomycin arabinoside ([18F]FAZA). *Radiat Oncol*. 2011;6:165.
- [125] Carlson DJ, Keall PJ, Loo BW, Chen ZJ, Brown JM. Hypofractionation Results in Reduced Tumor Cell Kill Compared to Conventional Fractionation for Tumors with Regions of Hypoxia. *Int J Radiat Oncol*. 2011;79(4):1188-95.
- [126] Ng WL, Huang Q, Liu X, Zimmerman M, Li F, Li CY. Molecular mechanisms involved in tumor repopulation after radiotherapy. *Transl Cancer Res*. 2013;2(5):442-8.
- [127] Supiot S, Lisbona A, Paris F, Azria D, Fenoglio P. ["Dose-painting": myth or reality?]. *Cancer Radiother*. 2010;14(6-7):554-62.
- [128] Overgaard J. Hypoxic radiosensitization: Adored and ignored. *J Clin Oncol*. 2007;25(26):4066-74.
- [129] Ferlay J, Soerjomataram I, Dikshit R, et al. Cancer incidence and mortality worldwide: sources, methods and major patterns in GLOBOCAN 2012. *Int J Cancer*. 2015;136(5):E359-86.
- [130] Kapiteijn E, Marijnen CA, Nagtegaal ID, et al. Preoperative radiotherapy combined with total mesorectal excision for resectable rectal cancer. *N Engl J Med*. 2001;345(9):638-46.
- [131] Yoshimura M, Itasaka S, Harada H, Hiraoka M. Microenvironment and radiation therapy. *Biomed Res Int*. 2013;2013:685308.
- [132] Bozec A, Formento P, Lassalle S, Lippens C, Hofman P, Milano G. Dual inhibition of EGFR and VEGFR pathways in combination with irradiation: antitumour supra-additive effects on human head and neck cancer xenografts. *Br J Cancer*. 2007;97(1):65-72.
- [133] Jiang Y, Allen D, Kersemans V, et al. Acute vascular response to cediranib treatment in human non-small-cell lung cancer xenografts with different tumour stromal architecture. *Lung Cancer*. 2015;90(2):191-8.

- [134] Bradley DP, Tessier JJ, Lacey T, et al. Examining the acute effects of cediranib (RECENTIN, AZD2171) treatment in tumor models: a dynamic contrast-enhanced MRI study using gadopentate. *Magn Reson Imaging*. 2009;27(3):377-84.
- [135] Becker MA, Farzan T, Harrington SC, et al. Dual HER/VEGF receptor targeting inhibits in vivo ovarian cancer tumor growth. *Mol Cancer Ther*. 2013;12(12):2909-16.
- [136] Hoff PM, Hochhaus A, Pestalozzi BC, et al. Cediranib Plus FOLFOX/CAPOX Versus Placebo Plus FOLFOX/CAPOX in Patients With Previously Untreated Metastatic Colorectal Cancer: A Randomized, Double-Blind, Phase III Study (HORIZON II). *J Clin Oncol*. 2012;30(29):3596-603.
- [137] Cunningham D, Wong RPW, D'Haens G, et al. Cediranib with mFOLFOX6 vs bevacizumab with mFOLFOX6 in previously treated metastatic colorectal cancer. *Br J Cancer*. 2013;108(3):493-502.
- [138] Schmoll HJ, Cunningham D, Sobrero A, et al. Cediranib With mFOLFOX6 Versus Bevacizumab With mFOLFOX6 As First-Line Treatment for Patients With Advanced Colorectal Cancer: A Double-Blind, Randomized Phase III Study (HORIZON III). *J Clin Oncol*. 2012;30(29):3588-95.
- [139] Williams KJ, Telfer BA, Shannon AM, Babur M, Stratford IJ, Wedge SR. Combining radiotherapy with AZD2171, a potent inhibitor of vascular endothelial growth factor signaling: pathophysiologic effects and therapeutic benefit. *Mol Cancer Ther*. 2007;6(2):599-606.
- [140] Laschke MW, Elitzsch A, Vollmar B, Menger MD. In vivo analysis of angiogenesis in endometriosis-like lesions by intravital fluorescence microscopy. *Fertil Steril*. 2005;84:1199-209.
- [141] Baker M, Wayland H. On-line volume flow rate and velocity profile measurement for blood in microvessels. *Microvasc Res*. 1974;7(1):131-43.
- [142] Norrby K. Microvascular density in terms of number and length of microvessel segments per unit tissue volume in mammalian angiogenesis. *Microvasc Res*. 1998;55(1):43-53.
- [143] Ceelen W, Smeets P, Backes W, et al. Noninvasive monitoring of radiotherapy-induced microvascular changes using dynamic contrast enhanced magnetic resonance imaging (DCE-MRI) in a colorectal tumor model. *Int J Radiat Oncol Biol Phys*. 2006;64(4):1188-96.
- [144] Ozerdem U. Measuring interstitial fluid pressure with fiberoptic pressure transducers. *Microvasc Res*. 2009;77(2):226-9.
- [145] Gatenby RA, Kessler HB, Rosenblum JS, et al. Oxygen Distribution in Squamous-Cell Carcinoma Metastases and Its Relationship to Outcome of Radiation-Therapy. *Int J Radiat Oncol*. 1988;14(5):831-8.
- [146] Bokacheva L, Kotedia K, Reese M, et al. Response of HT29 colorectal xenograft model to cediranib assessed with 18F-fluoromisonidazole positron emission tomography, dynamic contrast-enhanced and diffusion-weighted MRI. *NMR Biomed*. 2013;26(2):151-63.
- [147] Bradley DP, Tessier JL, Checkley D, et al. Effects of AZD2171 and vandetanib (ZD6474, Zactima) on haemodynamic variables in an SW620 human colon tumour model: an investigation using dynamic contrast-enhanced MRI and the rapid clearance blood pool contrast agent, P792 (gadomelitol). *NMR Biomed*. 2008;21(1):42-52.
- [148] Maeda A, Leung MKK, Conroy L, et al. In Vivo Optical Imaging of Tumor and Microvascular Response to Ionizing Radiation. *PLoS One*. 2012;7(8).



- [149] Pietras K, Ostman A, Sjoquist M, et al. Inhibition of platelet-derived growth factor receptors reduces interstitial hypertension and increases transcapillary transport in tumors. *Cancer Res.* 2001;61(7):2929-34.
- [150] Fan Y, Du W, He B, et al. The reduction of tumor interstitial fluid pressure by liposomal imatinib and its effect on combination therapy with liposomal doxorubicin. *Biomaterials.* 2013;34(9):2277-88.
- [151] Heldin CH, Rubin K, Pietras K, Ostman A. High interstitial fluid pressure - an obstacle in cancer therapy. *Nat Rev Cancer.* 2004;4(10):806-13.
- [152] Salnikow AV, Heldin NE, Stuhr LB, et al. Inhibition of carcinoma cell-derived VEGF reduces inflammatory characteristics in xenograft carcinoma. *Int J Cancer.* 2006;119(12):2795-802.
- [153] Hofmann M, Pflanzner R, Zoller NN, et al. Vascular endothelial growth factor C-induced lymphangiogenesis decreases tumor interstitial fluid pressure and tumor (vol 6, pg 394, 2013). *Transl Oncol.* 2013;6(5).
- [154] Landry JC, Feng Y, Prabhu RS, et al. Phase II Trial of Preoperative Radiation With Concurrent Capecitabine, Oxaliplatin, and Bevacizumab Followed by Surgery and Postoperative 5-Fluorouracil, Leucovorin, Oxaliplatin (FOLFOX), and Bevacizumab in Patients With Locally Advanced Rectal Cancer: 5-Year Clinical Outcomes ECOG-ACRIN Cancer Research Group E3204. *Oncologist.* 2015;20(6):615-6.
- [155] Salazar R, Capdevila J, Laquente B, et al. A randomized phase II study of capecitabine-based chemoradiation with or without bevacizumab in resectable locally advanced rectal cancer: clinical and biological features. *BMC Cancer.* 2015;15.
- [156] Nair DV, Reddy AG. Laboratory animal models for esophageal cancer. *Vet World.* 2016;9(11):1229-32.
- [157] Pham TH, Genta RM, Spechler SJ, Souza RF, Wang DH. Development and characterization of a surgical mouse model of reflux esophagitis and Barrett's esophagus. *J Gastrointest Surg.* 2014;18(2):234-40; discussion 40-1.
- [158] Hashimoto N. Expression of COX2 and p53 in Rat Esophageal Cancer Induced by Reflux of Duodenal Contents. *ISRN Gastroenterol.* 2012;2012:914824.
- [159] Choi SY, Lin D, Gout PW, Collins CC, Xu Y, Wang Y. Lessons from patient-derived xenografts for better in vitro modeling of human cancer. *Adv Drug Deliv Rev.* 2014;79-80:222-37.
- [160] Tran LBA, Bol A, Labar D, et al. Hypoxia imaging with the nitroimidazole F-18-FAZA PET tracer: A comparison with OxyLite, EPR oximetry and F-19-MRI relaxometry. *Radiother Oncol.* 2012;105(1):29-35.
- [161] Postema EJ, McEwan AJB, Riauka TA, et al. Initial results of hypoxia imaging using 1-alpha-D-(5-deoxy-5-[(18)F]-fluoroarabinofuranosyl)-2-nitroimidazole ((18)F-FAZA). *Eur J Nucl Med Mol Imaging.* 2009;36(10):1565-73.
- [162] Le QT, Fisher R, Oliner KS, et al. Prognostic and predictive significance of plasma HGF and IL-8 in a phase III trial of chemoradiation with or without tirapazamine in locoregionally advanced head and neck cancer. *Clin Cancer Res.* 2012;18(6):1798-807.
- [163] Mortensen LS, Johansen J, Kallehauge J, et al. FAZA PET/CT hypoxia imaging in patients with squamous cell carcinoma of the head and neck treated with radiotherapy: Results from the DAHANCA 24 trial. *Radiother Oncol.* 2012;105(1):14-20.
- [164] Sugie C, Shibamoto Y, Ito M, et al. Reevaluation of the radiosensitizing effects of sanazole and nimorazole in vitro and in vivo. *J Radiat Res (Tokyo).* 2005;46(4):453-9.
- [165] Overgaard J, Overgaard M, Nielsen OS, Pedersen AK, Timothy AR. A Comparative Investigation of Nimorazole and Misonidazole as Hypoxic Radiosensitizers in a C3h Mammary-Carcinoma In vivo. *Br J Cancer.* 1982;46(6):904-11.

- [166] Lei YY, Huang JY, Zhao QR, et al. The clinicopathological parameters and prognostic significance of HER2 expression in gastric cancer patients: a meta-analysis of literature. *World J Surg Oncol*. 2017;15(1):68.
- [167] Seshadri R, Firgaira FA, Horsfall DJ, Mccaul K, Setlur V, Kitchen P. Clinical-Significance of Her-2/Neu Oncogene Amplification in Primary Breast-Cancer. *J Clin Oncol*. 1993;11(10):1936-42.
- [168] Perez EA, Romond EH, Suman VJ, et al. Trastuzumab plus adjuvant chemotherapy for human epidermal growth factor receptor 2-positive breast cancer: planned joint analysis of overall survival from NSABP B-31 and NCCTG N9831. *J Clin Oncol*. 2014;32(33):3744-52.
- [169] Cunningham D, Allum WH, Stenning SP, et al. Perioperative chemotherapy versus surgery alone for resectable gastroesophageal cancer. *N Engl J Med*. 2006;355(1):11-20.
- [170] Bang YJ, Van Cutsem E, Feyereislova A, et al. Trastuzumab in combination with chemotherapy versus chemotherapy alone for treatment of HER2-positive advanced gastric or gastro-oesophageal junction cancer (ToGA): a phase 3, open-label, randomised controlled trial. *Lancet*. 2010;376(9742):687-97.
- [171] Fuchs CS, Tomasek J, Yong CJ, et al. Ramucirumab monotherapy for previously treated advanced gastric or gastro-oesophageal junction adenocarcinoma (REGARD): an international, randomised, multicentre, placebo-controlled, phase 3 trial. *Lancet*. 2014;383(9911):31-9.
- [172] Wilke H, Muro K, Van Cutsem E, et al. Ramucirumab plus paclitaxel versus placebo plus paclitaxel in patients with previously treated advanced gastric or gastro-oesophageal junction adenocarcinoma (RAINBOW): a double-blind, randomised phase 3 trial. *Lancet Oncol*. 2014;15(11):1224-35.
- [173] Souvatzoglou M, Grosu AL, Roper B, et al. Tumour hypoxia imaging with [F-18]FAZA PET in head and neck cancer patients: a pilot study. *Eur J Nucl Med Mol Imaging*. 2007;34(10):1566-75.
- [174] Schmoll HJ, Van Cutsem E, Stein A, et al. ESMO Consensus Guidelines for management of patients with colon and rectal cancer. A personalized approach to clinical decision making. *Ann Oncol*. 2012;23(10):2479-516.
- [175] Dewdney A, Capdevila J, Glimelius B, et al. EXPERT-C: A randomized, phase II European multicenter trial of neoadjuvant capecitabine plus oxaliplatin chemotherapy (CAPOX) and chemoradiation (CRT) with or without cetuximab followed by total mesorectal excision (TME) in patients with MRI-defined, high-risk rectal cancer. *J Clin Oncol*. 2011;29(15).

# **CURRICULUM VITAE**

## **PERSONAL DATA**

Name	Melsens
First Name	Elodie
Date and place of birth	February 5 <sup>th</sup> , 1989, Knokke-Heist, Belgium
Nationality	Belgian
Address Work	Laboratory of Experimental Surgery Department of Gastro-Intestinal Surgery University Hospital Ghent De Pintelaan 185 9000 Ghent Belgium
Home	Laurent Delvauxstraat 12, bus 3 9000 Gent Belgium
Contact	Work +32 9 332 21 34; elodie.melsens@ugent.be Home +32 495 57 09 71; elodie.melsens@gmail.com

## **EDUCATION**

2014 till now	PhD student, Laboratory of Experimental Surgery, Ghent University Hospital, Project: Tumor hypoxia in solid tumors Surgical Trainee, University Hospital Ghent, Prof. Dr. P. Pattyn
2010- 2014	Master of Medicine in Medicine, Ghent University (Graduated with High Distinction)
2007- 2010	Bachelor of Medicine, Ghent University (Graduated with High Distinction)
2001- 2007	Latin- Mathematics (8h), Sint- Andreaslyceum, Sint- Kruis

## **CERTIFICATES AND POSTGRADUATE COURSES**

2015	Certificate Radioprotection, Ghent University
2014-2015	Certificate Laboratory Animal Science (Level: Experiment Leader), Vrije Universiteit Brussel
2010- 2011	Principles of Electrocardiography, Ghent University

## PUBLICATIONS

### A1

- **Melsens E**, De Vlieghere E, Descamps B, Vanhove C, De Wever O, Ceelen W, Pattyn P. Improved xenograft efficiency of esophageal adenocarcinoma cell lines through in vivo selection. *Oncol Rep.* 38: 71-81, 2017. (IF 2015= 2.49; Ranking Oncology 2015= Q3 (130/213)).
- **Melsens E**, Verberckmoes B, Rosseel N, Vanhove C, Descamps B, Pattyn P, Ceelen W. The VEGFR Inhibitor Cediranib Improves the Efficacy of Fractionated Radiotherapy in a Colorectal Cancer Xenograft Model. *Eur Surg Res.* 2016;58(3-4):95-108. (IF 2015= 1.15; Ranking Surgery 2015, Q3 (127/200))
- van Geel N, Speeckaert R, **Melsens E**, Toelle SP, Speeckaert M, De Schepper S, Lambert J, Brochez L. The distribution pattern of segmental vitiligo: clues for somatic mosaicism. *Br J Dermatol.* 2013 Jan;168(1):56-64. (IF 2013= 4.1; Ranking Dermatology 2013= Q1 (7/61))

### C3

#### *Oral presentations*

- **Melsens E**, De Vlieghere E, Descamps B, Vanhove C, Kersemans K, Devos F, Goethals I, Brans B, De Wever O, Ceelen W, Pattyn P. Hypoxia in esophageal cancer, biomarker and target for therapy, a preclinical study. Joint Academic meeting with the Travelling Surgical Society (TSS) of Great Britain and Ireland 2017, Ghent, Belgium. *Winner of Registrar's Prize for best presentation.*
- **Melsens E**, Verberckmoes B, Rosseel N, Vanhove C, Descamps B, Pattyn P, Ceelen W. The VEGFR Inhibitor Cediranib Improves the Efficacy of Fractionated Radiotherapy in a Colorectal Cancer Xenograft Model. *Belgian Surgical Week (BSW) 2016, Brussels, Belgium.*
- **Melsens E**, Willaert W, Van Nieuwenhove Y, Monstrey S, Pattyn P. Vaginal elongation with descending colon in patients with gender identity disorder. *Belgian Surgical Week (BSW) 2014, Spa, Belgium.*
- **Melsens E**, Willaert W, Van Nieuwenhove Y, Monstrey S, Pattyn P. Vaginal elongation with descending colon in patients with gender identity disorder. *European Society for Surgical Research (ESSR) 2014, Budapest, Hungary.*

*Poster presentations*

- **Melsens E**, De Vlieghere E, Descamps B, Vanhove C, Kersemans K, Devos F, Goethals I, Brans B, De Wever O, Ceelen W, Pattyn P. Hypoxia imaging with <sup>18</sup>F-FAZA PET/CT to predict radioresistance in esophageal adenocarcinoma xenografts. Belgian Society of Nuclear Medicine (BELNUC) 2017, Ghent, Belgium.
- **Melsens E**, De Vlieghere E, Descamps B, Vanhove C, Kersemans K, Devos F, Brans B, Ceelen W, Pattyn P. Hypoxia imaging with <sup>18</sup>F-FAZA PET/CT predicts radioresistance in esophageal adenocarcinoma in mice. European Society for Diseases of the Esophagus (ESDE) 2016, Munich, Germany.
- **Melsens E**, Verberckmoes B, Rosseel N, Vanhove C, Descamps B, Pattyn P, Ceelen W. The VEGFR Inhibitor Cediranib Improves the Efficacy of Fractionated Radiotherapy in a Colorectal Cancer Xenograft Model. Society for Surgical Oncology (SSO) 2016, Boston, USA.



## **ACKNOWLEDGMENTS**

Arriving at the end of this thesis, I look back at an amazing 3 years that flew past. This work would not have been possible without the help of numerous people. I would like to thank everyone that contributed to this thesis, in a big or small way.

My promotor, Prof. Dr. Piet Pattyn. I am very thankful for the scientific and clinical opportunities you gave me. This research project has been a winding road and I would like to thank you for your endless confidence and support and perfect balance between guidance and freedom. Despite your fully booked agenda, you always made time for a meeting and advice. I also enjoyed my days in the clinic at the department of gastro-intestinal surgery, thank you for being an excellent teacher.

My co-promotor, Prof. Dr. Wim Ceelen, head of the laboratory of experimental surgery. Thank you for introducing me in the world of fundamental research. I enjoyed working in '*de kelder*'. Thank you for your confidence and support. You provided connections and scientific insights that helped me accomplish this thesis. I respect the way you combine science and clinical activities and how you made the laboratory evolve to what it is today. I am proud to have worked in your lab.

Members of the examination commission, Prof. Dr. Johan Vande Walle, Prof. Dr. Anne Hoorens, Dr. Louke Delrue, Prof. Dr. Boudewijn Brans, Prof. Dr. Philippe Nafteux and Prof. Dr. Marc Peeters, thank you for your time, thorough revision and constructive remarks.

I would like to thank everyone from the Laboratory of Experimental Cancer Research for showing me the way in '*de P7*'. Special thanks to Prof. Olivier De Wever and Elly De Vlieghe for the enlightening meetings and discussions, for your interest in my project, for your enthusiasm and help. Special thanks to Stephanie Decloedt and Glenn Wagemans for your practical assistance.

Prof. Ir. Chris Vanhove and Dr. Benedicte Descamps from Infinity, it was a pleasure working with you. Thanks for teaching me some scan-skills and for your insights in analyzing and interpreting results. Also, thanks for trusting me with the machinery to perform scans outside '*opening hours*'.

Prof. Dr. Boudewijn Brans, Prof. Dr. Ingeborg Goethals and Prof. Dr. Filip De Vos from the department of nuclear medicine and radiopharmacy, thank you for the introduction in the world of nuclear medicine, your positivity and insightful remarks. Special thanks to Ken Kersemans and Jan Courtyn for the flawless productions of  $^{18}\text{F}$ -FAZA and for your flexibility. Without you this project would not have been possible.

Thank you Prof. Anne Vral and Leen Pieters from the Department of Basic Medical Sciences for helping me with the complex  $\gamma$ -H2AX immunostaining.

The Department of Clinical Chemistry, Microbiology and Immunology and Leen Van Simaey for giving me access to the anaerobic work station.

Co-workers of the animalarium, thank you for taking care of the mice and providing good conditions to perform research.

Thanks to the staff-members, residents, assistants and nurses of the department of gastro-intestinal surgery for all your support and understanding in the clinic, and for the teaching during my traineeship. Thank you for your understanding and interest for my work in the lab. Thanks to the secretary of gastro-intestinal surgery and Maaïke Pauwels in specific, for helping me with logistics.

Heidi Maertens, thank you for the support and the tips-and-tricks to succeed this project.

My colleagues of the Laboratory of Experimental Surgery, Dr. Wouter Willaert, Dr. Félix Gremonprez, that were there from the start, thank you for sharing your knowledge and being good examples. Thank you Natacha Rosseel for the enormous help with immunohistochemistry, mice experiments, cell cultures... Also thanks for all the fun moments and for the advice in animal care and eco-lifestyle ;) Thank you Evelien Dierick 'mom of the lab', for taking over this difficult and sometimes chaotic job, for your help and distracting chats!

Charlotte Carlier and Kaat De Clercq, we had such a great time the last three years. Thank you for supporting me in the ups and downs. This PhD would not have been the same without you, 'vriesganzen'!

Annouck Philippron, thanks for the relaxing talks and discussions we had at 'closing time', thanks for your help in the clinic and the fun moments at the ESDE meetings!



Thanks Sarah Cosyns, Leen Van de Sande, Nick Lagast and Eva Pape for bringing new energy and inspiration to the lab and for the sportive lunch-breaks.

My family, friends and 'Lindseys', thanks for all your positive vibes, cheering words and distraction in sometimes stressful moments. You are the best!

Mama and papa, David, thank you for the unlimited support, interest and tolerance. Thank you for making home such a warm place to come back to and always, always, being there for me!

Toon, my love, thank you for being my Tonny. Thank you for always believing in me and supporting me in everything I do. You cheer me up like no one can. Thank you for all the adventures we had, up to the next! xxx